8-2010

PROBING THE MECHANISMS OF PLATELET ADHESION TO ADSORBED PLASMA PROTEINS

Balakrishnan Sivaraman
Clemson University, bsivaraman@gmail.com

PROBING THE MECHANISMS OF PLATELET ADHESION TO ADSORBED PLASMA PROTEINS

A Dissertation
Presented to
the Graduate School of
Clemson University

In Partial Fulfillment
of the Requirements for the Degree
Doctor of Philosophy
Bioengineering

---

by
Balakrishnan Sivaraman
August 2010

Accepted by:
Dr. Robert Latour, Committee Chair
Dr. Naren Vyavahare
Dr. Anand Ramamurthi
Dr. Alexey Vertegel

ABSTRACT

Despite over three decades of research in blood-material interactions, the biomaterials field has been unsuccessful in developing a truly non-thrombogenic biomaterial. This is due to an incomplete understanding of the factors underlying biomaterial-associated thrombosis, especially the mechanisms mediating the interactions of platelets with the adsorbed plasma protein layer(s) on the implant surface. The work presented here is motivated by the primary goal of delineating these mechanisms, and understanding the platelet receptors involved, as well as the domains/amino acid sequences they bind to in the protein molecules.

It is critical to differentiate between the amount and the conformation of the adsorbed protein, both of which are potential mediators of platelet adhesion, while designing hemocompatible biomaterials. We accomplished this by independently varying the surface chemistry and protein solution concentration, and illustrated that the platelet adhesion correlated strongly with the degree of adsorption-induced fibrinogen (Fg) unfolding, as measure by the loss in α-helix measured via circular dichroism (CD) spectropolarimetry. Additionally, platelet adhesion to adsorbed albumin (Alb), which is conventionally thought to be unable to bind platelets, strongly correlated with Alb unfolding beyond a critical level of unfolding (~34% α-helix loss).

A variety of blocking strategies were employed in order to identify the platelet receptors involved in the adhesion process, including soluble peptides, monoclonal antibodies, as well as a platelet antagonist drug. Our preliminary results suggested that

two platelet receptor sets were potentially mediating the adhesion, as a peptide containing the Arginine-Glycine-Aspartic Acid (RGD) sequence, which is a well known cell-binding sequence, was found to be a partial inhibitor of platelet adhesion to both adsorbed Fg and Alb. We therefore hypothesized that one set was specific to the RGD amino acid sequence, and mediated both platelet adhesion and activation. The other set was likely non-RGD-specific and mediated adhesion with little/no activation.

Targeting the GPIb-IX-V complex as the non-RGD-specific receptor set using monoclonal antibodies against GPIb, did not inhibit platelet adhesion to adsorbed Fg and Alb. However, the use of Aggrastat, a platelet antagonist drug against the RGD-specific GPIIb/IIIa platelet receptor, led to a near complete inhibition of platelet adhesion to both adsorbed Fg and Alb, clearly illustrating the critical role played by this receptor in platelet adhesion.

Chemical modification of the arginine residues in adsorbed Alb led to a significant decrease in platelet adhesion to Alb, thereby provided deeper insight into their role in mediating platelet-Alb interactions, while the modification of lysine residues did not affect platelet adhesion. Thus, we hypothesize that beyond a critical degree of adsorption-induced conformational changes in Alb, the arginine and aspartic/glutamic acid residues may become spatially oriented such that they form RGD-like motifs which are recognized by the GPIIb/IIIa platelet receptors. Additionally, we also showed that an irreversibly adsorbed, tightly packed Alb layer undergoes increased unfolding with

increasing residence times of up to 6 months, thereby enabling and enhancing platelet adhesion.

Overall, these studies present deeper insights into the molecular mechanisms mediating platelet interactions with adsorbed plasma proteins, and how these interactions can be controlled to improve the hemocompatibility of cardiovascular biomaterials.

DEDICATION

This work is dedicated to my parents, Ammu and Sivaraman. They have been pillars of support, encouragement, and inspiration over the years, in all my endeavors. Nothing can ever replace everything you have given me!

ACKNOWLEDGEMENTS

Kahlil Gibran once wrote, “The teacher who is indeed wise does not bid you to enter the house of his wisdom but rather leads you to the threshold of your mind”. I am deeply indebted to all my teachers, who have gone a long way in playing their role of Rodin, sculpting the thinker and analyzer in me.

I would like to express my sincere gratitude to my advisor, Dr. Robert Latour for his support and guidance over the past five years. In reality he was not only an advisor, but a mentor! I would also like to thank my committee members, Dr. Naren Vyavahare, Dr. Anand Ramamurthi and Dr. Alexey Vertegel for their advice, guidance and support from the beginning of my doctoral odyssey. They have all been constant sources of encouragement, through the ups and downs of this project.

Dr. Dan Simionescu and Dr. Agneta Simionescu have been a tremendous source of support and advice throughout my stint at Clemson. Special thanks to Dr. Jim Harriss for assistance with coating our substrates with gold. I would like to acknowledge assistance from Dr. Yonnie Wu with the mass spectrometric analysis experiments. The numerous volunteers who kindly volunteered to donate blood for my experiments deserve special mention.

Thanks are due to the members (past and present) of the Biomolecular Interactions & Biomolecular Modeling laboratories for being great sources of help, and for all the discussions (scientific and non-scientific) we have had. I am grateful to Dr. Kenan Fears

and John Marigliano for helping me take my first steps in the laboratory. Yang Wei and Aby Thyparambil have been an integral part of life in the laboratory, and I consider myself fortunate to have had them as friends and colleagues. Nihar, Jai, Aditee, Chandrasekhar, Betsy and Jeremy have taken time out from their own busy schedules to brainstorm and discuss many a point with me.

My parents have been a constant source of support, encouragement and inspiration. They have always pushed me to strive to achieve greater goals, and I am grateful for everything they have done for me. I would like to thank Gayathri Ramasubramanian for being a huge source of support, and being there for me, patiently caring and sharing!

All the staff in the Bioengineering department have gone a long way in making my Clemson experience a smooth and unforgettable one, with their disarming smiles. Merci beaucoup Mesdames!

TABLE OF CONTENTS

Page

LIST OF FIGURES

Page

List of figures (continued…..)

Page

List of figures (continued….)

Page

LIST OF TABLES

Page

CHAPTER 1

INTRODUCTION

The development of truly hemocompatible biomaterials for cardiovascular applications has been hindered by the failure to completely understand the molecular mechanisms underlying biomaterial-associated thrombosis, mainly due to the complexity of blood-material interactions. The adsorbed layer of plasma proteins on the biomaterial surface plays a critical role in the recruitment of platelets from the bloodstream to form thrombi, which in adverse cases may lead to thrombotic and thromboembolic complications, which are the primary factors mediating the blood incompatibility of biomaterials. Chapter 2 of this dissertation presents a critical review of blood-biomaterial interactions, focusing on the role of adsorbed proteins, especially fibrinogen (Fg) and albumin (Alb), and platelets in mediating the thrombogenicity of biomaterial surfaces.

The specific aims of this research project in delineating/probing the mechanisms of platelets to adsorbed Fg and Alb are listed in Chapter 3. The biomaterials literature has remained unclear on whether it is the conformation or the surface coverage of adsorbed proteins which influences the platelet response, and our research proposes to examine this critical question.

Studies covered in Chapter 4 involved the combined use of surface chemistry and protein solution concentration to independently vary the degree of structural change in the proteins from the surface coverage of adsorbed protein, which was examined using

circular dichroism (CD) spectropolarimetry. Using these surfaces with differing amounts and conformations of adsorbed protein, we were able to definitively delineate the critical role played by the adsorbed conformation in mediating the platelet response to adsorbed Fg (Chapter 5) and Alb (Chapter 6).

Both chapters provide deeper insight into the roles of specific platelet receptors and specific amino acid residues in the adsorbed protein in the platelet adhesion response, which were ascertained using blocking strategies on the platelets, as well as the adsorbed protein layer. The results presented in Chapter 6 provide conclusive information on the potential of adsorbed Alb to bind platelets, with the mechanisms of platelet adhesion to both Fg and Alb being similar in nature, as a function of adsorption-induced unfolding.

Chapter 7 builds on the results obtained in the previous two chapters, probing the role of the GPIIb/IIIa and GPIb-IX-V platelet receptors in mediating adhesion to adsorbed Fg and Alb. The role of Asp and Glu residues in the adsorbed Alb layer in mediating platelet binding was analyzed using chemical modification studies. Additionally, residence time-dependent conformational changes in an irreversibly adsorbed, tightly packed layer of adsorbed Alb and its potential in enabling and enhancing platelet attachment was analyzed in Chapter 8.

The appendix provides details on the formation and characterization of the SAM surfaces, protein adsorption, washed platelet preparation and platelet adhesion. Additionally, this section expands on the techniques for the side-chain modification of the native/adsorbed proteins, used for delineating the platelet adhesion mechanisms.

Overall, the experiments described in this dissertation provide deeper insights into the molecular mechanisms mediating platelet adhesion to adsorbed proteins on biomaterial surfaces, and hopefully will aid in the development of more blood-compatible biomaterials for cardiovascular applications.

CHAPTER 2

BACKGROUND INFORMATION

2.1 Blood-material interactions

2.1.1 Overview

Under normal conditions, blood comes into contact with an anticoagulant and antithrombotic endothelium, which represents the inner lining of the entire cardiovascular system. However, when a biomaterial is implanted in the body, it represents the introduction of a 'foreign surface' with non-endothelial properties into the circulation, as a result of which a series of complex, interlinked events occur including protein adsorption, platelet and leukocyte adhesion and activation, and activation of the coagulation and complement cascades [1].

Upon contact with blood, the implant surface is coated with a layer of plasma proteins within seconds to minutes. The cells which arrive at the implant surface after the proteins adsorb primarily 'see' a protein layer rather than the surface of the implant, and may respond to this layer of adsorbed proteins by adhering, spreading, releasing active compounds, and also recruiting other cells to the implant surface [2]. The cellular response is primarily mediated by the platelets, which are thought to adhere specifically to binding motifs/domains exposed in these adsorbed proteins.

Although they do not bind platelets strongly in their native state in the bloodstream, plasma proteins such as fibrinogen (Fg), von Willebrand factor (vWf), fibronectin (Fn) and vitronectin (Vn) are strongly adhesive towards platelets in their adsorbed state. This

adhesion is primarily mediated by receptors on the platelet membrane, which are conventionally thought to bind to the adhesive Arg-Gly-Asp (RGD) amino acid sequence present in these proteins, and leads to a complex set of reactions involving the generation and release of platelet agonists such as adenosine diphosphate (ADP) and thrombin and thromboxanes, which in turn act in concert to recruit other platelets, leading to platelet aggregation [3]. The surface of the aggregate serves as a site for rapid thrombin formation, the rate of which is higher than that of anticoagulant mechanisms in blood, thereby causing further platelet activation and catalyzing the formation of fibrin [3]. The formation of a fibrin clot is the final step of a series of proteolytic reactions called the coagulation cascade (schematic illustration in Fig. 2.1)

2.1.2 Blood coagulation cascade

In the coagulation cascade (in Fig. 2.1), inactive factors (zymogens) become enzymatically active due to surface contact or proteolytic cleavage by other factors, with the newly activated enzyme then activating another inactive factor [1]. This cascade is initiated either by the surface-mediated route (intrinsic pathway) or due to the cellular expression of tissue factor (extrinsic pathway). These two pathways converge into the common pathway, leading to the generation of thrombin from prothrombin, resulting in the formation of a fibrin clot due to the action of thrombin in catalyzing the conversion of fibrinogen to form the clot. The exact mechanisms underlying these pathways, as well as

their roles in blood coagulation, however, have remained unclear [1], and may potentially be dependent on a combination of synergistic factors.

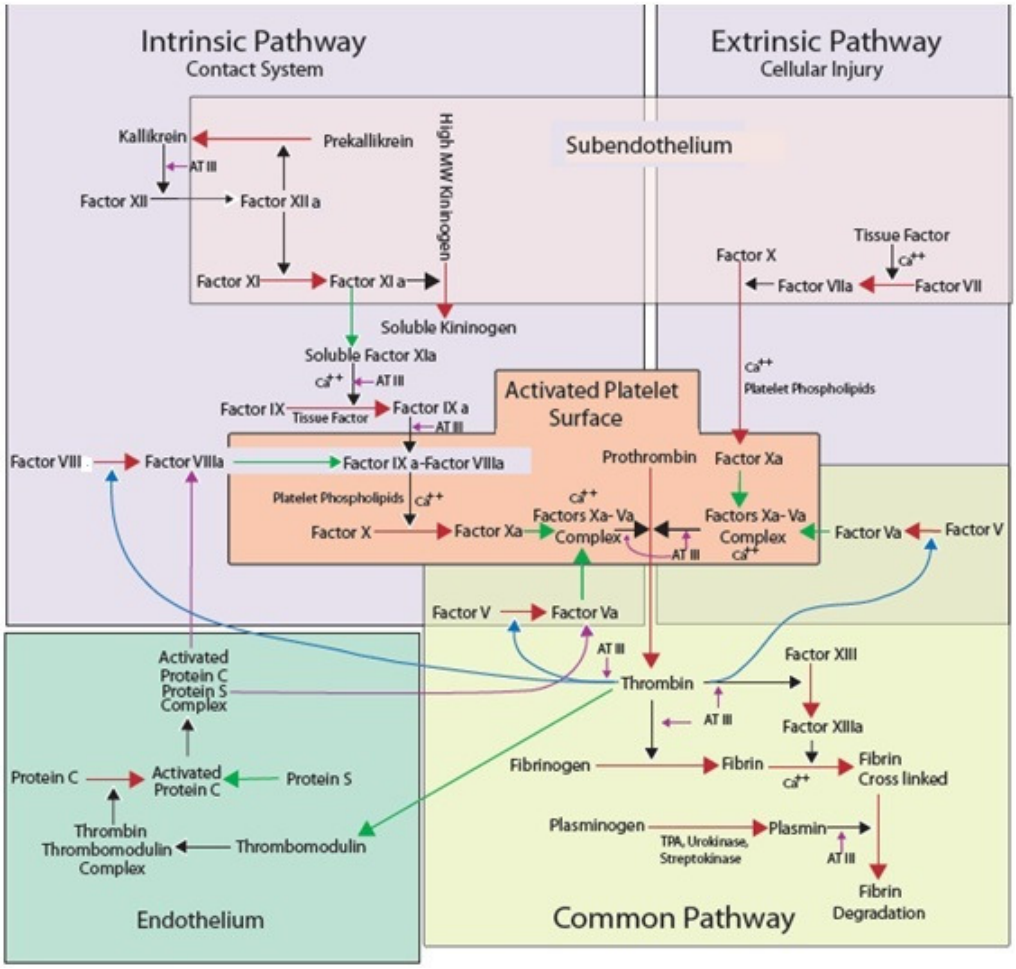

Figure 2.1. The coagulation cascade. (Figure taken from www.sigma-aldrich.com).

The zymogens associated with the initiation of the intrinsic pathway such as high molecular weight kininogen (HMWK), prekallikrein and Factor XII (FXII) have been conventionally thought to require contact with negatively charged surfaces for activation in vitro [4], although recent studies by Chatterjee *et al.* and Vogler and Siedlecki [5, 6]

have suggested that contact activation of FXII is not specific to anionic hydrophilic surfaces. Gorbet and Sefton in their review of biomaterial-associated thrombosis [1], suggested that the role of the intrinsic pathway in normal blood coagulation has been unclear. The fact that patients who have deficiencies in these zymogens do not necessarily have bleeding disorders lends credence to the argument that this contact activation system may not be relevant in vivo under normal, physiological conditions [4, 7].

On the other hand, FXII activation may occur when any artificial surface comes into contact with blood, with the surface along with the adsorbed protein layer then representing the activating surface [1]. Recent studies [5, 6, 8, 9] have provided strong evidence for the role of FXII and the contact activation pathway in mediating blood coagulation. However, studies have shown that despite the presence of moderate amounts of FXII on biomaterials used for vascular grafts [10] and hemodialyzers [11], it is often not present in its activated form (FXIIa) [12]. In vivo studies with hemodialyzer membranes have not indicated any significant increase in FXIIa [13], while there was no significant correlation between FXIIa and thrombin generation in another study [14]. These results potentially suggest that the contact-activation pathway may not play an important role in the activation of coagulation cascade by biomaterial surfaces, and instead the tissue factor (TF) pathway of blood coagulation is slowly being recognized by the biomaterials community [1].

TF expression by monocytes may result in blood coagulation via the extrinsic pathway, when a biomaterial comes into contact with blood. This has been observed in

vivo during or after cardiopulmonary bypass [15-17], and thus leukocytes (most likely due to TF on monocytes) may play a role in the activation of the coagulation cascade [18], suggesting that a TF-dependent pathway of coagulation initiation may occur on biomaterial surfaces.

Since the biomaterials field remains divided over the exact mechanisms of the extrinsic and intrinsic coagulation pathways and their roles in the bigger picture of biomaterial-associated thrombosis, further research studies investigating these pathways are essential in developing a more comprehensive understanding of the coagulation cascade.

2.1.3 Additional blood-biomaterial interactions in thrombosis

Biomaterials-induced thrombosis can also be directly mediated by platelet adhesion and activation to adsorbed proteins, thus skipping the initial activating processes of the coagulation cascade. The platelet-mediated thrombotic response to implanted biomaterials comprises (i) plasma protein adsorption, (ii) platelet adhesion, and (iii) fibrin formation or blood coagulation. Both white (platelet) and red (fibrin) thrombi form on valves and other cardiovascular implants, and under adverse conditions, these thrombi may get dislodged from the implant surface, leading to thromboembolic complications, which may even be fatal in some cases [19]. Virchow attributed the causes of thrombus formation and propagation in his triad (see Fig. 2.2) to abnormalities in (i) blood flow (circulatory stasis), (ii) vessel wall (vascular wall injury), and (iii) blood components (hypercoagulable state). In addition to the relative propensity for thrombus formation,

this triad also often predicts the location of thrombotic deposits associated with cardiovascular implants [20].

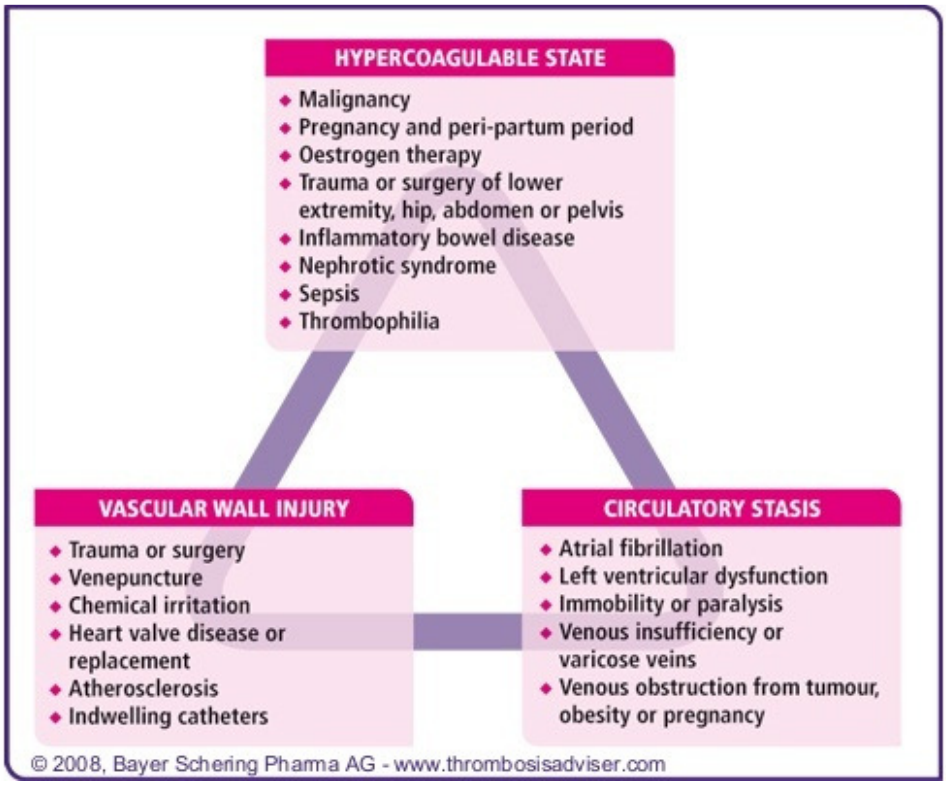

Figure 2.2. Virchow's triad illustrating the three broad categories of factors (and their causes) which contribute to thrombosis.

Thus, the blood compatibility (or hemocompatibility) of biomaterials can be defined as that property due to which these materials or devices can function in an environment where they come into contact with blood without inducing any adverse reaction, such as thrombosis [21]. Despite over three decades of research, no material has been found to be truly hemocompatible so far, although many cardiovascular biomaterials/devices have

been found to function with minimal or acceptable risks of complications [7]. The thrombotic and thromboembolic complications associated with these devices are fairly low and can be addressed using anticoagulant therapy, but the bleeding risks associated with anticoagulants still remain serious concerns [1].

The failure to design a completely hemocompatible biomaterial can be attributed to the insufficient understanding of the complexities underlying blood-material interactions. In addition to platelets and plasma proteins like fibrinogen (Fg) that are associated with the coagulation response, other proteins (notably the complement system) and a variety of cells (such as leukocytes) that are associated with the inflammatory response also play important roles in determining the blood compatibility of biomaterial implants [1].

The complement system consists of more than 20 plasma proteins which play an important role in mediating the body's defense mechanisms against infection and foreign elements [1] by coating the surface of the foreign body with complement fragments (such as C3b, C4b and iC3b). This process is known as opsonization [22], and facilitates the uptake of the foreign body by phagocytic cells. Biomaterials which activate the complement system are generally characterized by the presence of hydroxyl and amine surface groups which promote the binding of complement product C3b, leading to the formation of C3 and C5 convertase which propagate the complement cascade [23, 24]. Although the complement and coagulation cascades are generally treated as separate processes, they have been shown to modulate each other's activities [25]. Overall, although some of the consequences of complement activation by biomaterials are well

understood, more research needs to be done in order to fully understand the mechanisms underlying biomaterial-associated complement activation and how this can be inhibited.

Leukocytes consist of neutrophils, basophils, eosinophils, monocytes and lymphocytes, and play a critical role in the inflammatory response to biomaterials. Neutrophils and monocytes become activated on contact with cardiovascular biomaterial surfaces, leading to increased leukocyte adhesion on these surfaces [1]. Although the exact nature of the mechanisms of leukocyte adhesion to biomaterials remains unclear, preliminary results suggest that it is mediated in part by the complement product iC3b [26], as in vitro studies showed that inhibition of complement activation led to a decrease in leukocyte adhesion [27-29]. Platelets have also been found to associate with leukocytes in the presence of cardiovascular devices via P-selectin glycoprotein ligand-1 (PSGL-1) on the leukocyte membrane which binds to P-selectin on the platelet surface [30], but the exact implications of this association remains unclear.

Although platelets, plasma proteins, complement system and leukocytes all play critical roles in blood-biomaterial interactions, it is important to analyze the role of individual components prior to looking at the system as a whole while analyzing the mechanisms of biomaterial-associated thrombosis. Since the adsorbed plasma proteins and the platelets are the critical players in the cellular response to the implant, our studies specifically deal with understanding these interactions at the molecular level.

2.2 Protein adsorption on surfaces

2.2.1 Fundamentals of protein adsorption

As mentioned in Section 2.1, the layer of adsorbed proteins plays a critical role in determining the nature of the blood-material interface, with the properties of the protein and the surface influencing the interfacial interactions [31]. Surface properties such as charge, free energy, roughness, hydrophilicity/hydrophobicity, and functionality are important parameters which affect interactions with proteins [32]. Depending on the properties of the surfaces, proteins adsorb in differing densities, orientations and conformations [33], and a protein (or even a particular region of the protein molecule) may have different affinities for different surfaces [31]. Protein molecules have a greater affinity for hydrophobic surfaces, as a result of which hydrophobic surfaces exhibit greater surface coverage of protein compared to their hydrophilic counterparts [34]. In addition to the size and charge of the protein molecules, their structural properties such as stability and unfolding rate also affect their interactions with surfaces. Overall, the adsorption process is complex, and involves van der Waals, electrostatic, and hydrophobic interactions.

The adsorption process on any surface is driven by a combination of the thermodynamics and the kinetics of the system, as a result of which protein molecules undergo conformational changes in order to minimize the free energy of the system. The degree of conformational change is more prominent on hydrophobic surfaces, leading to the exposure of hydrophobic residues in the core of the protein to the adsorbent surface

[33, 35]. On the other hand, hydrophilic surfaces exhibit minimal unfolding, indicating that the hydrophobic interaction between the protein molecules and the surface is the primary driving force for post-adsorptive conformational changes in the protein molecules [34]. These adsorption-induced conformational changes may also expose integrin binding sites, which mediate subsequent cell adhesion.

Changes in conformation of adsorbed proteins may be (i) time-dependent and (ii) dependent on the bulk protein solution concentration. In the former, as the residence time of the protein on the surface increases, it forms more contacts with the surface, and as a result of this, the probability of desorption decreases. Fg has been found to bind more tightly [36] and undergo conformational changes with increasing residence time on surfaces, with evidence suggesting that this may cause the protein to become less recognizable by platelets [37, 38].

On the other hand, the bulk protein solution concentration affects the transport rate of protein molecules to the surface. At lower bulk protein solution concentrations, the rate of arrival of the protein molecules at the surface is slow, as a result of which they have more surface area over which they can spread (and form contacts) before they come into contact with neighboring protein molecules [31, 39]. Hence, the conformational changes in the adsorbed protein would be more prominent, while the surface coverage would be lower, at lower bulk protein concentrations.

Although much of our understanding of the mechanisms mediating protein adsorption on surfaces is from single-component solutions, adsorption from multi-component solutions is highly relevant to understanding the interactions at the blood-material

interface, since blood contains numerous biomolecules, including more than 150 proteins. The affinity (e.g., size, charge and conformational stability) and kinetic factors (e.g., size and concentration) associated with the proteins play a role in determining which proteins adsorb on the material surface [31]. Considering a diffusion-limited situation at the interface, protein molecules with higher concentration and/or higher diffusion coefficients (i.e., smaller size) arrive first at the surface. Over time, molecules with higher overall affinity for the surface, but slower diffusion rates (due to their larger size and/or lower solution concentration) will approach the surface. However, the surface may already be covered with a monolayer of protein molecules, in which case the newly arriving molecules can attach only if the adsorbed molecules detach. Although simple desorption rarely occurs, the protein molecules can exchange with one another, until the surface is occupied with molecules having strong interactions with the surface. This process of adsorption and subsequent exchange is called the Vroman effect [40].

Since the adsorbed protein layer mediates the subsequent cellular response and the biocompatibility of the implant, in the past decade, the design of protein-resistant surfaces, using techniques such as polyethylene oxide (PEO) immobilization, has been a popular approach to achieve biocompatibility. Most protein-resistant surfaces are evaluated on the basis of the amount of protein adsorbed under biological conditions over a relatively short period of time using a variety of techniques including surface plasmon resonance (SPR) spectroscopy [41, 42], ellipsometry [43], radiolabeling [36] and enzyme-linked immunosorbent assay (ELISA) [44]. However, these studies may not be appropriate for devices for long-term, blood-contacting applications. Additionally, the

efficacy of these PEO-coated surfaces in reducing protein adsorption and subsequent platelet adhesion has remained questionable with regard to thrombogenicity [1]. Studies have shown that surfaces functionalized with polyethylene glycol (PEG) or PEO cause increased complement activation compared to non-functionalized control surfaces [45, 46], and it has been hypothesized that this is due to the hydroxyl groups at the end of the PEG chain [45]. Hydroxyl and amino groups on surfaces have been shown to cause increased complement activation and increased binding of complement product C3b [24]. Thus, although PEG and PEO may be effective in creating relatively protein-resistant surfaces, they may be unsuitable from the aspect of hemocompatibility due to their ability to activate the complement system.

Although the elimination of protein adsorption may be desirable from the hemocompatibility aspect, the fact remains that under normal physiological conditions we have a multitude of proteins in solution in our blood plasma and interstitial fluids, which (generally) do not trigger any adverse cellular response in their native/solution state, but mediate cell attachment in their adsorbed state. Hence, rather than the presence of proteins themselves on the biomaterial surfaces, it is more likely that adsorption-induced conformational changes lead to the exposure of bioactive domains in the protein that are normally 'hidden' in its native conformation, which then mediate binding of platelets.

Standard analytical tools which have been used so far for studying protein adsorption such as quartz crystal microbalance (QCM) [47-49], surface plasmon resonance (SPR) [47, 48, 50], ellipsometry [48] and atomic force microscopy (AFM) [47, 51-53] provide

generalized information on the adsorbed protein, indicating that it undergoes conformational changes, but do not provide any quantitative data on the secondary structural composition of the adsorbed protein layer. Information on the conformation of the surface-bound protein and its role in mediating cell-surface interactions has come into prominence only recently using techniques such as circular dichroism (CD) spectropolarimetry, and grazing-angle Fourier transform infrared spectroscopy (GA-FTIR) [33, 54, 55].

2.2.2 Plasma proteins involved in mediating platelet-biomaterial interactions

Fg (plasma concentration = 3.0 mg/mL) is a 340 kDa glycoprotein, composed of two copies each of three distinct polypeptide chains – α, β and γ. It is essential for platelet-biomaterial interactions, as it mediates platelet adhesion and aggregation. Removal of Fg from plasma reduces platelet adhesion drastically, while removal of other plasma proteins such as vWf, Fn or Vn reportedly causes little or no change in platelet adhesion [56, 57], illustrating its critical role in platelet adhesion compared to other plasma proteins.

There are three likely platelet binding sites in the Fg molecule. Two of these are the well known RGD sequences, RGDF at α95-98 and RGDS at α572-575, in the Aα chains; the other is the C-terminal dodecapeptide (HHLGGAKQAGDV) at γ400-411 [58]. Studies have suggested that the γC-terminal dodecapeptide sequence is essential for platelet binding to adsorbed Fg [59], while the role of the RGD sequences remains unclear. Although this sequence does not contain the classic RGD cell adhesion

sequence, structural studies of the γC dodecapeptide complex with the GPIIb/IIIa platelet receptor have indicated that the role of Lys-406 in γC is functionally similar to that of Arg in RGD, and that the KQAGD sequence in γC occupies the same site as RGD when it binds GPIIb/IIIa [60].

However, recent studies have pointed to the possibilities that there may be other amino acid sequences in Fg which play important roles in platelet binding. A recent study by Remijn et al. using recombinant Fg as well as blood from patients with dysfibrinogenemia (i.e., congenitally defective Fg which leads to defective clot formation) showed that in addition to the γC chain, the γ316-322 sequence (DNDNDKF) may play a role in platelet interactions with adsorbed Fg [61]. This sequence is part of the fibrin-specific region in Fg, and is buried inside the Fg molecule in its native state, but becomes exposed on fibrin polymerization, and also when Fg is adsorbed on material surfaces. Another set of studies using recombinant Fg identified a new binding site for platelet GPIIb/IIIa receptors in the γC domain of Fg, spanning residues γ365-383 (also called P3) [62], which functions as a binding site of GPIIb/IIIa during clot retraction. Further studies subsequently narrowed this down to two sequences γ370-375 (ATWKTR) and γ376-381 (WYSMKK), which were found to be capable of independently mediating $\alpha_{IIb}\beta_3$ (synonymous with GPIIb/IIIa) recognition [63]. These residues are not exposed in soluble Fg, but become exposed like the γ316-322 sequence, when Fg is adsorbed on surfaces or when Fg is converted to fibrin [64]. Thus, it is possible to delineate the role of specific domains or amino acid sequences in mediating platelet attachment to Fg using recombinant fibrinogen.

Although the specific mechanisms underlying platelet adhesion to Fg remain to be fully defined, the amount of adsorbed Fg has been widely cited in biomaterials literature [65-67] to be the primary determinant of the hemocompatibility of biomaterials. However, other studies have shown that the conformation of the adsorbed Fg layer may actually be more important than the amount of adsorbed Fg [54, 55]. This is further supported by the fact that non-activated platelets are unable to strongly adhere to Fg in its native, soluble conformation in the bloodstream, but readily adhere and activate when they contact Fg in its adsorbed state on a surface, clearly indicating that adsorption-induced conformational changes in Fg may expose platelet-binding sites, which otherwise remain hidden in the native state.

Although Fg is the pre-eminent protein involved in platelet-protein interactions and subsequent thrombotic response, the initial interactions between the platelets and the vessel wall and subsequent platelet deposition at sites of vascular injury is mediated by von Willebrand factor (vWf). vWf is present in the Weibel-Palade bodies of endothelial cells, in the α-granules of platelets, and in plasma at a concentration of approximately 10 μg/mL [68]. It is a multimeric protein which binds to the two major platelet receptors GPIIb/IIIa and GPIb-IX-V, as well as to collagen [69]. The interaction between the GPIb platelet receptor and the A1 domain of vWf is pivotal in mediating the initial adhesion of platelets on the subendothelium under conditions of high shear stress [69], while the RGD sequence in the C1 domain of vWf serves as a binding motif for both GPIIb/IIIa and $\alpha_V\beta_3$ platelet integrins, which mediates subsequent platelet adhesion and aggregation.

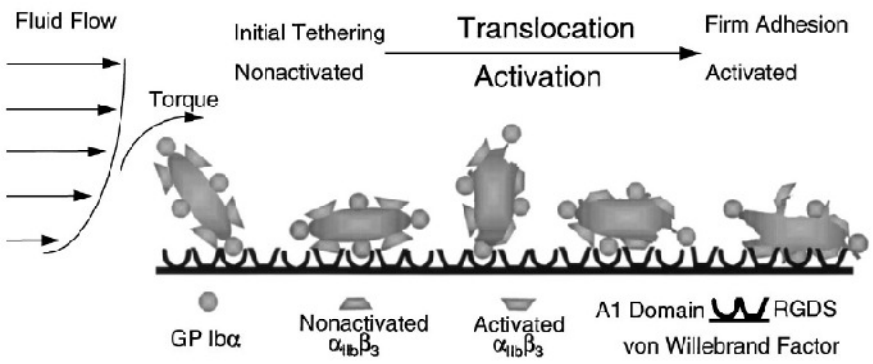

Figure 2.3. Schematic illustration of the dual-step mechanism of platelet adhesion to immobilized vWf [70].

Under normal conditions, the GPIb-IX-V platelet receptor complex does not interact strongly with soluble vWf, but when collagen is exposed at sites of vascular injury, vWf becomes immobilized and undergoes conformational changes in its A1 domain, which enables platelet binding [69]. As seen in Fig. 2.3, the initial capture of the platelets from flowing blood is due to the interactions between the platelet GPIbα receptor and the A1 domain of vWf. This bond however has a rapid dissociation rate [71] and therefore cannot mediate stable platelet adhesion. As a result of this, the platelets detach and translocate along the surface in a forward rolling movement due to the torque applied by the flowing blood [70]. During this translocation, the GPIb-IX-V receptor complex forms bonds with the underlying vWf and collagen, thereby decreasing the velocity of the platelets. Although the exact nature of the regulation of the interactions between GPIbα and vWf remains unclear, the changes in conformation of the ligand and receptor play important roles in these interactions [72]. The GPIb-IX-V receptor complex also

functions as a signal transducer, which activates platelet GPIIb/IIIa receptors, leading to the arrest and firm adhesion of the platelets on the surface due to the binding of these activated GPIIb/IIIa receptors to the RGD sequence in the C1 domain of vWf [73].

vWf-deficiency in plasma (also known as Bernard-Soulier syndrome) causes severe problems in hemostasis and coagulation in humans [74], and also has been shown to cause spontaneous bleeding and prolonged bleeding times in mice [75]. However, unlike GPIb, vWf is unlikely to be essential for in vivo thrombus formation, as platelet adhesion is only delayed, indicating that the GPIb-IX-V receptor complex interacts with some other ligand(s) such as Fg, to initiate platelet adhesion, although a study has suggested that thrombospondin-1 may also interact with GPIb-IX-V in the absence of vWf [76].

In addition to Fg, our research is also focused on the possible role of Alb in mediating platelet adhesion. Alb is the most abundant plasma protein (35-50 mg/mL in plasma) [77], and combined with its moderately low molecular weight (68.3 kDa) [78], is one of the first proteins adsorbing on the biomaterial surfaces [79]. Since it lacks any known amino acid sequences for binding platelet receptors, it has been considered to be unable to support platelet adhesion, and hence is widely used for blocking non-specific platelet-surface interactions in platelet studies [80], as well as for a blood-compatible coating on biomaterial surfaces [81, 82]. However, some studies have suggested that platelets can adhere to adsorbed Alb [54, 83, 84], and that the mechanisms underlying this adhesion can be attributed to the adsorption-induced conformational changes in Alb [54]. In fact, for the same degree of loss of α-helix in the protein, platelet adhesion levels have been found in one study to be comparable for both Alb and Fg [54].

In addition, other cell types, such as hepatocytes [85], as well as monocytes, macrophages and dendritic cells [86-88], have been shown to be able to bind to adsorbed Alb. For example, a recent study has shown that macrophages are able to bind to Alb adsorbed on perfluorocarbon surfaces, with the adhesion process shown to be primarily mediated by the Mac-1 ($\alpha_M\beta_2$) macrophage integrin [89]. These cell-types may be broadly categorized as 'defensive' cells, as they play a critical role in the inflammation and coagulation cascades [1], and their ability to adhere to Alb may possibly be attributed to an inherent ability to recognize and adhere to misfolded proteins, which are often a sign of degenerative diseases [90]. Hence, the role of Alb in mediating the blood-compatibility of implants cannot be ignored.

2.2.3 Protein adsorption studies on SAM surfaces

Surface properties are critical in controlling the interactions of plasma proteins and cells on biomaterial surfaces. Self-assembled monolayers (SAMs) of alkanethiols on gold are widely used as model surfaces for analyzing the effect of surface chemistry on protein adsorption, since they are easy to prepare, form highly ordered systems, and permit a broad range of surface functionalities to be produced [84, 91-93], thereby permitting us to clearly delineate the role of specific surface chemistries on protein adsorption [51, 94-96]. Their structural integrity coupled with the uniform surface chemistries obtained enables them to behave successfully like biomimetic surfaces, such as membranes [97]. The alkanethiols we use have the structural formula ($HS\text{-}(CH_2)_{11}\text{-}R$), with the thiol group

at one end which binds to gold, while the long alkyl chain orders the alkanethiol on the surface.

Defects in the SAMs (such as vacancies and grain boundaries) may occur and are dependent on the surface smoothness and cleanliness, concentration and purity of the alkanethiols, temperature and time of deposition, and solvent selection [98]. These defects may expose the underlying alkyl chain of the alkanethiols to the proteins that are adsorbing on the surface. Protein-surface interactions are dominated by hydrophobic interactions; hence Triton-X-100 (Fig. 2.4) has been used as a blocking agent to cover hydrophobic defects from proteins on SAMs with neutral non-methyl terminating groups [99]. The Triton-X-100 molecule contains ethylene glycol repeat units, which are known to resist protein adsorption and effectively fills defect sites in the SAM structure.

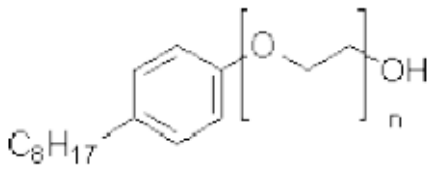

Figure 2.4. Chemical structure of Triton-X-100, which is used as a blocking agent on alkanethiol SAMs. (n= 9-10)

Studies have shown that Fg adsorption is higher on CH_3-terminated SAMs than on the COOH- and OH-functionalized surfaces [34, 100, 101], with a linear decrease in the amount of Fg adsorbed as the percentage of hydroxyl groups on the surface increased (i.e., increasing hydrophilicity) [84]. Additionally, the differential affinity of different

proteins on a given surface is illustrated in studies which showed that Fg exhibited higher levels of surface coverage on both hydrophobic and hydrophilic surfaces compared to Alb [51]. Alb has also been found to adsorb more firmly on hydrophobic surfaces, like CH_3-terminated SAMs, whereas adsorption on hydrophilic surfaces, such as OH-terminated SAMs, was low [50, 102]. In general, hydrophobic surfaces show higher amounts of adsorbed plasma proteins [84] due to their tendency to bind protein more strongly, thus packing proteins more tightly on the surface at surface saturation. These interactions between the protein and surface are also the driving force mediating the changes in conformation of the adsorbed protein and its irreversible adsorption on the surface [34, 35] that was confirmed in recent studies [33, 34, 101], which showed that adsorption-induced conformational changes in proteins are higher on CH_3-terminated surfaces than on OH-terminated ones.

Competitive protein adsorption studies with Fg and Alb indicated that the addition of Fg led to only modest desorption of Alb on hydrophilic and hydrophobic SAMs, suggesting the occurrence of minimal Vroman effects on these SAMs for the adsorption conditions used [34]. Thus, this clearly confirms that Alb adsorbs strongly even on hydrophilic SAMs, as a result of which the more surface-active protein (i.e., Fg) is unable to fully displace a less surface-active protein (i.e., Alb) from the surface. This behavior may have serious implications from the aspect of blood-biomaterial interactions, raising questions about the ability of Fg and other plasma proteins with high surface affinities to displace preadsorbed Alb molecules from a biomaterial surface.

2.3 Role of platelets in blood-biomaterial interactions

2.3.1 Platelets and platelet receptors involved in adhesion

Platelets are normally anucleate, discoid cells with a diameter of 3-4 μm, and play a critical role in hemostasis by maintaining the integrity of the vascular endothelium [1]. They accomplish this by (i) forming platelet plugs which stop the bleeding at injury sites, and (ii) catalyzing the reactions in the coagulation cascade leading to the formation of fibrin which stabilizes these platelet plugs [3], thereby preventing blood loss. As mentioned earlier, resting platelets do not bind to plasma proteins like Fg, vWf, Fn, and Vn in the bloodstream. However, the GPIIb/IIIa platelet receptor (80,000 copies per platelet) undergoes conformational changes upon platelet activation, leading to intra-platelet signaling, thereby enabling platelet binding to these proteins [3]. Resting platelets also have the ability to bind to adsorbed plasma proteins, which is believed to be due to the conformational changes in the proteins during the adsorption process.

Normal (non-activated) platelets are discoid in shape, but undergo a rapid change in morphology upon activation, spreading and forming filopodia, ultimately leading to the formation of platelet aggregates [103]. Minimal stimulation is required to elicit a platelet response, as a result of which they become activated when they contact any thrombogenic surface (such as an injured endothelium, subendothelium and synthetic surfaces), and are the first cells to adhere to the layer of adsorbed protein on a biomaterial surface [104]. The activation process is often associated with the coupling of a ligand to specific platelet receptors, leading to intra- and extra-cellular signaling (i.e., ‘inside-out’ and ‘outside-in’

signaling, respectively) [105]. These ligands include plasma proteins such as Fg, vWf and thrombin, parts of the vascular endothelium such as collagen, as well as platelet agonist molecules such as adenosine diphosphate (ADP) and thromboxane A2 secreted by inflammatory cells and activated platelets. Negatively-charged phospholipids (such as P-selectin) are translocated from the platelet α-granules to the platelet membrane [106] upon platelet activation, as a result of which coagulation factors Va and Xa can bind to the platelet membrane and form the prothrombinase complex. The thrombin generated by the prothrombinase complex stimulates thrombosis, which, in the case of an implant, ultimately may lead to its failure or adverse events such as the generation of thromboemboli. Thus, platelet activation is clearly linked to the thrombotic complications associated with cardiovascular devices.

Platelet receptors play a key role in mediating the thrombotic response, and hence are the main target of anti-thrombotic therapies. The GPIIb/IIIa receptor (also known as the $\alpha_{IIb}\beta_3$ integrin) is thought to be the main receptor mediating platelet-plasma protein interactions. It can bind to several ligands containing the RGD amino acid sequence, such as Fg, fibrin, vWf, Fn, Vn and thrombospondin [73]. In resting platelets, this integrin is in a highly bent, low-affinity or 'off' state, in which the RGD-binding region is believed to be hidden [73]. However, when the platelets are activated, the integrin undergoes a conformational switch into its high-affinity or 'on' state, leading to the exposure of the RGD-binding site, as a result of inside-out signaling. Previous studies have also shown that the RGDS peptide inhibits platelet attachment to Fg and other plasma proteins [107,

108] suggests that further research into the regulation of the RGD-binding domain on platelets is essential in understanding the mechanisms of platelet-protein interactions.

Savage *et al.* showed that the GPIIb/IIIa receptor was essential for platelet binding to adsorbed Fg using a monoclonal antibody LJ-CP3 to block the GPIIb/IIIa receptor [59]. At low shear rates (100 s^{-1} or lower, which are usually seen in the venous circulation) [109], non-activated GPIIb/IIIa selectively binds surface-immobilized Fg [59], in addition to contributing to platelet aggregation by cross-linking with the GPIIb/IIIa receptors on adjacent platelets. However, at high shear rates, the initial stages of platelet-surface interactions are mediated by the interactions between the platelet GPIb-IX-V receptor complex (about 25,000 copies per platelet) and surface immobilized vWf, independent of the activation state of the platelets. These newly adherent platelets are then activated by agonists, such as ADP, thrombin or epinephrine, released by other platelets that are already adherent and activated, as well as by shear stress [110], resulting in GPIIb/IIIa activation and irreversible platelet aggregation, finally leading to thrombus formation.

Other receptors involved in platelet adhesion include those for collagen (GPVI, $\alpha_2\beta_1$), fibronectin ($\alpha_5\beta_1$), and vitronectin ($\alpha_V\beta_3$). P2Y receptors for ADP, and PAR receptors for thrombin also play a subsidiary role in mediating platelet activation [111]. These 'secondary' platelet receptors may act in synergy with the primary platelet receptors (GPIIb/IIIa and GPIb-IX-V) in mediating adhesion to adsorbed proteins.

2.3.2 Platelet interactions with adsorbed proteins on surfaces

The platelet adhesion on a surface is typically quantified using a colorimetric LDH assay [54], in addition to microscopy techniques like scanning electron microscopy (SEM) [84, 97] or glutaraldehyde induced fluorescence technique (GIFT) [84, 112]. The activation state and the morphology of the adherent platelets is assessed by techniques such as confocal microscopy, total internal reflection fluorescence microscopy (TIR-FM) and immunofluorescence microscopy [113, 114], in addition to other conventional microscopic techniques such as GIFT and SEM.

Currently, it is unclear whether the adhesion and activation of platelets on a layer of adsorbed proteins is mediated by the conformation or the amount of adsorbed proteins. The conventional thought in the biomaterials field has been that the surface coverage of the adsorbed protein mediates platelet binding, with the investigation of the role of the conformation of the adsorbed layer coming into prominence very recently [54, 55]. Platelets exhibit a greater extent of spreading on a given surface coated with low-density Fg (0.003 mg/mL bulk solution concentration) compared to high-density Fg (0.1 mg/mL bulk solution concentration) [113]. GPIIb/IIIa activation was examined using the PAC-1 monoclonal antibody (mAb) which selectively recognizes activated GPIIb/IIIa [115], and it stained the spread platelets on low-density Fg four times more intensely than on high-density Fg [113]. The results from this study clearly suggest that the surface coverage of Fg affects both platelet adhesion and GPIIb/IIIa-mediated outside-in signaling, resulting

in differences in Ca^{2+} signaling, signal transduction mechanisms, platelet morphology, and inside-out signaling.

However, various groups have hypothesized that the platelet adhesion correlated with the amount of Fg that can be recognized by conformation-specific antibodies against Fg, rather than the total surface coverage of Fg [80, 116-118]. Thus, in addition to the surface coverage of adsorbed Fg, the conformational of this Fg layer also plays a critical role in mediating platelet adhesion and subsequent activation [119-121].

In a study by Tanaka et al. [55], although poly(2-methoxyethylacrylate) (PMEA) and poly(hydroxyethlylmethacrylate) (PHEMA) surfaces adsorbed the same amount of Fg, the PHEMA surface showed significantly greater levels of platelet adhesion compared to PMEA, which was attributed to the increased level of denaturation of Fg on the PHEMA surface. Thus, this suggests rather than the surface coverage of Fg, its adsorbed conformation mediates platelet binding.

Recent investigations [84, 97] have indicated that CH_3 SAMs with adsorbed proteins showed stronger platelet adhesion compared to OH-terminated SAM surfaces, with scanning electron microscopy (SEM) results revealing that the platelets adherent on the CH_3 SAM exhibited high levels of platelet activation, with the degree of activation and adhesion decreasing with increasing hydrophilicity (i.e., increase in percentage of OH groups on the surface) [84]. Accounting for the fact that proteins adsorbed on more hydrophobic surfaces exhibit a higher degree of adsorption-induced unfolding compared to hydrophilic surfaces [33], this seems to suggest that the adsorption-induced conformational changes in Fg lead to the exposure of platelet-binding sites which would

have normally remained ‘hidden’ in the native/solution state of the protein and thus cause increased platelet adhesion and activation. The lower extent of adsorption-induced unfolding on hydrophilic surfaces would maintain the structure of protein closer to that in its native state and thereby have lesser tendency to expose platelet-binding domains, explaining the low platelet adhesion.

The same explanation may hold true while explaining platelet adhesion observed on Alb-coated surfaces [54, 84]. In cases where platelet adhesion has been observed on Alb-coated surfaces in the past, it has been attributed to non-specific processes [80], such as the platelet interactions with exposed surface area of the substrate as opposed to actual binding to the adsorbed Alb. However, as mentioned in Section 2.2.3, the fact that Alb adsorbs firmly on hydrophilic surfaces, as a result of which Fg has been shown to be unable to displace it [34], suggests that the Alb adsorbed on biomaterial surfaces may not be easily displaced by more surface-active proteins from blood.

Two recent studies reported that platelet adhesion to Alb may actually be via specific mechanisms, which are linked to the conformational state of the adsorbed Alb [54, 84]. However, these studies did not rule out the possibility that the observed response maybe have been due to platelet interactions with some other residual protein in the system, leaving the question of the exact nature of platelet-Alb interactions still open to debate. Hence, it is imperative for us to definitively examine whether non-activated platelets can adhere to Alb; and if so, whether this is via a receptor-mediated process that can be directly correlated with the degree of adsorption-induced conformational changes in Alb on the surfaces.

Although the platelet adhesion is higher on more hydrophobic surfaces, it is also important to note that surfaces which cause a higher degree of adsorption-induced unfolding in proteins also adsorb larger amounts of proteins. Differentiating between these two potential mediators of platelet binding is essential, as they lead to two very different approaches to the design of hemocompatible biomaterials. If the platelet adhesion is mediated by the amount of adsorbed proteins, biomaterial surfaces must be designed so as to minimize the surface coverage of adsorbed protein, irrespective of its conformation. On the other hand, if the degree of adsorption-induced unfolding of the proteins mediates the platelet attachment, then the surfaces should be designed in a manner which retains the proteins as close to their native conformation as possible, irrespective of the surface coverage of adsorbed protein.

2.4 Assessment of adsorption-induced conformational changes in proteins

One of the primary questions this project aims to address is whether the surface coverage or the conformation of the adsorbed protein mediates subsequent platelet adhesion. By using a broad range of surface chemistries and a wide range of protein solution concentrations, it is possible to obtain a large set of systems with differing amounts and conformations of adsorbed protein. In order to accurately ascertain the conformation of the native protein in solution and adsorbed protein on the SAM surfaces, it is essential to use a highly sensitive experimental technique.

While post-adsorptive conformational changes in protein layers on surfaces have been evaluated using nuclear magnetic resonance (NMR) [122] and Fourier transform infra red-attenuated total internal reflection (FTIR) spectroscopy [123, 124], both methods have inherent disadvantages that limit their usefulness for this application. Although NMR provides an extremely powerful technique that can potentially reveal the complete three-dimensional structure of a protein on a surface, it requires samples with very high surface area density [125], while FTIR requires high protein surface concentrations, which may lead to protein aggregation and associated conformational changes [125]. As an alternative to these methods, circular dichroism (CD) spectroscopy is relatively simple and easy to use, and can be used to analyze samples with relatively low surface area and at relatively low degrees of surface coverage. Because of these advantages, CD has been increasingly used in recent studies as a means of examining protein-surface interactions at the molecular level [54, 55, 126-128].

2.4.1 Fundamentals of Circular Dichroism (CD) Spectropolarimetry

When asymmetric molecules interact with light, they absorb left- and right-handed circularly polarized light to different extents, and this difference in absorbance is defined as CD. On account of this, the plane of the wave of light is rotated such that the addition of the vectors representing the electric fields of left-handed (E_L) and right-handed (E_R) circularly polarized light, resulting in a vector which traces an ellipse and the light is said to elliptically polarized.

The absorbance of a solute at a given wavelength λ, $A_i(\lambda)$, is given by Beer's Law, and can be written as [129]:

$$A_i(\lambda) = \varepsilon_i(\lambda) \times C \times L \qquad (2.1)$$

where $\varepsilon_i(\lambda)$ is the extinction coefficient (in g/cm^2) of the chiral solute for a particular handedness of polarized light, C is the concentration of the solute (in g/mL), and L is the distance that the light travels through the medium containing the solute (in cm). (Note: A is unitless).

Therefore the difference in absorbance of left- and right-handed circularly polarized light (i.e., CD) can be defined as:

$$CD \equiv \Delta A = A_L - A_R = (\varepsilon_L \times C \times L) - (\varepsilon_R \times C \times L)$$

$$= \Delta\varepsilon \times C \times L \qquad (2.2)$$

Modern spectropolarimeters use a modulation technique that allows for the direct measurement of ΔA, which is generally very small [130]. Since the change in absorbance can be accurately measured, Δε can be easily calculated and used to report CD data. However, CD is often reported in terms of ellipticity [131].

The vector representing the electric field of a circularly polarized light beam rotates in the direction of propagation, completing one revolution per wavelength. When the electric field vectors of right- and left-handed circularly polarized light are in the same direction, the sum of their magnitudes is the major axis of the elliptically polarized light and the minor axis of the ellipse is given by their difference when the vectors are in the opposite direction. The ellipticity (θ, generally expressed in millidegrees) is the angle of which the tangent is the ratio of the minor axis of the ellipse to its major axis [132, 133].

Since this angle of ellipticity is very small, the tangent of θ is approximately equal to θ in radians, thus the measured ellipticity can be related to the difference in absorbance by the following expression [134].

$$\theta\ [\text{rad}] \approx \tan\theta = (\,|\,\mathbf{E}_L\,| - |\,\mathbf{E}_R\,|\,) / (\,|\,\mathbf{E}_L\,| + |\,\mathbf{E}_R\,|\,)$$

$$= [\exp(-A_L/2) - \exp(-A_R/2)]/[\exp(-A_L/2) + \exp(-A_R/2)] \qquad (2.3)$$

This expression can be simplified by converting θ to degrees and expanding the exponentials, while neglecting the higher terms of order of ΔA in comparison with unity, to yield the following expression [134]:

$$\theta\ [\text{deg}] = 180 \times \ln 10 \times \Delta A/4\pi = 32.98\ \Delta A \qquad (2.4)$$

Equation 2.4 shows that the ellipticity is directly proportional to the differential absorption of right- and left-handed circularly polarized light by the optically active medium. For protein analysis, the measured ellipticity is often converted into its corresponding molar ellipticity ([θ]) value by the following expression [135]:

$$[\theta] = (\theta \times M_0) / (10{,}000 \times C \times L) \qquad (2.5)$$

where [θ] is the molar ellipticity (deg·cm^2/dmol) and M_0 is the mean amino acid residue molecular weight (118 g/mol).

2.4.2 Analysis of protein structure

Proteins are considered to have four levels of structure – primary, secondary, tertiary and quarternary [136]. The primary structure of proteins consists of its defined sequence

of amino acids. The secondary structure of proteins refers to the segments of amino acid sequences that fold into regular conformations with well-defined, repeated torsion angles that are stabilized by hydrogen bonding. The tertiary structure of the protein is determined by the folding and binding together of the secondary components of the protein, which is mediated by nonbonded interactions between side-chain of the amino acid residues and possibly disulfide bond formation, giving the protein its overall three-dimensional shape. The quarternary structure of proteins contains multiple polypeptide chains, each with its own N and C termini, such as dimers and trimers, which are arranged in a regular manner [136].

Helices are the most common type of secondary structural unit occurring in proteins. The α-helix, which was first modeled in 1951 by Pauling, Corey, and Branson [137], is the most abundant type of helix found in proteins and its coiled structure consists of 3.6 residues per turn. Two alternative helices that have been found in proteins are 3_{10} helices, which have tighter coils consisting of 3.0 residues per turn, and the larger π helices that consist of coils containing 4.1 residues per turn [138]. The second most common type of secondary structure are β-sheets that are formed by β-strands, which consist of either parallel or anti-parallel stretches of amino acids whose peptide backbone chains are nearly in full extension, with hydrogen bonding between adjacent β-strands [139]. Turns are the third type of secondary structure that is often found in proteins, resulting due to the formation of hydrogen bonds between amino acid residues that are close to one another in the primary sequence along a polypeptide chain. For a turn to form, the C_α atoms of the amino acids involved must be within 7 Å of each other, with neither of the

amino acids being contained within another secondary structural unit. β-turns are the most frequent type of turn and are characterized by C_α atoms separated by three residues, while γ-, α-, and π-turns are characterized by C_α atoms separated by two, four, and five residues, respectively [140, 141]. The final type of secondary structure is the random loop, which consist of unstructured segments of the polypeptide chain that link the other types of secondary structural elements with one another.

As a result of 'exciton' interactions, when the chromophores of the amides in the polypeptide chain of proteins are aligned in arrays, their optical transitions are either shifted or split into multiple transitions [142]. Thus, the different secondary structural components in proteins have their own characteristic spectra, and the overall CD spectrum contains contributions from all the structural components within the protein. This causes the curves for each individual component of the secondary structure (such as α-helix and β-sheet) to overlap to give a single spectrum that can be deciphered to provide an estimate of the overall secondary structural composition of the protein.

For example, the CD spectra for α-helical proteins exhibit negative maxima at 222 nm and 208 nm, along with a positive maximum at 193 nm [143]. Proteins with well-defined β-sheets have negative bands in their spectra at 218 nm and positive bands at 195 nm [144], while those with disordered/random structure have very low ellipticity at wavelengths greater than 210 nm, and negative bands near 195 nm [145]. This is clearly illustrated in Fig 2.5 (below), for different conformations of poly-L-lysine.

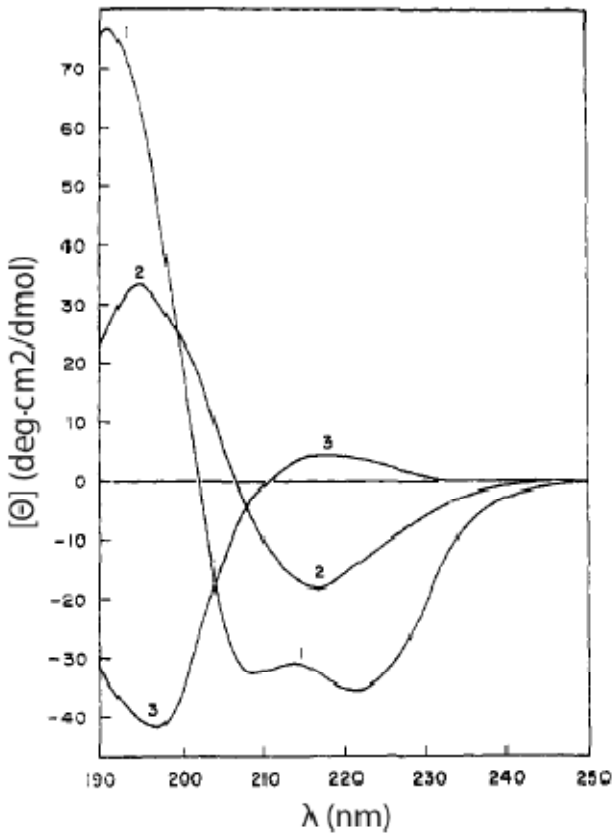

Figure 2.5. CD Spectra of poly-L-lysine in various conformations: (1) 100% α-helix, (2) 100% β-sheet, and (3) 100% random chain [144].

While performing CD experiments, it is imperative to take certain key points into consideration [132]. The protein used must be at least 95% pure, and the buffer used for preparing the protein solutions must be free of any other optically active materials that may interfere with the CD signal and complicate the analysis by masking the change in the CD signal due to the protein itself. Hence, nanopure water would be the best solvent suited for this method. But this does not represent physiological conditions, with the lack of salts in the buffer possibly influencing the structure of the protein. Additionally, so as

to obtain accurate data, the total absorbance of the sample (inclusive of the cuvette, sample and buffer) in the wavelength range of 190-200 nm must not exceed a critical value beyond which the high tension (HT) voltage limits for the instrument are exceeded [132]. The CD spectrum obtained within these experimental constraints is then deconvoluted using spectral analysis algorithms such as SELCON3 or CONTINLL [146, 147] to estimate the content of α-helix, 3_{10} helix, β-sheet, β-turn, polyproline type-II helix and unordered residues [142, 148]. This method provides a quantification of the secondary structural content of the proteins that has been shown to closely reflect the actual secondary structural composition of proteins.

Thus, CD spectropolarimetry is an accurate and sensitive experimental technique to quantify the degree of adsorption-induced conformational changes occurring for a given protein [54], and can potentially also be used to quantify the surface coverage of the adsorbed proteins.

2.5 Blockade of platelet receptors

The role of specific platelet receptors in mediating adhesion to adsorbed proteins such as Fg and Alb can be delineated via their blockade using monoclonal antibodies or fragment antigen binding (Fab) antibodies. The GPIIb/IIIa platelet integrin is the major platelet receptor supporting platelet aggregation and thrombus formation [149], and since platelets from patients with Glanzmann's thrombasthenia, which lack functional

GPIIb/IIIa, exhibit diminished binding function [150], the blockade of GPIIb/IIIa has been the main focus of anti-thrombotic therapies [151, 152].

Since GPIIb/IIIa platelet receptors are RGD-specific, RGD-containing peptides were among the first candidates to be examined for inhibition of platelet receptor function [108, 153, 154]. The RGDS peptide was found to inhibit agonist-induced platelet aggregation, as well as Fg-binding to ADP-stimulated platelets [107]. However, it was found to be a partial competitive inhibitor of platelet aggregation and Fg-binding, suggesting that the platelet receptors for Fg (i.e., GPIIb/IIIa) were likely to still be able to interact with Fg in their RGDS-bound low-affinity state. Additionally, studies by Du et al. [155] indicated that RGDS peptides function as partial agonists of platelet integrins, in addition to being competitive antagonists. RGDS induces conformational changes in both the α_{IIb} and β_3 subunits of the GPIIb/IIIa platelet receptors [156, 157], and it is this conformational shift in the β_3 subunit which mediates GPIIb/IIIa-mediated outside-in signaling, leading to the activation of the $\alpha_2\beta_1$ platelet integrin for collagen [158]. These results are in agreement with other studies which have reported that the cytoplasmic domain of the β_3 subunit plays an important role in GPIIb/IIIa-mediated outside-in signaling [159-161]. Hence, in analyzing the role of the GPIIb/IIIa platelet receptor in platelet adhesion to adsorbed proteins, it is imperative to use an antagonist which inhibits the receptor without causing any associated induced platelet signaling.

The peptide-mimetic GPIIb/IIIa antagonist Aggrastat (or tirofiban, MW = 495.08 g/mol) has been shown to bind to GPIIb/IIIa on non-activated platelets [157], inhibiting their ability to bind Fg, and also preventing overall platelet activation (as measured by P-

selectin exposure), $\alpha_2\beta_1$ activation and subsequent collagen binding [158]. This is due to the fact that it induces a conformational change only in the α_{IIb} but not the β_3 subunit, which is consistent with other studies [156, 157]. However, the anti-GPIIb/IIIa monoclonal antibody fragment ReoPro (or abciximab, MW = 145,651 g/mol) has been found to be more therapeutically potent clinically [162], as it has been shown to inhibit the $\alpha_V\beta_3$ platelet receptor as well as the macrophage Mac-1 integrin, in addition to the platelet GPIIb/IIIa receptor [163].

The GPIb-IX-V platelet receptor complex is the second most abundant platelet receptor set with 25,000 copies per platelet, and the interaction between vWf and the GPIbα platelet receptor is important for platelet adhesion, especially at high shear stress. The inhibition of the GPIb receptor as a highly potent target for anti-thrombotic drug development has come into prominence only in the last decade [164]. One of the first studies examining the anti-thrombotic effect of blockade of the GPIb-IX-V receptor used a novel murine anti-GPIb mAb 6B4 [165]. The results from this study indicated that the mAb and its $F(ab')_2$ and Fab fragments were highly effective in inhibiting GPIb binding to vWf under static and flow conditions. Recent studies carried out using murine anti-GPIbα mAbs 24G10 and 6B4 [166] as well as platelets from patients with Bernard-Soulier syndrome which display GPIb-deficiency [111] showed complete inhibition of platelet adhesion to immobilized vWf. Phage display studies have narrowed the epitope for 6B4 to the amino acid sequences 230-242 and 259-262 in GPIb, while the epitope for 24G10 has been mapped to the amino acid sequence 1-81 in GPIb [166]. Blockade of GPIb using these agents led to a moderate decrease of 29% and 26% in the activation of

GPIIb/IIIa and platelet integrin $\alpha_2\beta_1$ receptors, respectively [111], suggesting that it functions primarily as an adhesive receptor and does not have any major role in platelet activation. Inhibition of GPIbα has also been shown to lead to reduced thrombus formation when atherosclerotic plaques were exposed to flowing blood [167]. Studies involving the blocking of GPIIb/IIIa, GPIbα, or both by monoclonal antibodies has been shown to inhibit arterial thrombosis in baboons without increasing the bleeding time [168, 169], illustrating the critical roles played by both receptors in thrombosis. Hence, the analysis of the interactions of both of these receptor sets with adsorbed Fg and Alb form an important part of this doctoral work.

2.6 Chemical modification of amino acid residues in proteins

Site-specific chemical modification of amino acid residues in proteins is potentially a quick and highly effective technique for examining the role of specific amino acid residues in proteins [170, 171]. It stoichiometrically alters a protein with the covalent transformation of a single set of amino acid residues, usually without any change in conformation of the protein or altering any other amino acid residues [171]. Hence, this technique has the potential to be a powerful tool in determining the role of specific amino acid residues in platelet adhesion.

The site-specific modification reaction depends on the protonation state of the amino acid residue of interest [171]. The local microenvironment surrounding this residue affects the physical and chemical properties of its functional group, especially for

nucleophiles such as amine groups, hydroxyl groups, phenolic hydroxyl groups, and sulfhydryl groups. The effective pK of these nucleophilic groups is affected by various factors in addition to solvent accessibility including electrostatic interactions with neighboring residues, hydrogen bonding with adjacent residues, and steric interference [172]. Thus, although the residue of interest may be solvent-accessible, it may not undergo chemical modification due to the non-uniform microenvironments surrounding all residues within the same protein or the same residue from protein to protein. Reaction conditions may be altered to shift the protonation state of these functional groups so that the desired modification reaction may occur, but may lead to undesirable conformational changes and modify multiple amino acid types in the protein. However, residues carrying the same charge (e.g., arginine and lysine) can be preferentially modified by suitable selection of reaction conditions (pH, ionic strength, solvent and temperature), illustrating the use of the effect of local chemistry on the pK of individual residues [171, 172]. Although many restrictions may apply regarding the ability to selectively modify specific amino acid types in a protein, several analytical procedures have been developed and applied over the past few decades to successfully accomplish this for designed types of amino acids.

The Arg-Gly-Asp (RGD) sequence is one of the main cell-binding motifs present in proteins, playing a critical role in the binding of platelet receptors [173]. 2, 3-butanedione has been used for neutralizing Arg residues under mild reaction conditions (pH 8.0) [174], and this Arg modification has been shown to inhibit fibroblast adhesion to plasma lipoproteins [175]. The reaction scheme is illustrated in Fig. 2.6.

Acetylation of proteins using acetic anhydride is one of the oldest and most widely used experimental approaches for the chemical modification of proteins [171]. This modification strategy has been shown to lead to extensive modification of amino groups [176], and is influenced by the relative accessibility of these residues, which depends on the microenvironment around them.

Overall, based on the information discussed in this chapter, studies were carried out to analyze the mechanisms of protein adsorption on varying surface chemistries, and delineate the mechanisms of platelet adhesion to adsorbed Fg and Alb.

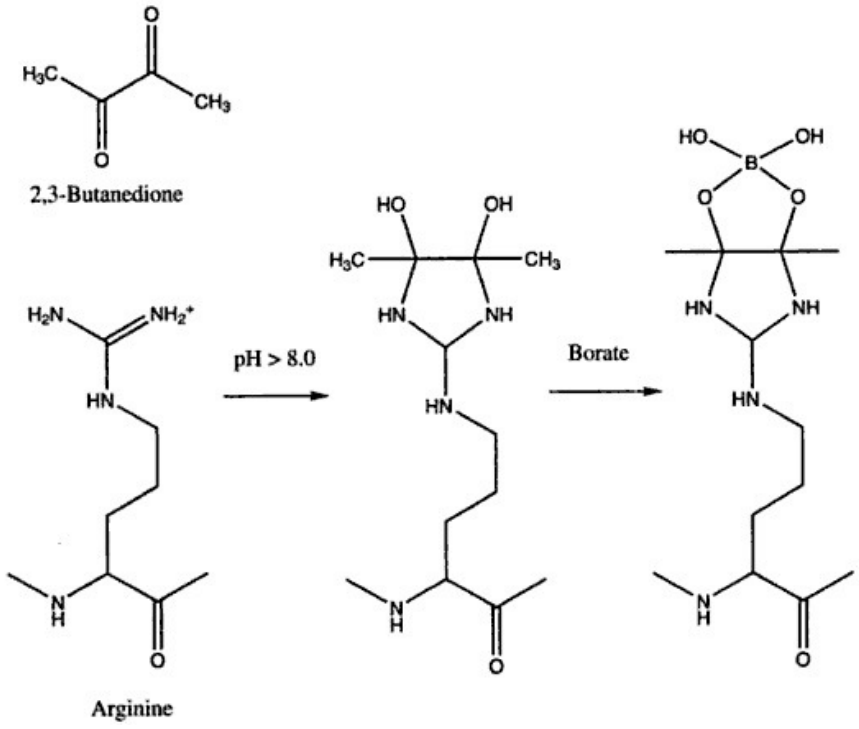

Figure 2.6. Reaction scheme for site-specfic modification of arginine residues using 2,3-butanedione [171].

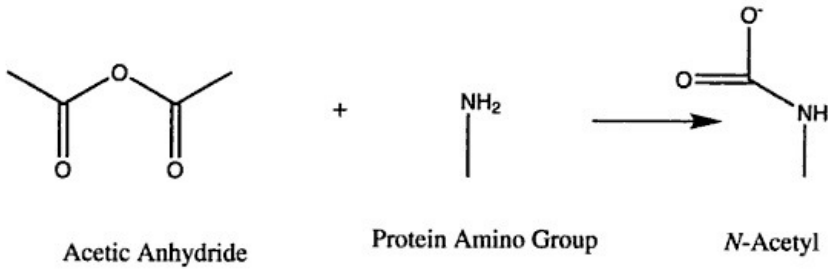

Figure 2.7. Schematic representation for the reaction of acetic anhydride with amino groups of proteins [171].

CHAPTER 3

SPECIFIC AIMS AND SIGNIFICANCE

3.1 Hypothesis

The molecular mechanisms mediating platelet adhesion to adsorbed proteins on biomaterial surfaces have not been completely understood by the biomaterials field despite over three decades of research into blood-biomaterial interactions [2]. The role of Fg in platelet-biomaterial interactions is well known, although it has remained unclear whether these are mediated by the surface coverage or the conformation of the adsorbed Fg. Additionally, although Alb is the most abundant plasma protein [77] and is the first protein to adsorb on biomaterial surfaces [79], the possible role for Alb in blood-biomaterial interactions has not been critically examined. Recent studies have highlighted the potential role of Alb in mediating platelet attachment [54, 84], which is a surprising finding given that Alb does not have any known amino acid sequences that mediate platelet binding. The mechanisms governing these interactions therefore remain to be elucidated.

Previous studies [54, 55] have focused on the role of the conformation of adsorbed proteins in mediating platelet adhesion, but have not put forward a definitive hypothesis on whether the conformation or the surface coverage of the adsorbed protein is the main parameter involved in platelet adhesion, nor have they determined the mechanisms responsible for the apparent ability of platelets to adhere to adsorbed albumin. Hence, our research was targeted on definitively delineating the mechanisms mediating platelet

adhesion to adsorbed Fg and Alb, with a critical focus on clearly determining whether this platelet response is actually driven by the amount of surface-adsorbed protein or the degree of the adsorption-induced conformational changes in the protein when it adsorbs on the surface. Since platelets do not interact strongly with proteins in their native state in the bloodstream, but can readily bind to adsorbed proteins, *we hypothesize that adsorption-induced conformational changes in blood proteins lead to the exposure and/or formation of platelet-binding sites/domains in the protein molecules, which would have otherwise remained hidden or not present in their native state*. To provide support for our hypothesis, we planned and carried out a series of studies that were designed to definitively show that platelet adhesion response is directly related to the degree of adsorption-induced protein unfolding rather than the amount of protein adsorbed (Specific Aims I and II). We also planned and conducted a series of studies employing a variety of blocking strategies on the adsorbed protein as well as on specific platelet receptors to provide deeper insight into the exact nature of these platelet-protein interactions (Specific Aims III and IV). Finally, we conducted aging studies of adsorbed Alb to begin to investigate how this factor may be expected to influence the structure of adsorbed proteins and how this subsequently influences the platelet response (Specific Aim V).

Overall, this research provides deeper and newer perspectives on the molecular mechanisms mediating platelet interactions with adsorbed proteins, and how these interactions can be controlled to enhance the hemocompatibility of biomaterials used for cardiovascular applications.

3.2 Specific Aims and Significance

Specific Aim I. Analysis of adsorption-induced conformational changes in Fg and Alb as a function of protein solution concentration using CD spectropolarimetry

Since surfaces that tend to adsorb proteins strongly, leading to a large amount of protein adsorption on the surface, also tend to cause a greater degree of conformational change in the adsorbed protein, it is difficult to differentiate which of these two factors is more critical in mediating subsequent platelet adhesion. To address this question, it was necessary to design a protein adsorption study to independently vary the amount of protein adsorbed and the degree of adsorption-induced unfolding in the adsorbed protein layer. To accomplish this, protein adsorption studies were planned and conducted using a broad range of surface chemistries using alkanethiol SAM surfaces and a wide range of protein solution concentrations (0.1, 1.0, and 10 mg/mL), which permitted us obtain a large set of systems with widely differing amounts and conformational states of the adsorbed proteins. CD analyses were then conducted to assess the degree of adsorption-induced conformational change that occurred relative to the protein's solution-state structure, with the surface coverage of the adsorbed protein being obtained from the absorbance spectra for the adsorbed protein layer.

Specific Aim II. Analyze the role of the conformation of the adsorbed protein vs. amount of adsorbed protein as a critical determinant of platelet adhesion

SAM surfaces with varying functionalities were preadsorbed with Fg and Alb at three different bulk solution concentrations (as described in Specific Aim I), following which

they were incubated with washed human platelets. Platelet adhesion was quantified via a colorimetric Lactate Dehydrogenase (LDH) assay, while the morphology of the adherent platelets was visualized via scanning electron microscopy (SEM). The changes in secondary structure of the adsorbed plasma proteins as well as the amount of adsorbed protein (Specific Aim I) were then correlated with the platelet adhesion levels on the different surfaces in order to determine which of these two factors plays a more important role in mediating platelet binding.

Specific Aim III. Probing the molecular mechanisms of platelet adhesion to adsorbed Fg and Alb

A variety of blocking strategies were utilized on the adsorbed layer of protein, as well as the platelets, in order to examine the mechanisms underlying platelet adhesion to adsorbed protein. The analysis of platelet adhesion mechanisms to Alb is an important component of our work, as recent studies have suggested that platelets may actually adhere to Alb via specific mechanisms [54, 84], and this may be linked to the conformation of adsorbed Alb [54].

The Arg-Gly-Asp-Ser (RGDS) peptide, a potent inhibitor of platelet-plasma protein interactions in solution [107, 108], was used to examine the specific mechanisms involved in platelet adhesion to both adsorbed Fg and Alb. Additionally, we used polyclonal antibodies against Fg (pAb-Fg) and Alb (pAb-Alb) to definitively determine whether the platelets were adhering to Fg or Alb, respectively, with polyclonal antibodies against the other protein as negative controls. These pAb studies provided further insight

into the role of non-specific interactions in mediating platelet adhesion to adsorbed Fg and Alb.

While Fg contains numerous known platelet adhesion sites, Alb does not contain any, and thus we were particularly interested in trying to determine which amino acids in the Alb were involved in platelet adhesion. Chemical neutralization of Arg [174, 177] and Lys [176, 178] residues in Alb, under reaction conditions close to physiological conditions, permitted us to examine the role of these residues in mediating platelet binding. Control studies conducted to modify these residues in solution were followed up with mass spectrometric analysis to confirm that the reactions caused the intended site-specific modification. CD studies of both the solution and adsorbed structure of Alb were also conducted to ensure that these modifications did not significantly alter the secondary structure of Alb.

Specific Aim IV. Examining the role of specific platelet receptors in mediating adhesion to adsorbed Fg and Alb

Our preliminary results pointed to the possibility that there are at least two distinct sets of receptors associated with platelet adhesion to adsorbed Fg and Alb; one RGD-specific receptor that mediates adhesion along with activation, and another non-RGD specific receptor set that mediates adhesion with minimal activation. We specifically targeted the the GPIIb/IIIa receptor, which is the pre-eminent platelet receptor [1] and is well known to be RGD-specific, as well as the GPIb-IX-V receptor complex which has been found to

primarily mediate adhesion and not activation [111]. These studies were performed by blocking these receptors using a peptidomimetic GPIIb/IIIa antagonist called Aggrastat (or tirofiban), along with GPIbα-specific monoclonal antibodies (mAbs), thereby examining their abilities to inhibit platelet adhesion and/or activation.

Specific Aim V. Time-dependent conformational changes in adsorbed Alb and platelet adhesion

As addressed below in Chapter 4, the results from our Aim II studies showed that there is a strong correlation between the solution concentration from which Alb is adsorbed from and the degree of subsequent adsorption-induced unfolding, with adsorption of Alb from more dilute solutions resulting in a greater degree of unfolding. Our results also then showed that platelets are able to specifically adhere to adsorbed Alb, but only after Alb undergoes a substantial degree of adsorption-induced unfolding (i.e., > 34% loss in α-helix), with a negligible degree of platelet adhesion occurring otherwise. In particular, we found that preadsorption of Alb from a 10.0 mg/mL bulk solution concentration on SAM surfaces led to a minimal degree of adsorption-induced unfolding and negligible platelet adhesion. Based on these results, it can therefore be assumed that the adsorption of Alb at even higher solution concentrations than 10 mg/mL will result in even less unfolding and negligible platelet adhesion to the adsorbed Alb. Since the concentration of Alb in blood plasma is about 40 mg/mL, it can thus be assumed that, in

vivo, Alb will largely retain its native state when adsorbed from blood to a biomaterial surface, with minimal exposure/formation of platelet binding sites. Therefore, it could be argued that our findings that platelets adhere to adsorbed Alb after it undergoes substantial adsorption-induced unfolding is only of academic interest with little relevance to clinical applications.

However, it is important to realize that competitive adsorption studies have indicated that Alb adsorbs irreversibly and with only modest displacement by larger proteins such as Fg on both hydrophilic and hydrophobic surfaces [34]. This means that once adsorbed on a biomaterial surface, Alb will be permanently retained on the surface. This then raises the question of whether an irreversibly adsorbed, tightly packed Alb layer on an implant surface will permanently retain its native-state conformational structure for the rest of the life of the patient, or will this adsorbed layer of protein undergo structural changes, including unfolding, over time. If so, the question must be asked whether aging-induced unfolding will then result in the exposure/formation of platelet binding sites and subsequent platelet adhesion and activation in a manner similar to that which occurs when the unfolding of adsorbed Alb is induced by adsorption from dilute solution. This question of the aging behavior of irreversibly adsorbed proteins may also apply to other plasma proteins, such as Fg, and may provide important further insight into the nature of platelet interactions with adsorbed plasma proteins on implants used in cardiovascular applications.

To address this question, we therefore planned and conducted a set of studies to investigate the effect of aging on the structure of an adsorbed layer of Alb and the

subsequent influence of aging-induced Alb unfolding on platelet adhesion. For these studies, Alb was adsorbed to a SAM surface from 10 mg/mL, thus inducing a negligible amount of initial unfolding in the adsorbed protein, and these adsorbed Alb layers were then aged at 37°C for over a six-month time period with periodic CD and platelet adhesion studies performed to follow aging-induced unfolding of the adsorbed proteins secondary structure and subsequent platelet response.

CHAPTER 4

ASSESSMENT OF CONFORMATION OF ADSORBED PROTEIN LAYER USING CIRCULAR DICHROISM SPECTROPOLARIMETRY

4.1 Introduction

When a biomaterial is implanted in the human body, the adsorption of plasma proteins to the surface of the implant is one of the first events to occur, subsequently influencing the cellular response to the biomaterial. Understanding the molecular mechanisms underlying these protein-surface interactions is important for the design of hemocompatible cardiovascular biomaterials, as the adsorption of plasma proteins influence the onset of a variety of adverse responses, such as thrombi and emboli formation and complement activation on the biomaterial surface [1].

Protein adsorption is a complex process, and is dependent on a variety of material properties, especially surface chemistry [32]. Conventional thinking holds that surfaces that adsorb the least amount of plasma proteins support less platelet adhesion and thus exhibit lower surface thrombogenicity. However, recent studies have suggested that the critical determinant of the hemocompatibility of a surface may actually be the conformational state of the adsorbed protein rather than the total amount of adsorbed protein on the surface [54, 55]. This likelihood is further supported by the fact that proteins do not induce adverse reactions when they are in their native soluble state in the blood. Based on this understanding, we hypothesize that adsorption processes cause the exposure and/or the creation of bioactive motifs that are ‘hidden’ or not in a active

conformation within the protein in its native conformation, which then stimulate adverse cellular responses. The effect of surface chemistry in inducing post-adsorptive conformational changes in proteins may thus be an important consideration for biomaterials surface design.

Alkanethiol SAMs on gold are widely used as model systems for studying the effects of surface chemistry on protein adsorption [51, 94-96] since they are easy to prepare, form highly ordered systems, and permit a wide variety of surface functionalities to be produced [84, 91-93]. While studies using these SAM surfaces have clearly shown that both the amount of protein adsorbed on a surface and the level of cellular response to the adsorbed protein layer generally increase with increasing surface hydrophobicity, it is difficult to clearly determine if the cellular response is actually driven by the amount of the protein on the surface or the degree of adsorption-induced refolding of the protein on the surface. This is because it is generally true that surface chemistries that adsorb a larger amount of protein (i.e., strong protein-surface interactions) also tend to cause a higher degree of conformational change in the proteins when they adsorb. To investigate this issue, a sensitive method is needed that is able to accurately measure the degree of structural change that occurs when a protein adsorbs to a surface and experimental conditions are needed that are able to vary the degree of conformational change that occurs during adsorption in a manner that can be separated from the amount of protein that is adsorbed.

Circular dichroism (CD) spectroscopy can be used to analyze samples with relatively low surface area and at relatively low degrees of surface coverage, and information on

the conformational state, as well as the surface coverage of the protein is easily obtained using this instrument. Because of these advantages, CD has been increasingly used in recent studies as a means of examining protein-surface interactions at the molecular level [54, 126-128].

Important considerations that should be taken into account when performing CD experiments and subsequent data analysis have been described previously [179]. Additionally, in order to obtain accurate data for protein adsorption experiments, the total absorbance of the sample (including the cuvette, sample, and buffer) in the 190 nm – 200 nm wavelength range must not exceed a critical value for a given instrument beyond which the high tension (HT) voltage limits of the instrument are exceeded [179]. Once conditions are set that allow a CD spectrum to be successfully obtained within these designated constraints, it is then analyzed via curve fitting algorithms [146-148, 180] that are used to quantify the fractions of the different secondary structural components that it contains.

In this chapter, we present the refinement of experimental methods for CD spectropolarimetry using a cuvette that was specifically designed for protein adsorption studies to increase the sensitivity and reproducibility of our measurements by maximizing the number of surfaces that can be used in a single sample while minimizing the path-length through the buffer solution, thereby substantially improving the signal-to-noise ratio of the CD spectra. These methods were then applied to investigate the effects of surface chemistry and solution concentration on the secondary structure of adsorbed Fg and Alb as a means of separately varying the amount of protein adsorbed and degree of

adsorption-induced changes in the protein's secondary structure [39]. From these studies, we show that our refined CD methods provide a very sensitive and reproducible means to measure the conformation of adsorbed proteins. Our results indicate that for these surfaces and proteins, an increase in surface hydrophobicity for a given solution concentration results in an increase in both the amount of protein adsorbed and the degree of adsorption-induced changes in their secondary structure, while an increase in solution concentration for a given surface chemistry results in an increase in the amount of protein adsorbed but a decrease in the degree of conformational change, with this latter effect being more pronounced on the more hydrophobic surfaces.

4.2 Materials and methods

4.2.1 Protein Solutions

Human fibrinogen (FIB3, plasminogen, von Willebrand factor and fibronectin depleted) was purchased from Enzyme Research Laboratories (South Bend, IN) and human serum albumin was purchased from Sigma (Catalog No. A 9511). The buffer used for all experiments was a 25 mM potassium phosphate buffer, consisting of appropriate amounts of monobasic potassium phosphate (Sigma) and dibasic potassium phosphate (Sigma) combined as necessary to adjust the solution pH to 7.4.

4.2.2 Gold substrates

Quartz slides (0.375" x 1.625" x 0.0625", Chemglass) were cleaned at 50°C by immersion in a piranha solution (7:3 v/v H_2SO_4/H_2O_2) for at least 30 minutes, followed by a Radio Corporation of America (RCA) basic wash (1:1:5 v/v $NH_4OH/H_2O_2/H_2O$), and this procedure was repeated twice. These slides were then rinsed with 100% ethanol (Pharmco-Aaper; Catalog No. 11100200), followed by nanopure water and then dried under a stream of nitrogen gas.

The quartz substrates were then coated with a 30 Å chromium adhesion layer followed by 100 Å of gold via a thermal vapor deposition (TVD) evaporator (Model E 12 E, Edwards High Vacuum Ltd.), prior to SAM formation on these substrates. The thicknesses of the gold and chromium layers were verified using a DekTak profilometer and a GES5 ellipsometer (Sopra, Inc., Palo Alto, CA).

4.2.3 Formation of self-assembled monolayers (SAMs) of alkanethiols

The following alkanethiols were used (as received) for our experiments:

1-Dodecanethiol ($SH-(CH_2)_{11}CH_3$; Aldrich; CH_3),

11-(2,2,2-Trifuoroethoxy) undecane-1-thiol) $SH-(CH_2)_{11}OCH_2CF_3$; Asemblon; CF_3),

11-Amino-1-undecanethiol, hydrochloride ($SH-(CH_2)_{11}NH_2HCl$; Prochimia; NH_2)

11-Mercaptoundecanoic acid ($SH-(CH_2)_{11}COOH$; Aldrich; COOH), and

11-Mercapto-1-undecanol ($SH-(CH_2)_{11}OH$; Aldrich; OH).

SAM surfaces were prepared as per established protocols.[181, 182] Briefly, pure alkanethiol solutions were prepared in 100% ethanol (Pharmco-Aaper; Catalog No.

111000200) to yield a final concentration of 1.0 mM. The gold substrates were cleaned by dipping them for 1 minute each in a modified piranha wash (4:1 v/v H_2SO_4/H_2O_2), followed by an RCA basic wash (1:1:5 v/v $NH_4OH/H_2O_2/H_2O$), rinsed copiously with ethanol, and then immersed in the alkanethiol solutions for 24 hours to form the SAM surfaces.

After SAM formation on the gold substrates, the SAM surfaces were cleaned to remove any traces of hydrophobic contaminants, prior to surface characterization and protein adsorption [99, 172]. The CH_3 and CF_3 SAM surfaces were sonicated in ethanol, hexane and ethanol, and finally rinsed with nanopure water. The NH_2, COOH and OH SAMs were sonicated in ethanol, prior to incubation in a 25 mM potassium phosphate buffer solution containing 0.005 volume % Triton-X-100 (Sigma-Aldrich, Catalog No. T-9284), to block off any hydrophobic defect sites (e.g., grain boundaries). These SAM surfaces were then sonicated in acetone, followed by ethanol, to remove any traces of residual/loosely-bound Triton, and finally rinsed with nanopure water.

4.2.4 Surface characterization

4.2.4.1 Contact angle goniometry

Advancing contact angle measurements were measured on the SAM surfaces using a CAM 200 Optical Contact Angle/Surface Tension Meter (KSV Instruments Ltd) and CAM 200 software provided with the instrument. The surfaces were sonicated in ethanol for 10 minutes, rinsed with nanopure water and dried with flowing nitrogen gas, and

mounted on the sample stage. The advancing water contact angles from six separate drops of nanopure water (pH=7.0) were measured on each surface.

4.2.4.2 X-ray photoelectron spectroscopy

XPS measurements of each type of SAM surface were conducted at the National ESCA and Surface Analysis Center (NESAC/BIO, University of Washington, Seattle, WA), using a Surface Science Instrument X-Probe spectrometer (Mountain View, CA) or a Kratos-Axis Ultra DLD spectrometer, equipped with a monochromatic Al Kα source (KE = 1486.6 eV), a hemispherical analyzer and a multichannel detector. The XPS spectra were collected at a nominal photoelectron takeoff angle (with respect to the sample surface normal) of 55°, at a pass energy of 80 eV for survey spectra and 20 eV for high resolution C1s and S2p spectra. The elemental composition was determined from the peak areas in the spectra, using the SSI data analysis software or Kratos Vision 2 software program.

4.2.4.3 Ellipsometry

Ellipsometry measurements were performed using a Sopra GES5 variable angle spectroscopic ellipsometer (Sopra Inc., Palo Alto, CA) and the accompanying GESPack software package. The substrates used were 18 mm square coverslips (VWR), coated with 50Å of chromium and 1000Å of gold via thermal vapor deposition to ensure high reflectivity. Ellipsometry was performed on these gold-coated samples before and after incubation in alkanethiol, to determine the thickness of the SAM monolayer. Briefly, the spectra for five test points on each sample were scanned from 250 nm to 850 nm using an incident angle of 70°. The thickness of the SAM monolayer was calculated via the

regression method in the Sopra WinElli software package (version 4.07) by setting the *n* and *k* values for the alkanethiol layer as 1.5 and 0.0, respectively. The results presented are the average of five measurements on each surface for each SAM.

4.2.5 Protein adsorption

Protein stock solutions were prepared by dissolving human Fg and Alb in 25 mM phosphate buffer solution (pH 7.4). Each set of cleaned SAM-coated surfaces was incubated in the phosphate buffer in a Pyrex petri dish and then a suitable amount of protein stock solution was pipetted into the buffer. It is important to ensure that the pipette tip was below the air-water interface, to avoid denaturation of the protein at this interface. Protein adsorption was conducted under two different protein solution concentrations, 0.1 mg/mL and 1.0 mg/mL, in order to investigate the effect of bulk protein solution concentration on the adsorption-induced conformational changes. The SAMs were incubated in protein for 2 hours, after which the protein solutions over the SAM surfaces were infinitely diluted to remove the bulk protein solution and wash away any loosely adherent protein prior to removal of the SAMs from the buffer solution. Following this infinite dilution step, the SAM surfaces were able to be safely removed from the pure buffer solution without dragging the surfaces through the denatured protein film that can be expected to be present at the liquid-air interface if the protein solution had not been replaced with pure buffer prior to surface removal.

4.2.6 Determination of solution structure, adsorbed concentration, and adsorption-induced conformational changes of proteins using circular dichroism spectroscopy

The structure of Fg and Alb in solution, the adsorption-induced conformational changes in these proteins on the various SAM surfaces, and the amount of protein adsorbed on each surface were determined using CD spectropolarimetry. The CD spectra (consisting of the ellipticity and absorbance values over wavelengths ranging from 190 nm to 240 nm) were obtained at room temperature using a Jasco J-810 spectropolarimeter (Jasco Inc., Easton, MD). The solution structure of the proteins was determined using special high-transparency quartz cuvettes (Starna Cells Inc., Atascadero, CA) while the structure of the adsorbed proteins was determined using cuvettes that we custom-designed for maximum signal-to-noise ratio (addressed below, see Fig. 4.1). Prior to running the instrument, it was calibrated using a 1.0 cm path-length quartz cuvette containing a solution of (1S)-(+)-10-camphorsulfonic acid, which has an ellipticity of +190.4 millidegrees (mdeg) at a wavelength of 290.5 nm [183].

4.2.6.1. Solution structure of proteins

The background spectrum (i.e., buffer only in the cuvette) was measured first, followed by that of the protein solution. Each CD spectrum was the average of ten scans done at a scan rate of 50 nm/min, using a data pitch of 0.1 nm, in a 0.1 mm path length quartz cuvette. The background spectrum was subtracted from the CD spectrum of protein solution to yield the spectrum of the protein solution alone. The contribution of any protein adsorbed on the walls of the cuvette while measuring the CD spectra for the

solution structure of the proteins was found to have negligible influence on the determination of the structure of the protein in solution (see Table 4.S.1 and Fig. 4.S.1.)

The ellipticity value (θ, in mdeg) was converted to molar ellipticity with standard units of deg·cm^2/dmol (designated as [θ]) using the following equation [135, 179]:

$$[\theta] = (\theta \cdot M_0)/(10{,}000 \cdot C_{soln} \cdot L) \qquad (4.1)$$

where θ is the molar ellipticity in mdeg, L is the path length of the cuvette in cm, C_{soln} is the solution concentration of the protein in g/mL, and M_0 is the mean residue molecular weight of 118 g/mol.

Proteins exhibit a peptide absorbance peak at 195 nm (A_{195}), and hence we use the height of the absorbance peak at this wavelength to determine C_{soln} [184]. The absorbances of serial dilutions of 2.0 mg/mL stock protein solutions were measured at 195 nm, with the concentrations of the stock solutions being verified using a bicinchoninic acid assay (BCA, Pierce Biotechnology). Calibration plots of A_{195} vs. C_{soln} were first plotted for both Fg and Alb, with the slope of these plots representing "$\varepsilon_{protein} \cdot L$" from Beer's Law, which is expressed as:

$$A_{195} = \varepsilon_{protein} \cdot C_{soln} \cdot L \qquad (4.2)$$

where $\varepsilon_{protein}$ is the extinction coefficient of the protein in mL $\cdot$ g^{-1} $\cdot$ cm^{-1} (or cm^2/g) and L is the path length of the cuvette in cm.

The data of the molar ellipticity as a function of wavelength that were obtained from the CD scans were deconvoluted using the SP-22X algorithm and analyzed using the SELCON and CONTIN/LL software packages [142, 148] to yield the percentages of secondary structure components (α-helix and β-sheet). These programs analyze the

ellipticity values at each wavelength and compare them with a library of proteins with known secondary structure in order to estimate the percentages of the various secondary structural components.

4.2.6.2. Adsorbed protein concentration

It should be noted that the term "$C_{soln} \cdot L$" in Eqn. (4.2) has units of g/cm^2, which is equivalent to the units of surface concentration of adsorbed protein. Assuming that the absorbance is dependent only on the total mass of protein per unit area that the light beam passes through, irrespective of whether the protein is in solution or adsorbed to a surface, the same calibration plots used for the proteins in solution along with Eqn. (4.2) can also be used to directly determine the amount of protein adsorbed per unit area on the SAM surfaces, Q_{ads}, by replacing $C_{soln} \cdot L$ in Eqn. (4.2) with Q_{ads}. The validity of using this relationship to measure the amount of protein adsorbed on the SAM surfaces was confirmed by the independent measurement of Q_{ads} using ellipsometry (see supplementary information, Section 4.5, Table 4.S.2).

4.2.6.3. Adsorbed protein structure

As noted above, the CD spectra for the analysis of adsorbed protein structure on the different SAM surfaces were obtained using a specially modified quartz cuvette that we custom-designed to enhance the signal-to-noise ratio for these experiments, by increasing the number of surface samples and reducing the path-length of buffer through which the beam of light passes (as seen in Figure 4.1). The cuvette was designed to hold four SAM surfaces with 1/16" (0.159 cm) as the total path-length of the buffer through which the CD beam passes. By reducing this path-length, we were able to keep the total absorbance

and HT voltage below their critical values while maximizing the number of surfaces being scanned, thereby minimizing the signal-to-noise ratio to obtain a high level of sensitivity for the measurement of the CD spectra of the adsorbed protein layers.

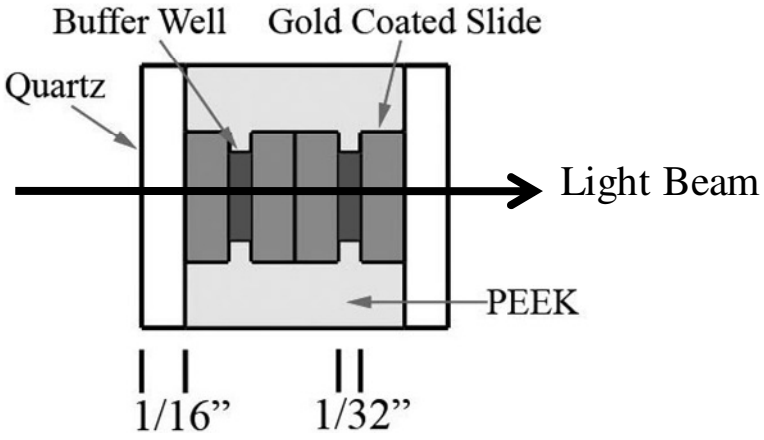

Figure 4.1. Top-view of the custom-designed cuvette used for measuring the CD spectra of adsorbed protein on the SAM surfaces.

To evaluate the structure of the adsorbed protein layer on each SAM surface, the background spectra for the SAM-coated quartz slides were first obtained prior to protein adsorption. After the completion of the protein adsorption process, the modified cuvette was filled with 1.0 mL of the 25 mM phosphate buffer and the protein-coated SAM surfaces were inserted into the slots provided for the slides, taking care to ensure minimal exposure of the protein-coated slides to air, (to avoid any potential drying-induced conformational changes). The spectra for the SAM-coated quartz slides with the adsorbed protein layer were then taken.

The collected spectra were prepared for analysis by subtracting the background spectrum taken for each SAM without the adsorbed protein from the corresponding

spectrum of the same SAM surface after protein adsorption, with this difference then representing the contribution to the overall spectrum from the adsorbed protein layer alone. The absorbance of the adsorbed protein layer at 195 nm (A_{195}) was measured and the amount of protein adsorbed on the SAM surface was obtained from the calibration curve of A_{195} vs. Q_{ads}. The resulting ellipticity values (θ, in mdeg) were then converted to molar ellipticity values ([θ], in standard units of deg·cm^2/dmol) using the following equation [135, 179]:

$$[\theta] = (\theta \cdot M_0)/(10{,}000 \cdot Q_{ads}) \qquad (4.3)$$

This is the same as Eqn.4.1, with the "$C_{soln} \cdot L$" term being replaced by Q_{ads}, which represents the surface concentration of the adsorbed protein. The molar ellipticity data was then analyzed using the SP-22X algorithm and analyzed using the SELCON and CONTINLL algorithms to determine the percentage composition of the secondary structural components in the adsorbed protein layer.

4.2.7 Statistical analysis

The results we present are the mean values with 95% confidence interval (CI). The statistical significance of differences between mean values for different samples/conditions was evaluated using Student's t-test, with values of $p < 0.05$ considered as statistically significant.

4.3 Results and Discussion

4.3.1 Surface characterization

The contact angle and ellipsometry data for the SAM surfaces is presented in Table 4.1 and is in excellent agreement with previously reported values for these types of surfaces [181, 185]. The contact angle for the OCH_2CF_3-terminated SAM (CF_3) was approximately 90°, which was lower than that observed for a CH_2-CH_2-CF_3-terminated SAM (estimated to be around 100°), but was consistent with a previous study [79]. It has been shown previously that water exerts its influence on atomic layers at a distance of approximately 5 Å from the upper surface of the thiol layer, penetrating these layers and forming hydrogen bonds [186]. The ether group of the OCH_2-CF_3 SAM is located at a distance of ~3Å from the surface, as a result of which water may be able to form hydrogen bonds with the oxygen atoms of the ether groups. This explains the lower contact angle observed for the OCH_2CF_3 SAM, compared to the CH_2-CH_2-CF_3-terminated SAM. The XPS data for the SAM surfaces is presented in Table 4.2, with these data also providing values within the expected range for each type of surface chemistry.

Table 4.1. Contact angle and ellipsometry data for the SAM surfaces. (Mean ± 95% CI, n =7)

Parameter	CH_3	OCH_2CF_3	NH_2	COOH	OH
Contact Angle (°)	100.9 ± 1.9	90.2 ± 0.8	47.6 ± 1.8	17.9 ± 1.3	17.6 ± 1.9
Thickness (Å)	11.5 ± 2.2	22.1 ± 4.9	14.7 ± 2.5	15.8 ± 1.9	12.1 ± 1.4

Table 4.2. Atomic composition of Au-alkanethiol SAM surfaces as determined via XPS (mean ± 95% C.I., n = 3)

Surface moiety	C (%)	S (%)	N(%)	O (%)	F (%)
CH_3	64.9 ± 2.6	2.8 ± 0.9	Negligible	Negligible	Negligible
OCH_2CF_3	44.1 ± 1.8	1.7 ± 0.2	Negligible	6.2 ± 1.0	13.0 ± 0.4
NH_2	54.0 ± 0.8	2.0 ± 0.2	4.0 ± 0.3	3.3 ± 0.3	Negligible
COOH	47.6 ± 1.6	1.6 ± 0.1	Negligible	7.6 ± 0.3	Negligible
OH	56.7 ± 3.0	2.8 ± 2.2	Negligible	7.5 ± 0.9	Negligible

4.3.2 Determination of conformational changes using CD spectroscopy

The CD spectra for human Fg and Alb in solution are shown in Figure 4.2. As seen in this figure, both Fg and Alb show a shoulder at 222 nm and a negative minima at 208 nm, as well as a positive maxima at 193 nm, which are characteristic of α-helical proteins [55, 179]. The α-helix and β-sheet content for native Fg and Alb was quantified using the CDPro software package, and the results are tabulated in the Table 4.3. These values agree well with those reported previously in literature [187-190], and in the Protein Data Bank (PDB) files [191, 192].

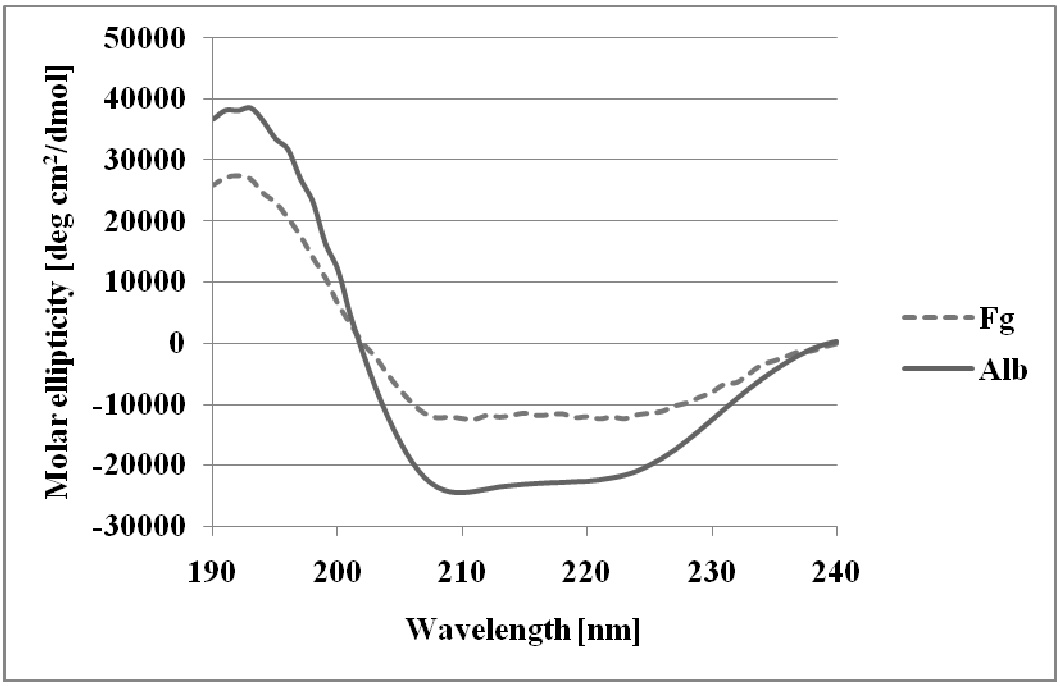

Figure 4.2. Representative CD spectra for human fibrinogen (Fg) and human serum albumin (Alb) in solution.

Table 4.3. Structural composition of human fibrinogen (Fg) and human serum albumin (Alb) in solution, as determined by CD spectra. The values for α-helix and β-sheet reported in literature (lit) and the Protein Data Bank (PDB) are included for comparison (mean ± 95% CI, n = 6).

Sample	**α-helix (%)**	**β-sheet (%)**
Fg	39.9 ± 1.1	9.5 ± 1.1
Fg – lit [193]	33.0	Very little
Fg-PDB [194]	30.0	14.4
Alb	65.1 ± 1.3	2.6 ± 1.1
Alb- lit [77]	67.0	0.0
Alb-PDB [192]	70.0	0.0

The CD data quantifying the secondary structural composition of the adsorbed Fg and Alb on the SAM surfaces are shown in Figures 4.3 and 4.4, respectively, and are compared with the α-helix and β-sheet content of native Fg and Alb in solution. As clearly shown in these plots, the degree of adsorption-induced conformational changes is dependent on the SAM surface chemistry, with a prominent decrease in α-helix content ($p < 0.05$) for both Fg and Alb with increasing hydrophobicity of the surfaces (as indicated by the water contact angle values presented in Table 4.1). This is consistent with observations made by other groups suggesting that proteins undergo greater conformational changes as they adsorb on hydrophobic surfaces [33, 35].

This appears to be a characteristic response from adsorption-induced protein unfolding; or since the β-sheet content increases it may be more appropriate to refer to

this as adsorption-induced protein refolding. We believe that this overall behavior is caused by the thermodynamic driving force of the reduction in free energy of the system, which causes the hydrophobically associated secondary structures of the protein to separate from each other to form hydrophobic interactions with the non-polar functional groups of the SAM surface, thus reducing the overall solvent-exposed surface area of the hydrophobic functional groups in the system. This apparently destabilizes the α-helix structures of the protein, causing them to unravel, with the relatively flat SAM surface then acting as a template that favors the formation of β-sheet structure in their place.

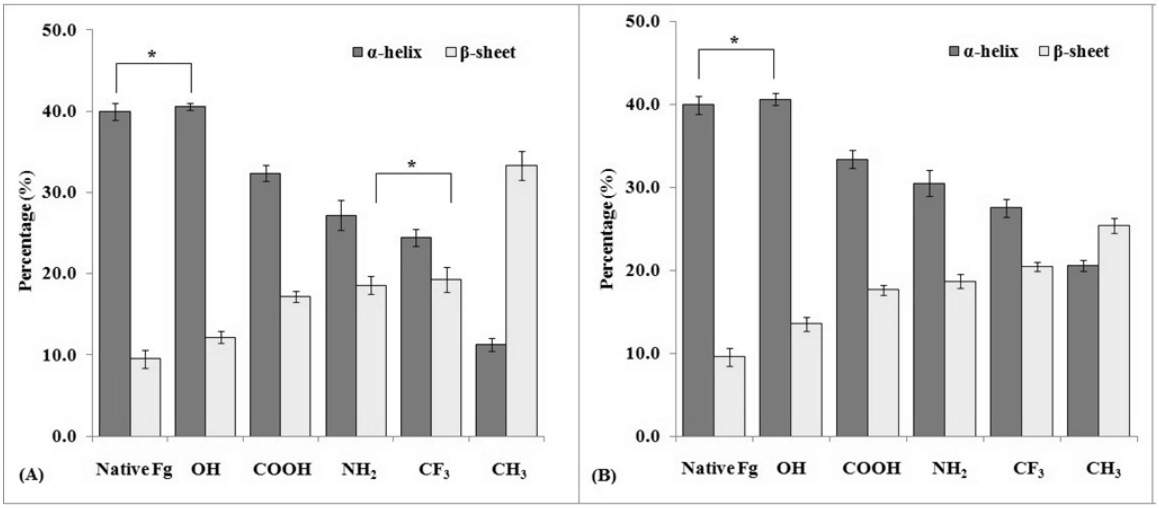

Figure 4.3. Changes in secondary structure of adsorbed human fibrinogen (Fg) adsorbed at (A) 0.1 mg/mL and (B) 1.0 mg/mL on SAM surfaces, determined by CD compared to its native conformation. (n=6, mean ± 95% CI). (* denotes not significant, all other values are significantly different from one another; $p < 0.05$)

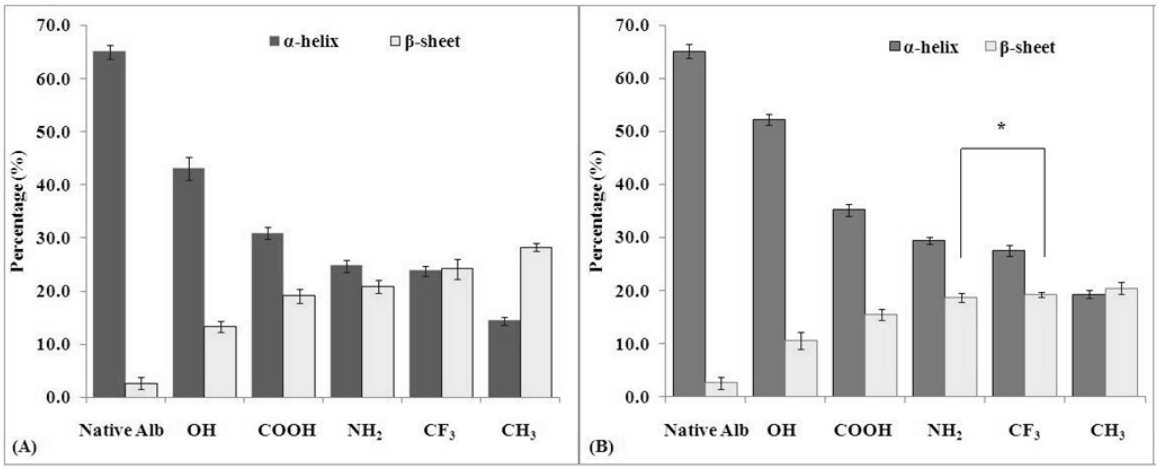

Figure 4.4. Changes in secondary structure of adsorbed human serum albumin (Alb) adsorbed at (A) 0.1 mg/mL and (B) 1.0 mg/mL on SAM surfaces, determined by CD compared to its native conformation. (n=6, mean ± 95% CI). Note: * denotes not significant, all other values are significantly different from one another; $p < 0.05$)

Although the OH and COOH SAMs exhibited similar levels of hydrophilicity ($p > 0.05$), as inferred from the contact angle data in Table 4.1, there was a significant difference ($p < 0.05$) in the way both Fg and Alb adsorbed and rearranged on these different surfaces, with the COOH SAM surfaces causing both a significantly greater loss of α-helix and a significantly greater increase in β-sheet in the protein structure compared to the OH SAM. As shown in Figures 4.3A and 4.3B (Fg) and Figures 4.4A and 4.4B (Alb), the structures of the proteins adsorbed on the OH SAM surfaces were closest to their native structures, with no statistical difference ($p > 0.05$) between the α-helix values for Fg adsorbed on the OH SAM surface at both protein concentrations. This may be attributed to the fact that the internal hydrophobic interactions within the proteins

dominate over their tendency to unfold and form contacts with the polar groups of the OH surface, thereby helping in preserving the native structure of fibrinogen and albumin [34]. In other words, due to the hydrophilicity of the surfaces (i.e., the lack of a hydrophobic driving force to cause protein refolding), the OH groups on the SAM surface primarily interact with the proteins by forming hydrogen bonds and van der Waal's interactions with the hydrogen-bondable groups present on the polar and charged amino acid residues presented on the outer surface of the protein. As a result of this, the thermodynamic stability of the proteins adsorbed on the OH-surfaces is minimally perturbed, thereby largely causing it to retain its native structure following adsorption to the surface.

On the other hand, the proteins adsorbed on the COOH SAM surface showed significantly greater ($p < 0.05$) structural rearrangement (i.e., loss of α-helix accompanied by gain of β-sheet) compared to their native structures. We attribute this behavior to the negatively charged carboxyl groups on the SAM surface (pK = 7.4) [195] interacting with positively charged amino acid residues on the protein's surface, or possibly salt-bridges formed by oppositely charged amino acid residue pairs within the core of the protein. We believe that these types of interactions apply new external forces on the proteins, leading to a situation where the native states of the Fg and Alb no longer represent the lowest free energy states of the protein-SAM-solution complexes, with the proteins then subsequently refolding to the new lowest free energy state conformations.

As also clearly evident from the results presented in Figures 4.3 and 4.4, the NH_2 SAM surface resulted in a significantly greater degree of structural changes in the

adsorbed protein ($p < 0.05$) than the COOH SAM surface. One explanation for this is that Fg (pI = 5.5) [196] and Alb (pI = 4.7) [196] should both have a greater number of negatively charged amino acid residues on their surface compared to the number of positively charged residues for a buffer solution of pH 7.4. This should then cause the positively charged NH_2 SAM surface (surface pK = 8.9) [195] to have a stronger electrostatic interaction with these proteins than the COOH SAM (surface pK = 5.0) [195]. In addition to these electrostatic effects, the NH_2 SAM surface also exhibits a much lower degree of attraction to water molecules (as evident by its relatively high contact angle, as presented in Table 4.1), with this tending to minimize the free energy penalty associated with dehydrating the functional groups on the SAM surface as the protein adsorbs.

These results clearly illustrate that the hydrophobicity of the surface is not the sole factor that governs protein adsorption behavior, but that the characteristics of the specific functional groups involved also play a significant role.

Finally, statistical comparisons between the data shown in Figures 4.3A versus 4.3B, and 4.4A versus 4.4B, indicates that the amount of loss in α-helix structure and the increase in β-sheet structure in both Fg and Alb were significantly greater when these proteins were adsorbed from 0.1 mg/mL solution concentration than from the 1.0 mg/mL solution concentrations ($p < 0.05$), with the exception of Fg adsorbed on the OH SAM. These results can be explained by kinetic arguments based on the relative kinetics of mass transport of the protein to the SAM surfaces compared to the kinetics of the refolding of the protein on the SAM surfaces. When the proteins adsorb from a dilute

solution, mass transport to the surface will be substantially slower than from a concentrated solution, thus giving the protein molecules more time to unfold, refold, and spread out over the surface before the entire surface becomes saturated, which inhibits further spreading of the protein over the surface [33, 39]. Further evidence is provided for this type of adsorption behavior in the following subsection.

4.3.3 Quantification of protein adsorption on the SAM surfaces

Figures 4.5 and 4.6 illustrate the amount of Fg and Alb, respectively, adsorbed on the SAM surfaces from bulk solutions of 0.1 mg/mL and 1.0 mg/mL solutions.

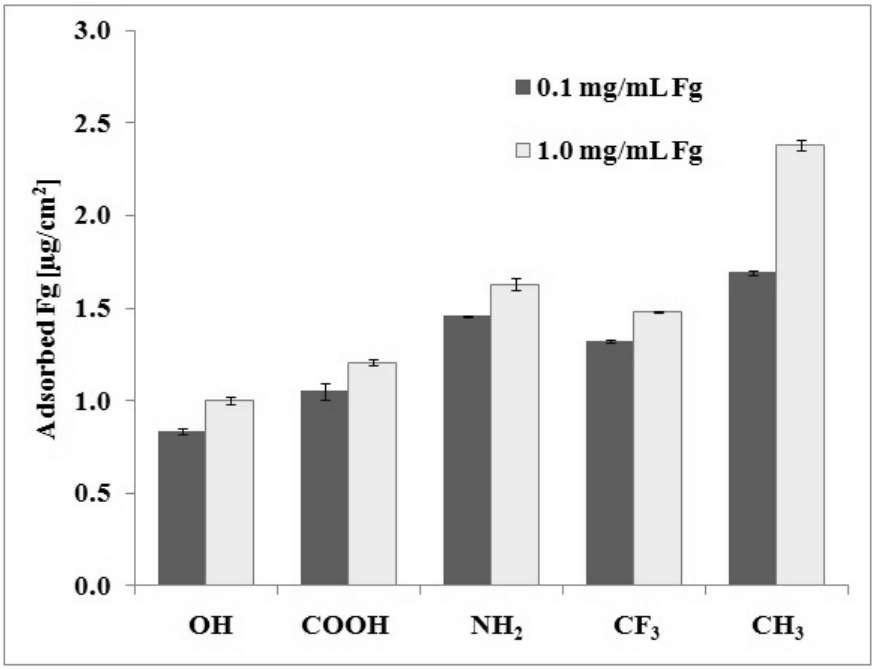

Figure 4.5. Fibrinogen (Fg) adsorption (Q_{ads}) from bulk solutions of 0.1 mg/mL and 1.0 mg/mL on SAM surfaces. (n=6, mean ± 95% CI).

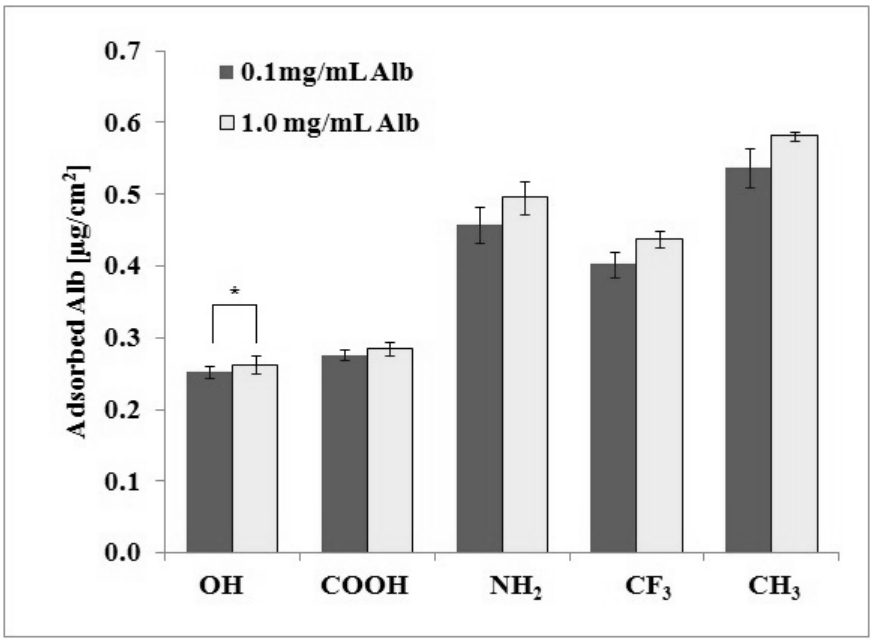

Figure 4.6. Albumin (Alb) adsorption (Q_{ads}) from bulk solutions of 0.1 mg/mL and 1.0 mg/mL on SAM surfaces. (n=6, mean ± 95% CI). Note: * denotes not significant, all other values are significantly different; $p < 0.05$)

Fg has dimensions of about 5.0 x 5.0 x 47.0 nm^3 [50], yielding a surface coverage of 2.26 µg/cm^2 when it is adsorbed end-on (25 nm^2 per adsorbed molecule of Fg), whereas a side-on adsorption configuration yields a surface coverage of 0.24 µg/cm^2 (235 nm^2 per adsorbed molecule of Fg) [34]. On the basis of the Alb molecule having dimensions of approximately 4.0 x 4.0 x 14 nm^3 [50], it was estimated [34] that the area occupied per adsorbed molecule of Alb for end-on adsorption would be 16 nm^2, thereby yielding a coverage of 0.72 µg/cm^2, and the surface area for side-on adsorption was similarly estimated as 56 nm^2, yielding a surface coverage of 0.21 µg/cm^2.

Our results (shown in Figures 4.5 & 4.6) suggest that our surfaces are saturated with protein and these protein molecules are arranged on the surface in a mixture of side-on and end-on configurations, as the values for surface coverage, with one exception, lie between the theoretical values for side-on and end-on protein adsorption for both of these proteins.

An interesting result from the quantification of protein adsorption is the fact that the levels of protein adsorption were much lower for both Fg and Alb on the CF_3 SAM compared to the CH_3 SAM, despite the fact that both of these types of surfaces are considered to be strongly hydrophobic. This can be attributed to the role of water, which can be expected to be able to interact with the subsurface ether group of the CF_3 SAM via hydrogen bonding to a much greater extent than a hydrogen-bondable group from the protein because of the much smaller size and increased mobility of a water molecule [39, 197], thus providing a thermodynamic mechanism to resist the dehydration of this surface by an adsorbing protein. In fact, the CF_3 SAM surface even adsorbed a significantly lower amount ($p < 0.05$) of each protein than the NH_2 SAM surface, even though the NH_2 SAM is a much more hydrophilic surface. The higher protein adsorption on the NH_2 SAM than OCH_2CF_3 SAM is attributed to the favorable attractive forces between the positively charged SAM surface and the negatively charged proteins combined with the ability of the subsurface ether group of the CF_3 SAM to preferentially hydrogen bond with water compared to an adsorbing protein.

As clearly shown in Figures 4.5 and 4.6, the amount of protein adsorbed is significantly influenced by solution concentration. At the lower solution concentration

(0.1 mg/mL), the rate of arrival of the protein molecules at the surface by diffusion is slower than from the solution with higher concentration (1.0 mg/mL). This provides a condition where an adsorbed protein has more time to undergo adsorption-induced refolding and spreading before it "bumps" into proteins adsorbed to neighboring sites, thus enabling each adsorbed protein molecule to occupy a larger amount of surface area and subsequently saturate the surface with a lower total amount of adsorbed protein. As a direct result of this phenomenon, and as we observed in this study, surface saturation occurred with a lower amount of adsorbed protein per unit area ($p < 0.05$) for all SAM surfaces when the protein was adsorbed from the more dilute solution, with the exception of Alb adsorbed on the OH SAM, which exhibited similar levels of surface coverage for both 0.1 mg/mL and 1.0 mg/mL solution concentrations. Most importantly for our interests, this decrease in the amount of adsorbed protein with decreased solution concentration coincides with an increase in the degree of protein refolding, as shown by the CD results of the adsorbed protein structure in Figures 4.3 and 4.4. This then provides conditions where the degree of structural change in the proteins following adsorption is no longer directly proportional to the amount of protein adsorbed to the surface, which will subsequently enable us to investigate which of these two parameters most strongly influences platelet adhesion behavior, as is shown in the next chapter.

4.4 Conclusions

This study examined the use of CD spectropolarimetry for measuring the adsorption-induced conformational changes in Fg and Alb as a function of surface chemistry and solution concentration. As an important component of these studies, we developed a custom-made sample-holding cuvette that was specifically designed in such a manner to minimize the path length of the buffer solution through which the CD beam passes while providing multiple surfaces with adsorbed protein. The use of this new cuvette was found to substantially improve the signal-to-noise ratio for these types of measurements compared to our previous studies [54].

Based on the results presented in this section, we conclude that both surface chemistry and the concentration of the protein solution play a significant role in influencing the amount of protein adsorbed to the surfaces and the degree of conformational change that these proteins undergo when they adsorb. Furthermore, these results show that by varying both surface chemistry and solution concentration, we can uncouple the relationship between the amount of protein adsorbed and the degree of adsorption induced refolding of the protein. We also conclude that the specific characteristics of the functional groups presented by a surface, and not simply their relative degrees of hydrophobicity, influence the amount of protein adsorbed and the degree of protein refolding that occurs following adsorption.

Recent studies [54, 55, 84] have shown that the conformation of the adsorbed protein layer, and not just the amount of adsorbed protein, is an important determinant of cellular response (e.g., platelet response) to biomaterial surfaces. CD spectropolarimetry

provides an excellent means to quantitatively investigate these types of interactions. Further studies (presented in Chapter 4) were carried out to correlate cellular response to both the amount of protein adsorbed and the degree of adsorption-induced structural changes in proteins in order to develop a more comprehensive understanding of how protein adsorption influences the biocompatibility of implanted biomaterials; and most importantly, to gain further insights into how surfaces can be engineered to control protein adsorption behavior and thereby direct biological response.

4.5 Supporting Information

4.5.S.1 Analysis of contribution of protein adsorbed on the cuvette in the determination of secondary structure of proteins in solution

It is important to examine the contribution of protein adsorbed on the inner surfaces of the cuvette, if any, in the CD measurements of the solution structure of the protein. In order to accomplish this, we obtained the CD spectrum of phosphate buffer first (buffer background, in Fig. 4.S.1) in the 0.1 mm quartz cuvette. The two removable quartz slides which form the front and back surfaces of the cuvette were then removed and preadsorbed with human fibrinogen (Fg) for a duration equal to the total scanning time per sample (i.e., about 20 min) and then infinitely diluted with phosphate buffer to remove any weakly adherent protein. The cuvette was then filled with phosphate buffer and CD measurements were then carried out to obtain the CD spectrum of the buffer along with any contribution from adsorbed Fg (modified background, in Fig. 4.S.1).

The cuvette was then cleaned thoroughly, filled with Fg solution, and the CD spectra for the Fg solution were obtained as per the procedures mentioned in Section 4.2.6.1. The buffer and modified backgrounds were subtracted from the CD spectra for Fg solution, and the resultant spectra were deconvoluted and analyzed (as per Section 4.2.6.1) to determine the percentages of α-helix and β-sheet in native fibrinogen, which are listed in Table 4.S.1.

Table 4.S.1. Structural composition of human fibrinogen in solution, as determined by CD spectra using different background conditions (mean ± 95% CI, n = 6).

Background condition	**α-helix (%)**	**β-sheet (%)**
Buffer background	39.3 ± 0.7	10.5 ± 0.5
Modified background	39.4 ± 0.6	10.3 ± 0.3

As shown in Table 4.S.1, there was no significant difference ($p > 0.05$) between the values of percentage α-helix and β-sheet for fibrinogen, irrespective of the background spectra used. The CD spectra for Fg solution obtained using either background spectrum overlapped, as observed in Fig. 4.S.1. Thus, we can conclude that the protein adsorbed on the walls of the cuvette during CD measurements of the solution structure of Fg had negligible contribution to the overall CD spectrum of the Fg solution.

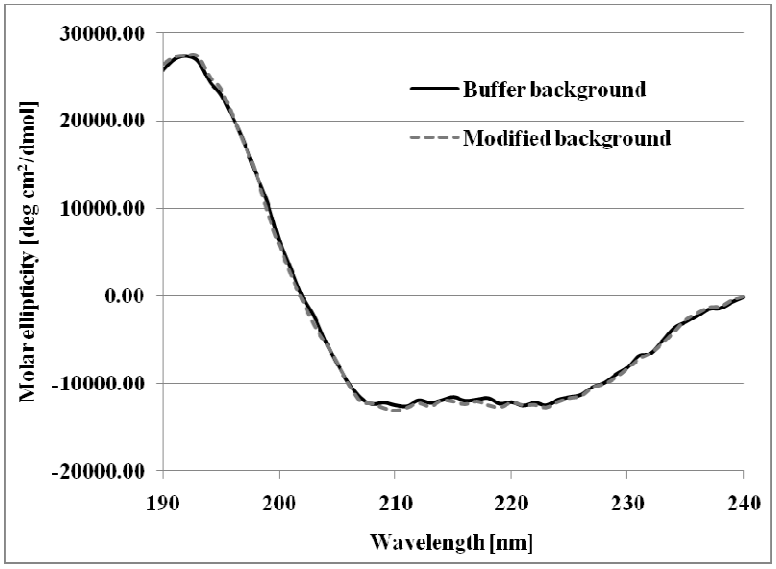

Figure 4.S.1. CD spectra of human fibrinogen (Fg) in solution, determined using different background spectra (Average of 6 samples).

4.5.S.2 Ellipsometry vs. Absorbance for Measurement of Protein Surface Concentration

To verify the validity of the relationship that we used for quantifying the amount of protein adsorbed based on the absorbance measurement at 195 nm (i.e. $C_{soln} \cdot L = Q_{ads}$) that was used in Section 4.2.6.2 (Adsorbed Protein Concentration), surface concentrations were confirmed by ellipsometry. In these preliminary studies, CH_3 SAM surfaces were incubated in 0.1 mg/mL and 1.0 mg/mL fibrinogen and albumin bulk solutions for 2 hours. The thicknesses of the adsorbed protein layers were then converted to surface coverage (in $\mu g/cm^2$) using the formula of de Feijter [198]:

$$\Gamma_{ads} = 0.1\, d_f\, (n_f - n_b) / (dn/dc) \qquad (4.S.1)$$

In equation (4.S.1) above, d_f = film thickness (in nm), n_f = refractive index of the adsorbed protein film ≈ 1.42 (values lie between 1.36 and 1.50), [102, 199] n_b = refractive index of the buffer ≈ 1.33 (measured using a refractometer), and dn/dc = increment of refractive index of protein solution versus protein solution concentration ≈ 0.188 for all proteins. [199] The thickness of the protein layers (in nm) and calculated surface coverage for albumin and fibrinogen adsorbed on the CH_3 SAM surfaces are shown in Table 4.S.2.

The values for protein adsorption on the CH_3 SAM calculated using de Feijter's equation (Γ_{ads}) are not statistically different ($p > 0.05$) from those obtained from relationship we used for quantifying the amount of protein adsorbed using circular dichroism (i.e. $C_{soln} \cdot L = Q_{ads}$), thus validating the use of the absorbance method to directly measure surface concentration of adsorbed protein.

Table 4.S.2. Thickness and adsorbed amounts of the fibrinogen (Fg) and Albumin (Alb) layers on a CH_3 SAM, adsorbed from 0.1 mg/mL and 1.0 mg/mL bulk solutions, as measured by ellipsometry (Γ_{ads}) and absorbance (Q_{ads}). (n =5, mean ± 95% CI)

Bulk protein concentration (mg/mL)	**Thickness of protein layer (nm)**	**Protein adsorbed, Q_{ads} (µg/cm^2)**	**Protein adsorbed, Γ_{ads} (µg/cm^2)**
0.1 Fg	32.9 ± 6.0	1.69 ± 0.01	1.57 ± 0.29
1.0 Fg	44.7 ± 5.0	2.37 ± 0.03	2.13 ± 0.23
0.1 Alb	11.6 ± 2.0	0.54 ± 0.03	0.55 ± 0.10
1.0 Alb	12.3 ± 1.8	0.58 ± 0.01	0.59 ± 0.09

CHAPTER 5

PLATELET ADHESION AS A FUNCTION OF ADSORBED CONFORMATION VS. SURFACE COVERAGE OF FIBRINOGEN

5.1 Introduction

While blood contains numerous different types of proteins, any of which may adsorb to a biomaterial surface, fibrinogen (Fg) has been identified as one of the most important types of adsorbed proteins that induces a platelet adhesion response. Although the specific mechanisms mediating platelet adhesion to adsorbed Fg remain to be fully defined, it is widely cited in the biomaterials field that the amount of adsorbed Fg is one of the most important determinants of the biocompatibility of a given biomaterial [65-67, 200]. Others, however, have found evidence that the conformational state of adsorbed Fg may actually be the more important mediator of platelet adhesion response [54, 55, 116]. This belief is further supported by the simple fact that non-activated platelets do not strongly interact with Fg when it is in its soluble, native conformation in the blood stream, but readily adhere and activate after contacting this same protein when Fg is adsorbed on a surface. This implies that adsorption induces some conformational change in Fg that exposes and/or creates otherwise hidden or non-active sites that are recognized by platelet receptors.

One of the primary problems in differentiating between these two factors (i.e., amount versus conformation of Fg) is that surfaces that tend to strongly adsorb Fg,

leading to a large amount of protein on the surface, also tend to induce a large degree of conformational unfolding of the protein when it adsorbs. Although commonly coupled in this manner, it is very important to differentiate between these two potential mediators of platelet adhesion because they lead to two very different approaches for biomaterials design to promote blood compatibility. If the amount of adsorbed Fg mediates platelet adhesion, then biomaterial surfaces should be designed to minimize the amount of Fg adsorbed irrespective of its conformational state. Alternatively, if platelet adhesion is mediated by the degree of adsorption-induced Fg unfolding, then surfaces should be designed to adsorb Fg in a manner that maximally retains its native-state structure irrespective of the amount of Fg that is adsorbed.

To address this critical issue, we conducted a set of platelet adhesion studies that were specifically designed to uncouple the amount of adsorbed Fg from the degree of adsorption-induced Fg unfolding and thereby definitively determine which of these two factors is the most important mediator of platelet adhesion response. This was accomplished by adsorbing Fg to a broad range of surface chemistries from a wide range of solution concentrations to obtain a large set of systems with differing amounts and conformational states of adsorbed Fg. The amount of Fg adsorbed and its degree of adsorption-induced unfolding was then determined by absorbance and circular dichroism (CD) spectropolarimetry, respectively, with a lactate dehydrogenase (LDH) assay and scanning electron microscopy (SEM) used to assess the platelet response. Additional studies were conducted using Arg-Gly-Asp-Ser (RGDS) peptides in the platelet suspension to block $\alpha_{IIb}\beta_3$ platelet integrins, to assess how adsorption-induced unfolding

of Fg influences the involvement of this receptor in the overall platelet adhesion response.

5.2 Materials and methods

5.2.1 Gold substrates

18 mm square cover glasses (VWR Scientific, Catalog No. 48368-040) were used as substrates for the platelet adhesion experiments, while quartz slides (0.375" x 1.625" x 0.0625", Chemglass) were used for CD experiments. All substrates were cleaned at 50°C by immersion in a piranha solution (7:3 v/v H_2SO_4/H_2O_2) for at least 30 minutes, followed by a Radio Corporation of America (RCA) basic wash (1:1:5 v/v $NH_4OH/H_2O_2/H_2O$), and this procedure was repeated twice. These substrates were then rinsed with 200-proof ethanol (Pharmco-Aaper; Catalog No. 11100200), followed by nanopure water and then dried under a stream of nitrogen gas.

The cleaned cover glasses were then coated with a 50 Å chromium adhesion layer followed by 1000 Å of gold, while the quartz slides for CD were coated with 30 Å of chromium and 100 Å of gold, via a thermal vapor deposition (TVD) evaporator (Model E 12 E, Edwards High Vacuum Ltd.), prior to SAM formation on these substrates. The thicknesses of the gold and chromium layers were verified using a DekTak profilometer and a GES5 ellipsometer (Sopra, Inc., Palo Alto, CA).

5.2.2 Formation of self-assembled monolayers (SAMs) of alkanethiols

The following alkanethiols were used for creating the SAM surfaces:

1-Dodecanethiol ($SH-(CH_2)_{11}CH_3$; Aldrich; CH_3),

11-(2,2,2-Trifuoroethoxy) undecane-1-thiol) $SH-(CH_2)_{11}OCH_2CF_3$; Asemblon; CF_3),

11-Amino-1-undecanethiol, hydrochloride ($SH-(CH_2)_{11}NH_2HCl$; Prochimia; NH_2),

11-Mercaptoundecanoic acid ($SH-(CH_2)_{11}COOH$; Aldrich; COOH), and

11-Mercapto-1-undecanol ($SH-(CH_2)_{11}OH$; Aldrich; OH).

SAM surfaces were prepared as per the established protocols [181, 182] described earlier (in Section 4.3). Pure alkanethiol solutions (1.0 mM) were prepared in 100% ethanol (Pharmco-Aaper; Catalog No. 111000200). Prior to immersion in the alkanethiol solutions for 24 hours, the gold substrates were cleaned by dipping them for 1 minute each in a modified piranha wash (4:1 v/v H_2SO_4/H_2O_2), followed by a Radio Corporation of America (RCA) basic wash (1:1:5 v/v $NH_4OH/H_2O_2/H_2O$), and then rinsed copiously with 100% ethanol.

All SAM surfaces were cleaned to remove any traces of hydrophobic contaminants on their surface prior to surface characterization and protein adsorption [99]. The CH_3 and CF_3 SAMs were cleaned by sonication in ethanol, hexane and ethanol, and then rinsed with nanopure water. The NH_2, COOH, and OH SAMs were sonicated in ethanol, and then incubated in a 25 mM potassium phosphate buffer containing 0.005 volume % Triton-X-100 (Sigma; Catalog No. T-9284), in order to block off any hydrophobic defect

sites (e.g. grain boundaries), and then rinsed thoroughly with acetone, ethanol and nanopure water to remove loosely-bound Triton.

5.2.3 Contact angle measurement

The advancing contact angle measurements on the SAM surfaces were carried out using a CAM 200 Optical Contact Angle/Surface Tension Meter (KSV Instruments Ltd.) and the CAM 200 software provided with the instrument. The cleaned SAM surfaces were mounted on the stage of the instrument, and the contact angles for six separate drops of nanopure water were measured on each surface.

5.2.4 Buffers

The protein adsorption experiments were carried out using a 25 mM potassium phosphate buffer (PBS, pH 7.4), which was prepared by combining appropriate amounts of the mono- and dibasic salts (Sigma-Aldrich) to maintain the pH at 7.4. The platelet suspension buffer (PSB, pH 7.4) contained 137 mM NaCl, 2.7 mM KCl, 5.5 mM Dextrose, 0.4 mM sodium phosphate monobasic, 10 mM HEPES and 0.1 U/mL apyrase [201]. 2.5 mM $CaCl_2$ and 1.0 mM $MgCl_2$ was added to the PSB to give a platelet suspension buffer with metal ions (PSB+MI).

5.2.5 Protein adsorption

Human Fg (FIB3, plasminogen, von Willebrand factor and fibronectin depleted; Enzyme Research Laboratories, South Bend, IN) was dissolved in the 25 mM phosphate buffer solution (pH 7.4), to prepare the protein stock solutions, and protein adsorption was carried out. Briefly, protein adsorption on the SAM surfaces was carried out at three different protein concentrations of 0.1 mg/mL, 1.0 mg/mL, and 10.0 mg/mL, in order to obtain adsorbed Fg layers with a wide range of surface conformations and coverages. These are essential in delineating the effect of secondary structure and surface coverage of the adsorbed Fg layer on the SAM surfaces on platelet adhesion.

The cleaned SAM surfaces were incubated in phosphate buffer in a six-well-plate (Corning Costar, Catalog No. 3506) and then a suitable amount of protein stock solution was added to give the desired bulk protein solution concentration, ensuring that the tip of the pipette was held below the air-water interface to avoid denaturation of the protein at this interface. The SAM surfaces were maintained fully immersed in the protein solution for 2 h, after which an infinite dilution step was carried out to wash away the bulk protein solution, in addition to any loosely adherent protein prior to removal of the SAMs from the buffer solution. Following this infinite dilution step, the SAM surfaces were able to be safely removed from the pure buffer solution without dragging the surfaces through the denatured protein film that can be expected to present at the liquid-air interface if the protein solution had not been replaced with pure buffer prior to surface removal.

The SAM surfaces with preadsorbed protein were then either used for CD studies to analyze the structure of the adsorbed protein layer, or incubated with the platelet suspension.

5.2.6 CD studies to quantify the adsorption-induced conformational changes and total surface coverage of Fg on SAM surfaces

CD spectropolarimetry was done using a Jasco J-810 spectropolarimeter (Jasco, Inc., Easton, MD) to determine the native and adsorbed secondary structures of Fg, as well as the surface coverage of adsorbed protein, as described earlier (in Section 4.2.6). Special high-transparency quartz cuvettes (Starna Cells, Inc., Atascadero, CA) were used for determining the native solution structure, while the adsorbed structure of Fg on the SAM surfaces was determined using a cuvette specially custom-designed for maximizing the signal-to-noise ratio (see Fig. 4.1). The ellipticity of the samples (θ, in mdeg) was converted to molar ellipticity (designated as $[\theta]$, with standard units of deg·cm^2/dmol) using the following equation [132, 135]:

$$[\theta] = (\theta \cdot M_0)/(10{,}000 \cdot C_{soln} \cdot L) \qquad (5.1)$$

where θ is the molar ellipticity in mdeg, L is the path length of the cuvette in cm, C_{soln} is the solution concentration of the protein in g/mL, and M_0 is the mean residue molecular weight of 118 g/mol.

Since proteins exhibit an absorbance peak at 195 nm [184], we used the height of this absorbance peak (A_{195}) for constructing a calibration curve of A_{195} vs. C_{soln} for various

known concentrations of Fg, as described in Section 4.2.6. The slope of this plot is "$\varepsilon_{protein} \cdot L$" from Beer's Law, which can be written as:

$$A_{195} = \varepsilon_{protein} \cdot C_{soln} \cdot L \qquad (5.2)$$

where $\varepsilon_{protein}$ is the extinction coefficient of the protein in $mL \cdot g^{-1} \cdot cm^{-1}$ (or cm^2/g) and L is the path length of the cuvette.

The term "$C_{soln} \cdot L$" in eq. 5.2 (above) has units of g/cm^2, which is equivalent to the amount of protein adsorbed per unit area. Assuming that the absorbance is dependent on the total amount of protein present per unit area through which the beam of light passes, irrespective of whether the protein is in the solution or the adsorbed state, the calibration curve of A_{195} vs. C_{soln} can also be used for calculating the amount of Fg adsorbed per unit area on the SAMs (i.e., Q_{ads}). The validity of this method for measuring the surface coverage of adsorbed protein has been confirmed by independent measurement of Q_{ads} from the thickness of the adsorbed protein film obtained by ellipsometry (see Section 4.S.2) using de Feijter's formula [198].

Hence, while calculating the molar ellipticity for the adsorbed Fg layer on the SAMs, the term "$C_{soln} \cdot L$" in eq. 5.1 can be replaced by the term Q_{ads} to give the following equation:

$$[\theta] = (\theta \cdot M_0)/(10{,}000 \cdot Q_{ads}), \qquad (5.3)$$

The CD spectra (molar ellipticity vs. wavelength) thus obtained were deconvoluted using the SP-22X algorithm and analyzed using the SELCON and CONTIN/LL software

packages to quantify the percentage of α-helix and β-sheet content of the native/adsorbed protein [148].

5.2.7 Platelet adhesion

All protocols pertaining to the use of whole blood and platelets were approved by the IRB (Institutional Review Board) and IBC (Institutional Biosafety Committee) at Clemson University. The blood (25 mL) was collected via venipuncture from healthy, aspirin-free human volunteers at the Redfern Health Center at Clemson University in BD Vacutainer tubes (Catalog No. 364606, Becton-Dickinson, Franklin Lakes, NJ) containing an acid-citrated dextrose (ACD) anticoagulant. It is important to note that the first few mL of blood was discarded, as it is rich in clotting factors, and then the remaining 25 mL was collected.

Platelet rich plasma (PRP) was generated by centrifuging the ACD-anticoagulated blood (225 g, 15 min, 25°C) using a Beckman Coulter Allegra 6R centrifuge (Beckman Coulter, Fullerton, CA) . Platelets were separated from the PRP via a gel separation method [201]. A liquid chromatography column (Sigma-Aldrich, Catalog No. C4169) was filled Sepharose 2B (Sigma, Catalog No. 2B-300) and the column was allowed to equilibrate with PSB. The PRP was then carefully pipetted onto the column and then allowed to pass into the column. PSB was added to top of the column from a reservoir, while the setup was kept running. Fractions were collected from the outlet of the column, with the platelet-rich fractions being identified by their increased turbidity. The platelet-

rich fractions that had maximum turbidity were pooled, and then the platelet concentration was measured using a Beckman Coulter Z2 Coulter Particle Count and Size Analyzer (Beckman Coulter, Fullerton, CA). The platelet concentration was adjusted to 10^8 platelets/mL with PSB, and $CaCl_2$ and $MgCl_2$ were added to yield 2.5 mM and 1.0 mM final concentrations of these salts in the platelet suspension, respectively. The platelet suspension was allowed to rest for 30 min at 37°C, and then added to the protein-coated SAM surfaces and allowed to adhere for 1 h at 37°C.

At the end of the platelet adhesion step, the suspension was aspirated from each well, and the non-adherent platelets were rinsed away by filling and aspirating the wells five times with PBS. The samples were then removed to a fresh well-plate and the platelet adhesion levels were quantified using a lactate dehydrogenase (LDH) assay, while the morphology of the adherent platelets was visualized using scanning electron microscopy (SEM).

A control platelet adhesion study was also performed with the PSB being supplemented with 4 mg/mL bovine serum albumin (BSA; Sigma-Aldrich), which is conventionally used as a blocking agent for non-specific interactions, in order to examine its effect on the adhesion of the washed platelets to the adsorbed Fg on the SAM surfaces. The results from this study showed that the addition of BSA had no significant effect on platelet adhesion (see Figure 5.S.1 of the Supporting Information, Section 5.6, provided after the conclusions section of this chapter).

5.2.8 SDS-PAGE analysis of platelet suspension

It is essential to ensure that the platelet suspension was free of any plasma proteins, which may have been retained in the platelet suspension from blood plasma or released from the platelets due to platelet activation during the separation process. The platelet suspensions obtained from two separate gel separation runs were centrifuged at 1200 rpm, 1500 rpm, and 1800 rpm, and the supernatant was aspirated and analyzed via sodium dodecyl sulfate polyacrylamide gel electrophoresis (SDS-PAGE) for any traces of residual plasma proteins. Silver staining was done using a Silver SNAP Stain Kit II (Pierce, Rockford, IL), which provides a rapid and highly sensitive detection system for sub-nanogram levels of proteins in polyacrylamide gels.

5.2.9 Measurement of platelet adhesion using lactate dehydrogenase (LDH) assay

Platelet adhesion was quantified by measuring the lactate dehydrogenase (LDH) released when the adherent platelets were lysed with a Triton-PSB buffer (2 % v/v Triton-X-100 in PSB), using a CytoTox96® Non-Radioactive Cytotoxicity Assay (Promega Corporation, Madison, WI). This is a modification of the methods used previously [202, 203]. A calibration curve was constructed using a known number of platelets, counted using a Beckman Coulter Z2 Coulter Particle Count and Size Analyzer (Beckman Coulter, Fullerton, CA), and the platelet adhesion on the SAM surfaces was determined from this calibration curve.

5.2.10 Scanning electron microscopy (SEM)

The samples for SEM were fixed for 30 min at room temperature using a special fixing buffer (3% glutaraldehyde, 0.1 M sodium cacodylate, pH 7.4), after which they were rinsed with PBS thrice. To dehydrate the adherent platelets, the samples were incubating in ascending ethanol:water mixtures (50%, 60%, 70%, 80%, 90% and 99% ethanol) for 10 min. The samples were finally treated with 0.02 mL of hexamethyldisilazane (Sigma) and allowed to dry overnight. The morphology of the adherent platelets was examined using a FESEM-Hitachi S4800 scanning electron microscope (Electron Microscopy Facility, Advanced Materials Research Laboratory, Clemson University, Pendleton, SC).

5.2.11 Inhibition of platelet-protein interactions using Arg-Gly-Asp (RGD)-containing peptides

In order to inhibit interactions between RGD-binding platelet receptors and Fg, the platelet suspension was incubated for 30 min at room temperature with 300 μM of an Arg-Gly-Asp-Ser (RGDS) peptide (Calbiochem, La Jolla, CA), which has been shown to be sufficient to inhibit platelet aggregation [107]. These platelets were then allowed to adhere on the CH_3 and OH SAMs preadsorbed with 0.1 mg/mL protein solution, after which the platelet adhesion was quantified using an LDH assay and the morphology of the adherent platelets was examined using SEM.

As a control, platelets incubated with 300 μM of an Arg-Gly-Glu-Ser (RGES) peptide (American Peptide Company, Sunnyvale, CA) were allowed to adhere on the SAM surfaces preadsorbed with Fg, and the adhesion characteristics were analyzed.

5.2.12 Study using polyclonal antibodies against Fg and Alb

Polyclonal antibodies against human Fg and Alb (Anti-Fg/Alb Rabbit pAb; Calbiochem, La Jolla, CA) at a concentration of 4 μg/mL were incubated for 30 min at room temperature, on the Fg coated surfaces in order to examine the role of any non-specific platelet binding to the adsorbed Fg layer. Platelet adhesion was characterized using an LDH assay.

5.2.13 Statistical analysis

The results we present are the mean values with 95% confidence intervals (CI). Statistical significance of differences between mean values for different samples and conditions was evaluated using a Student's t-test, with $p \leq 0.05$ considered as statistically significant.

5.3 Results and Discussion

5.3.1 Amount of Fg adsorbed on SAM surfaces

The amount of Fg adsorbed on alkanethiol self-assembled monolayer (SAM) surfaces on gold functionalized with OH, COOH, NH_2, CF_3, and CH_3 function groups under solution concentration conditions of 0.1, 1.0, and 10 mg/mL of Fg was measured spectroscopically by absorbance at 195 nm (as described in Section 4.2.6.1). The results presented in Figure 5.1 show that the amount of Fg generally increased with increased surface hydrophobicity (see Table 5.1), and indicate that the amount of Fg adsorbed was dependent on the solution concentration from which it was adsorbed, with significantly greater amounts of Fg being adsorbed on a given SAM surface for each increasingly higher solution concentration. This can be explained by the fact that at a high solution concentration, the rate of diffusion of protein molecules to the surface is higher than that from a more dilute solution [31], and has been shown to be independent of the surface chemistry by Wertz et al. [34]. Therefore, an adsorbed protein molecule has less time to unfold and spread out over the surface before other protein molecules adsorb next to it, blocking further spreading on the surface [31, 39], leading to higher surface coverages of adsorbed Fg.

Table 5.1. Contact angle data for the SAM surfaces. (mean ± 95% CI, n =7).

	OH	COOH	NH_2	CF_3	CH_3
Contact Angle (°)	17.6 ± 1.9	17.9 ± 1.3	47.6 ± 1.8	90.2 ± 0.8	100.9 ± 1.9

The minimum amount of Fg adsorbed under any our conditions was 0.8 $\mu g/cm^2$, as shown in Figure 5.1. Given that the Fg molecule has dimensions of about 5.0 x 5.0 x 47.0 nm^3 [50], which yields a theoretical surface coverage at saturation between 0.24 $\mu g/cm^2$ and 2.26 $\mu g/cm^2$ for side-on versus end-on adsorption [34], respectively, the amounts of Fg adsorbed on the SAM surfaces from each bulk solution condition clearly show that our surfaces were saturated with the adsorbed protein. The values of surface coverage obtained for preadsorption with 0.1 and 1.0 mg/mL Fg lie between the theoretical maxima for side-on and end-on adsorption of Fg, suggesting a tight monolayer coverage. Adsorption from the 10.0 mg/mL Fg solution concentration led to surface coverage values well beyond the theoretical maximum for monolayer coverage of Fg, indicating multilayer adsorption.

We expect the Fg molecules to adsorb on the SAMs in a wide range of orientations, which would play a role in the platelet adhesion response. Unfortunately, CD spectropolarimetry does not provide information on the orientation of the adsorbed Fg layer. Overall, our results indicate that the Fg molecules preadsorbed from 0.1 mg/mL and 1.0 mg/mL bulk solution concentrations are arranged in a mixture of side-on and end-on orientations, since the surface coverage lies between the theoretical maxima for

these two orientations. A recent study of Fg adsorption showed that the majority of Fg molecules are adsorbed end-on when adsorption is carried out at Fg solution concentrations greater than 0.2 mg/mL [119], which suggests that as the Fg solution concentration for preadsorption increases, the fraction of Fg molecules adsorbed in an end-on orientation will increase, thereby increasing the surface coverage at higher Fg solution concentrations.

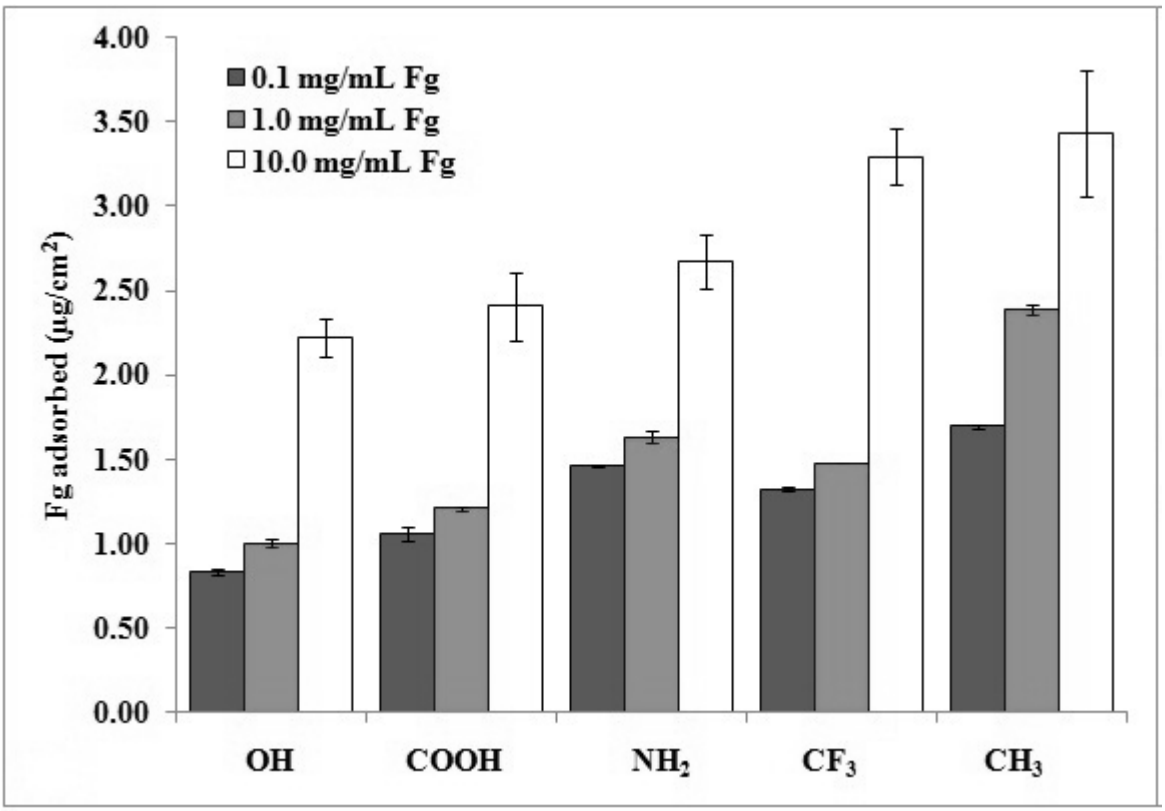

Figure 5.1. Fg adsorption from bulk solutions of 0.1 mg/mL, 1.0 mg/mL and 10.0 mg/mL on SAM surfaces functionalized with OH, COOH, NH_2, CF_3, and CH_3 surface groups (n=6, mean ± 95% CI).

5.3.2 Conformation of adsorbed Fg on SAM surfaces

The secondary structural composition (percentage α-helix and β-sheet content) of Fg adsorbed on the SAM surfaces, which was determined by adsorbed-state CD spectropolarimetry is presented in Figure 5.2, with the native/solution structure included for comparison. As shown, the combined variation of surface chemistry and protein solution concentration provided a wide range of average conformational states of the adsorbed Fg on the SAM surfaces. As the surfaces became more hydrophobic (see Table 5.1), Fg underwent a higher degree of adsorption-induced conformational change (i.e., loss of α-helix, accompanied by increase in β-sheet), which is consistent with observations made by other groups [33, 35]. This effect can be understood based on the increasingly strong thermodynamic driving force to induce protein unfolding on a surface to reduce the overall solvent accessible surface area of the system as a surface becomes increasingly hydrophobic. Similarly, the degree of adsorption-induced loss of α-helix was more prominent when the protein was absorbed from lower solution concentrations. This effect is particularly evident when Fg was adsorbed from the 10.0 mg/mL Fg solutions (Figure 5.2C), in which case the Fg adsorbed so rapidly that it had little time to unfold before the surface became saturated, resulting in minimal conformational changes such that the secondary structure of the adsorbed protein was much closer to the native solution structure of Fg.

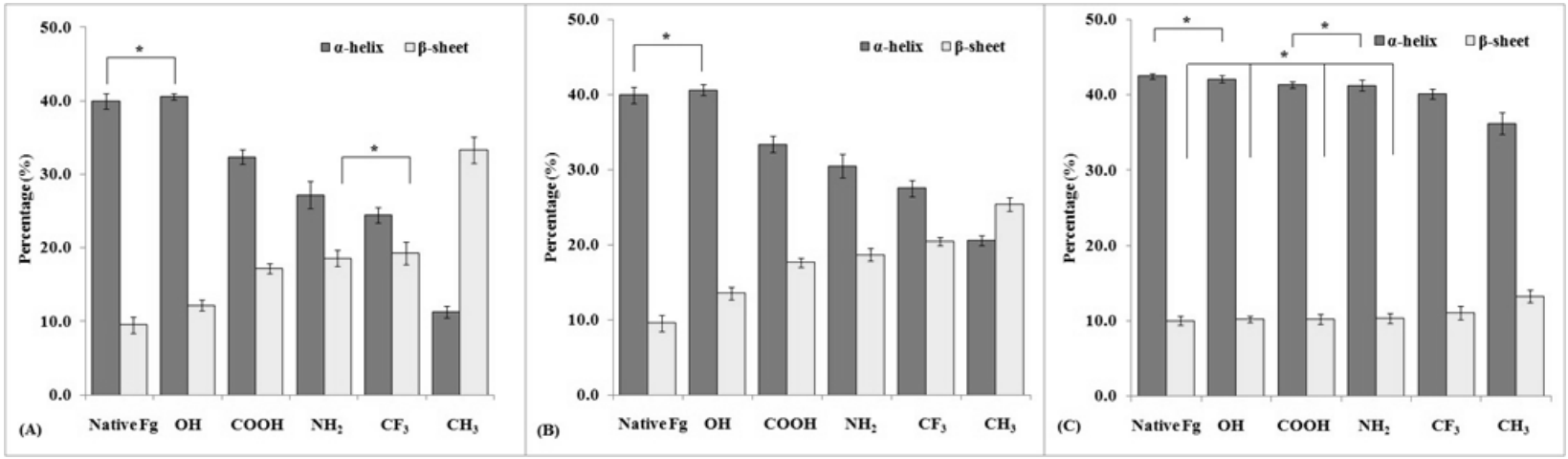

Figure 5.2. Changes in secondary structure of adsorbed human fibrinogen (Fg) adsorbed at (A) 0.1 mg/mL, (B) 1.0 mg/mL, and (C) 10.0 mg/mL on SAM surfaces determined by CD compared to its native conformation. (n=6, mean ± 95% CI). * denotes not significant, all other values are significantly different from one another; $p < 0.05$.

As with the amount of Fg adsorbed, this concentration effect can be understood to be due to the relationship between the kinetics of transport of the protein to the surface by diffusion compared to its rate of unfolding on the surface after it adsorbs. At lower protein solution concentrations, the transport of protein molecules to the surface has been shown to be much slower [34], thus providing adsorbed protein molecules with more time to unfold and spread out on the surface before they come in contact with neighboring adsorbed protein molecules, which inhibits further spreading [31, 39].

Although it would be ideal to know the full structural composition of the adsorbed protein layers in each of these cases, this information cannot be obtained using CD studies. Results obtained via CD represent the single average secondary structural content of the adsorbed Fg, and CD studies cannot distinguish between discrete sub-populations of states and a uniform distribution of a single population. Hence, we cannot rule out the possibility that the multilayer observed for preadsorption with 10.0 mg/mL Fg solution may be composed of more than one population, with varying degrees of unfolding.

5.3.3 Platelet adhesion to adsorbed Fg on SAM surfaces

Prior to conducting platelet adhesion experiments, SDS-PAGE analysis was carried out to test for traces of residual proteins in the platelet suspension which may either have entered the platelet suspension from the platelet-rich plasma (PRP) or released due to platelet activation during the separation process from whole blood. These could

complicate our study by potentially displacing the preadsorbed Fg through Vroman effects [39, 204].

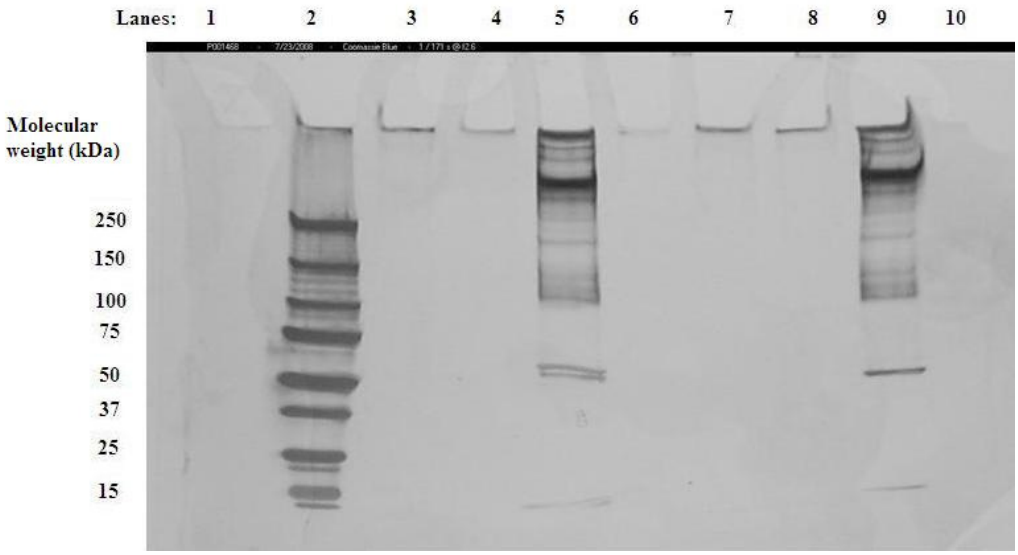

Figure 5.3. SDS-PAGE results for analysis of residual protein content in supernatant of platelet suspension. (Lanes 1, 6, 10: Blank, Lane 2: Protein ladder, Lanes 3 & 7: Platelet suspension centrifuged at 1200 rpm, Lanes 4 & 8: Platelet suspension centrifuged at 1500 rpm, Lanes 5 & 9: Platelet suspension centrifuged at 1800 rpm). Staining was done using a SilverSNAP® Stain Kit II.

The platelet suspension obtained from two different gel chromatographic separation processes was centrifuged at three different speeds and then examined for traces of residual plasma proteins via SDS-PAGE analysis. The SilverSNAP® Stain Kit II used for staining is highly sensitive and can detect sub-nanogram levels of proteins. As seen in Figure 5.3, only the platelet suspension sample centrifuged at 1800 rpm showed traces of

plasma proteins, suggesting that platelet lysis occurred at this high speed, releasing intracellular proteins into the supernatant. This suggests that the residual plasma proteins in the platelet suspension were below detectable limits, thus providing confidence that the measured platelet adhesion response was directly mediated by the preadsorbed layer of Fg.

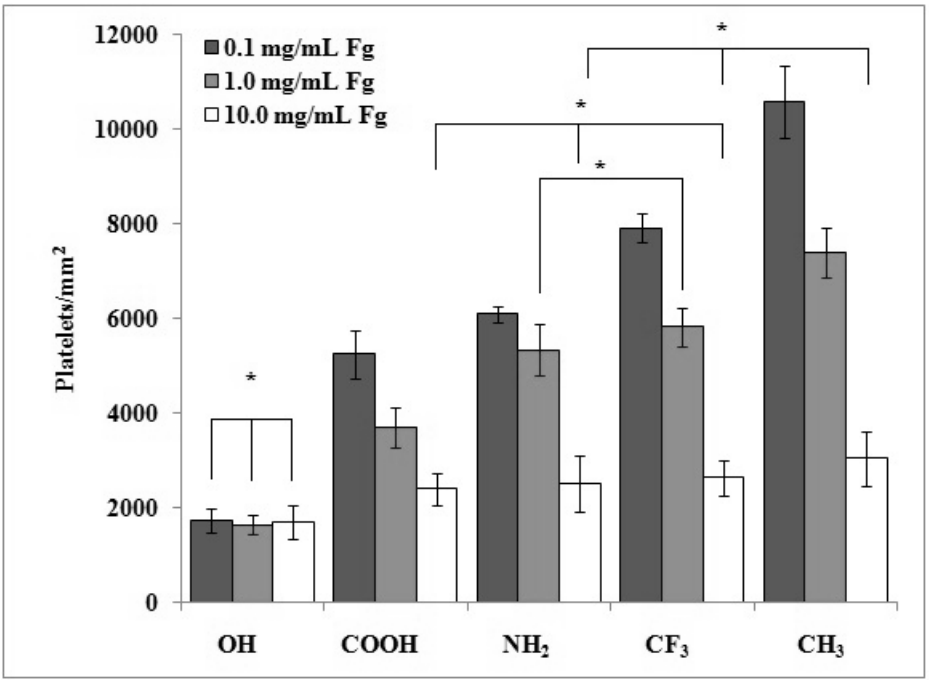

Figure 5.4. Platelet adhesion on SAM surfaces preadsorbed with Fg, assessed by LDH assay (n=6, mean ± 95% CI). * denotes no statistically significant difference, $p > 0.05$.

Figure 5.4 shows the platelet adhesion levels to preadsorbed Fg on each of the five SAM surfaces at each of the three different Fg solution concentrations. Each platelet adhesion value represents the mean of a set of six independent measurements (n = 6),

with each measurement being conducted using a different blood sample. As is clearly evident, the platelet adhesion levels observed were strongly influenced by both the surface chemistry as well as the solution concentration from which the protein was adsorbed. The platelet adhesion response increased with increasing surface hydrophobicity for each solution concentration and decreased with increased solution concentration for each surface chemistry, except for the OH SAM surface, where solution concentration did not significantly influence the platelet adhesion response.

To investigate whether platelet adhesion was more strongly mediated by the amount of adsorbed Fg or the conformation of adsorbed Fg, the data presented in Figures 5.1, 5.2 and 5.4 were re-plotted to show the platelet adhesion response versus the amount of adsorbed Fg (Figure 5.5A) and versus the degree of adsorption-induced Fg unfolding as represented by the percent loss in α-helix content of the protein (Figure 5.5B). As shown in Figure 5.5A, platelet adhesion appears to correlate fairly strongly with the amount of Fg adsorbed when the protein is adsorbed from a given solution concentration. However, when the universal data set is considered, the correlation between platelet adhesion and the amount of adsorbed Fg is essentially zero (r^2 = 0.04). In distinct contrast to this, the platelet adhesion response correlates very strongly with the adsorption-induced loss in α-helix (r^2 = 0.96), as seen in Figure 5.5B, when the results for all surfaces and Fg solution conditions are combined. These results strongly indicate that under these experimental conditions platelet adhesion is actually not in response to the amount of Fg adsorbed, but rather it is controlled by the conformational state of the protein on the surface, and provide an explanation for why many previous studies have reported results that imply

that platelet adhesion is in response to the amount of adsorbed Fg. Referring to the data presented in Figure 5.5A, platelet response does correlate with the amount of adsorbed Fg for a given solution concentration. However, close evaluation for each of the three individual data sets shown in Figure 5.5A for each solution concentration in comparison with Figure 5.5B reveals that within a given solution concentration, the change in the conformation of the adsorbed protein also tracks very closely with the adsorbed amount of Fg. It is only when the results are presented as a universal data set combining the results from each different solution concentration that these two effects are clearly separated, which then reveals that platelet adhesion is actually responding to the change in adsorbed structure of the Fg with little influence from the amount of Fg adsorbed. This situation is particularly demonstrated by comparing the platelet response to the COOH and OH SAMs with Fg preadsorbed from the 10.0 mg/mL Fg solution in comparison to the platelet response to the CH_3 SAM with Fg preadsorbed from the 1.0 mg/mL Fg solution (see associated data points in Fig. 5.5A). In each of these cases, the amount of adsorbed Fg was nearly the same while the degree of change in conformation of the adsorbed Fg on the CH_3 SAM was much greater than on either the COOH or the OH SAMs (see associated data points in Fig. 5.5B). If platelet adhesion was primarily governed by the amount of adsorbed Fg, then the platelet response would be expected to be nearly the same for each of these conditions. However, the platelet response on the CH_3 SAM (with the much greater degree of structural change in the adsorbed Fg) is nearly four times greater than on the COOH and OH SAMs. This clearly illustrates that the platelets are responding to something other than simply the amount of Fg adsorbed on

the surface. The strong correlation shown in Fig. 5.5B indicates that the degree of structural unfolding of the adsorbed Fg is the much greater determinant of the platelet response than the amount of Fg adsorbed.

Additionally, it is also important to keep in mind that this study was focused on comparing the role of the conformation verses the amount of adsorbed Fg in mediating the platelet response. Other factors, such as the orientation, packing arrangement, and structural heterogeneity of the adsorbed Fg layer can be expected to also influence the overall bioactive state of the adsorbed layer of protein, and in turn the platelet adhesion response. However, the results from these present studies indicate that these other variables, which were not controlled or measured in this study, do not obscure the effect of the adsorbed conformation of Fg on platelet adhesion, as indicated by the strong correlation between these two factors as shown in Fig. 5.5B.

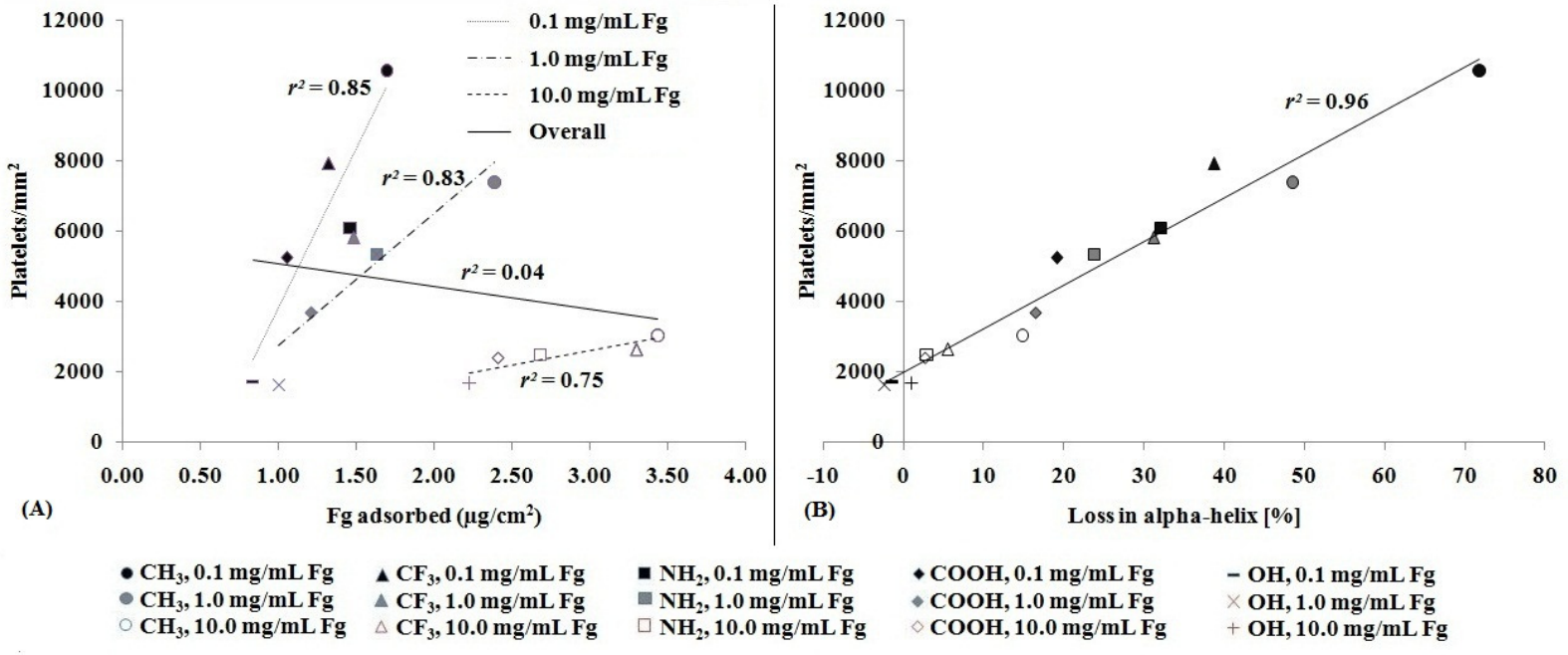

Figure 5.5. Platelet adhesion to Fg adsorbed on SAM surfaces as a function of (A) the amount of adsorbed Fg, and (B) the loss of α-helix. (Each point represents the mean of six values for each SAM surface.)

5.3.4 The role of RGD-specific receptors in mediating platelet adhesion to adsorbed Fg

Previous studies have shown that $\alpha_{IIb}\beta_3$ platelet integrins are involved in platelet adhesion to adsorbed Fg, with this receptor being effectively blocked by Arg-Gly-Asp-Ser (RGDS) peptide [107, 108]. In order to probe the extent of the involvement of this platelet receptor as a mediator of the platelet adhesion response as a function of the degree of adsorption-induced Fg unfolding, we conducted additional studies for Fg adsorbed from the most dilute solution concentration (0.1 mg/mL) on the two SAM surfaces representing the extremes in hydrophobicity (OH and CH_3 SAMs). The platelet suspensions were treated with an RGDS peptide (300 μM solution concentration) prior to exposure to the SAM surfaces preadsorbed with Fg to determine the extent that platelet adhesion is mediated by RGD-specific receptors (e.g., $\alpha_{IIb}\beta_3$ and $\alpha_V\beta_3$ platelet integrins) [173], with an Arg-Gly-Glu-Ser (RGES) peptide used as a non-bioactive control. The results of these studies are shown in Figure 5.6.

As presented in Figure 5.6, treatment of the platelets with the RGDS peptide resulted in a substantial decrease in platelet binding to adsorbed Fg on both of the SAM surfaces, while the RGES peptide had no significant effect ($p > 0.05$) on platelet adhesion to Fg for either surface. RGDS-treatment of the platelets led to a similar extent of inhibition of platelet adhesion to adsorbed Fg on both the CH_3 and OH SAMs (58.3% on CH_3, 45.7% on OH SAM) compared to the normal (unblocked) platelet control. These results indicate

that RGD-specific platelet receptors play a key role in mediating the interactions with adsorbed proteins, but only account for about half of the total platelet adhesion response.

This not surprising, considering the fact that the RGDS peptide has been shown to be a partial inhibitor of platelet-Fg interactions in a previous study [107], leading to a hypothesis that RGDS-bound platelet receptors can still interact with Fg but with lower affinity compared to their unbound state. Additionally, RGDS peptides have been shown to 'activate' the GPIIb/IIIa platelet receptors [155], and a recent study indicated that RGDS-treatment of washed platelets led to powerful activation of the $\alpha_2\beta_1$ platelet integrin without overall platelet activation [158]. This suggests that the role of GPIIb/IIIa in its RGDS-bound low-affinity state, as well as other platelet receptors cannot be ruled out in mediating the adhesion to RGDS-treated platelets to adsorbed Fg.

The fact that the RGDS peptide was unable to completely inhibit platelet interactions with adsorbed Fg suggests that the remaining level of platelet adhesion was either due to (*i*) non-specific platelet adhesion to exposed areas of the SAM surfaces and/or (*ii*) a specific receptor mediated process by non-RGD-specific platelet receptors to the adsorbed Fg.

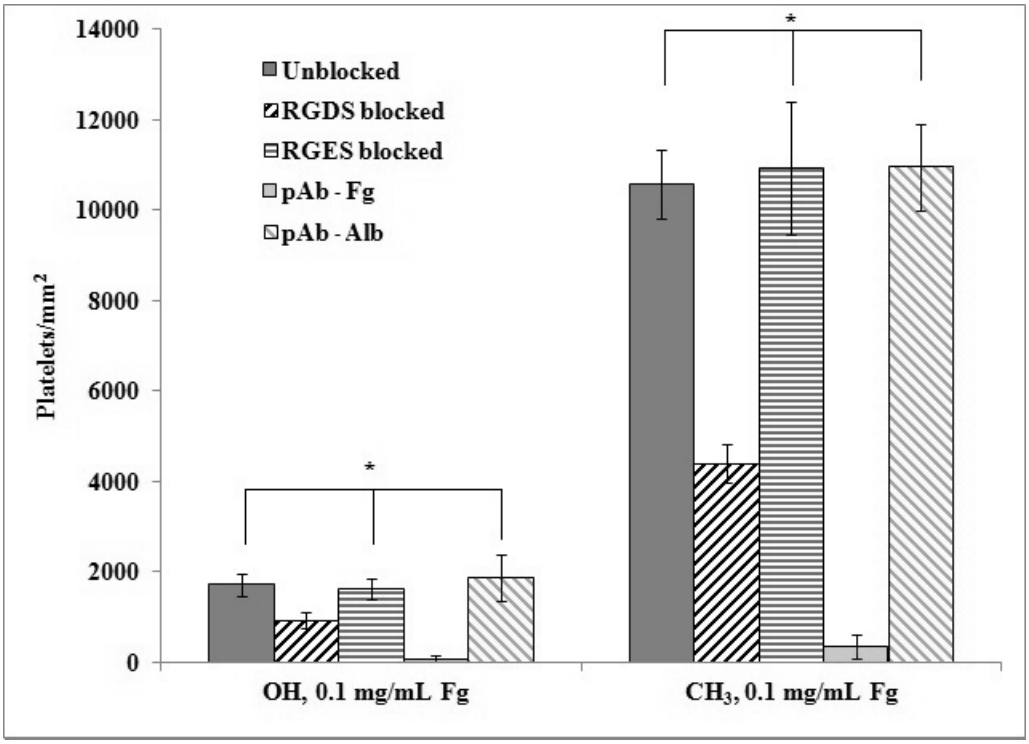

Figure 5.6. Platelet adhesion on OH- and CH_3 SAM surfaces preadsorbed with Fg from 0.1 mg/mL solutions under various blocking treatments. The blocking treatments included RGDS and RGES peptides and polyclonal antibodies specific for human Fg (pAb - Fg) and human albumin (pAb - Alb); (n=6, mean ± 95% CI). * signifies no significant difference, $p > 0.05$.

To address this issue, we treated the adsorbed Fg with polyclonal antibodies against Fg (pAb-Fg), with polyclonal antibodies against Alb (pAb-Alb) serving as a control. As seen in Figure 5.6, the pAb-Fg inhibited platelet interactions with adsorbed Fg almost entirely, while the pAb-Alb had no significant effect on platelet adhesion. These results thus clearly indicate that the adhesion of RGDS-treated platelets to adsorbed Fg was not

due to a non-specific platelet adhesion mechanism, but rather suggests that nearly 50% of the platelet adhesion response on both SAM surface may be mediated by non-RGD-specific platelet receptors. Alternatively, these data may also indicate that RGDS is only a partial inhibitor of the GPIIb/IIIa receptor, with this receptor still able to competitively bind to adsorbed Fg even in the presence of RGDS peptide. Future studies are planned to elucidate what these non-RGD-specific receptors may be and what the motifs are that they are binding to in the adsorbed, unfolded Fg. One method to investigate whether this behavior is due to a competitive binding mechanism would be to investigate the effect of RGDS solution concentration on the degree of inhibition of platelet binding.

5.3.5 SEM analysis of platelet adhesion to adsorbed Fg

Scanning electron microscopy (SEM) was carried out to assess the morphology of the adherent platelets to Fg on the CH_3 and OH SAMs, as well as to analyze the effect of platelet-receptor blocking with RGDS-peptides on the adherent platelet morphology.

The platelets adherent to both the CH_3 SAM (Figure 5.7A) and the OH SAM (Figure 5.7C) preadsorbed with 0.1 mg/mL Fg were considerably spread, with the expression of extensive filopodia (thus showing that our platelets were sensitive to activating surface conditions), with the primary difference between these two surfaces only being the number of adherent platelets per unit area as opposed to their morphology. In distinct contrast to this, the RGDS-treated platelets adherent to Fg adsorbed on both the CH_3

SAM surface (Figure 5.7B) and the OH SAM surface (Figure 5.7D) did not exhibit any filopodial extensions and were only moderately spread with prominent granulomeres.

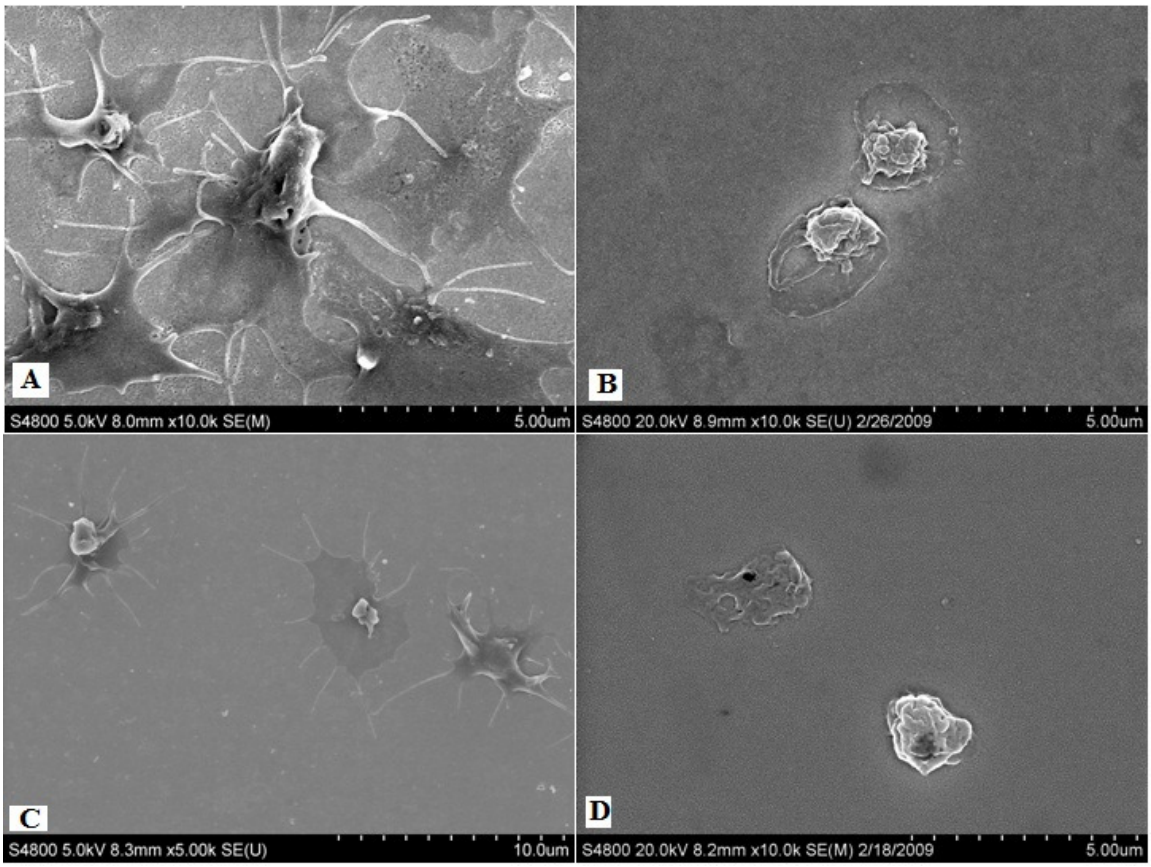

Figure 5.7. Platelet adhesion to the CH_3 (top row) and OH SAMs (bottom row) preadsorbed with 0.1 mg/mL Fg, under different blocking conditions: (A,C) unblocked Fg, (B,D) platelets treated with RGDS.

The difference in morphology of the RGDS-treated platelets compared to untreated platelets also strongly suggests that there may be at least two distinct set of receptors associated with platelet adhesion to adsorbed Fg. The RGD-specific receptor set is shown

to mediate adhesion along with a high degree of activation (i.e., spreading, accompanied by extension of filopodia), while the non-RGD-specific receptor set mediates platelet adhesion with minimal activation (i.e., minimal spreading, with no expression of filopodia). Alternatively, the decrease in the degree in platelet activation with RGDS in solution may indicate that platelet response is related to the number of receptors per unit area of the platelet that are activated upon binding, with the partial inhibition of platelet receptors leading to a decrease in the severity of platelet activation.

5.4 Conclusions

The results from these studies indicate that the platelet response correlates strongly with the adsorption-induced conformational changes in Fg, as measured by the loss of α-helix. Adsorption-induced conformational changes apparently lead to the exposure and/or creation of platelet binding motifs in Fg that are otherwise not accessible to platelet receptors in the native/solution state of this protein. The facts that the RGDS peptides only partially inhibited platelet adhesion to adsorbed Fg while pAb vs. Fg nearly totally blocked platelet adhesion suggests that either non-RGD-binding platelet receptor(s) are also substantially involved in mediating platelet adhesion to adsorbed Fg or that RGDS only serves as to partially block RGD-binding receptors, with these receptors then being still able to bind to sites in the adsorbed Fg in a competitive manner. Further studies are planned to elucidate the specific platelet receptors and their recognition sites in Fg that

mediate platelet adhesion responses to adsorbed Fg as a function of adsorption-induced unfolding.

These results call for a re-evaluation in the biomaterials field of our understanding of how Fg adsorption influences platelet response and our approach to design surfaces for improved hemocompatibility. Based on these results, studies that use adsorbed Fg as a measure of blood compatibility of biomaterials surfaces should be based on the ability of surfaces to maximally retain the native state of adsorbed Fg as opposed to focusing merely on the amount of Fg that is adsorbed. While the determination of adsorbed conformation of a protein is more difficult to assess than the adsorbed amount, this factor should correlate much more strongly with platelet response, and thus serve as a much more sensitive indicator of the tendency of a surface to resist a platelet-induced thrombotic response.

5.5 Supporting information

5.5.S.1 Effect of BSA on the adhesion of washed platelets to adsorbed Fg

In most platelet adhesion studies reported in the literature, the platelet suspension buffer generally contains 4 mg/mL BSA [201], which functions as an agent for blocking non-specific platelet adhesion interactions to exposed areas of the surface. Platelet adhesion to Fg preadsorbed on the CH_3 and OH SAMs from 0.1 mg/mL Fg bulk solutions was carried using a platelet suspension supplemented with 4 mg/mL BSA. The addition of BSA had no significant effect ($p > 0.05$) on the platelet adhesion levels, which concurs with our results using polyclonal antibodies (Figure 5.6), confirming that the contribution of non-specific interactions in platelet adhesion to adsorbed Fg was minimal.

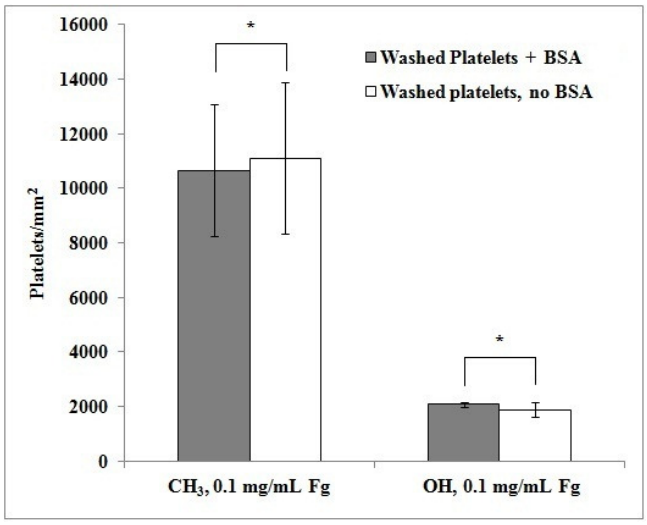

Figure 5.S.1. Adhesion of platelet suspensions supplemented with 4 mg/mL BSA (grey bars) and without 4 mg/mL BSA (white bars) to CH_3 and OH SAMs preadsorbed with 0.1 mg/mL Fg, assessed by LDH assay (n=6, mean ± 95% CI). * denotes no statistically significant difference, $p > 0.05$.

CHAPTER 6

RECEPTOR-MEDIATED RECOGNITION OF BINDING SITES EXPOSED BY ADSORPTION-INDUCED UNFOLDING UNDERLIES PLATELET ADHESION TO ADSORBED ALBUMIN

6.1 Introduction

Human albumin (Alb), with a plasma concentration of 40 mg/mL [77], is the most abundant protein in blood. Its high concentration, combined with a moderately low molecular weight (68.3 kDa) [78] causes it to be one of the first proteins to adsorb on the surface of implanted biomaterials [79]. Since Alb lacks any known amino acid sequences for binding platelet receptors, this protein has been considered to be unable to support platelet adhesion and hence is widely used for blocking non-specific platelet-surface interactions in platelet adhesion studies [80] as well as for a hemocompatible coating for biomaterial surfaces [81, 82]. In cases where platelet adhesion has been observed to occur on Alb-coated surfaces, it has generally been attributed to some non-specific process [80], such as the interaction between the platelets and exposed surface area of the substrate, as opposed to actually representing an interaction with Alb itself.

Two recent studies, however, have suggested that platelets may actually have specific mechanisms to adhere to adsorbed Alb [54, 84], and that these mechanisms may be linked to the conformational state of the protein [54]. Unfortunately, these studies did not rule out the possibility that these responses may have been due to platelet interactions with some other residual protein in the system, thus leaving this question still open to

debate. To clarify this issue, we conducted studies to definitively determine whether non-activated platelets can adhere to adsorbed Alb; and if so, whether the adhesion response is due to receptor-mediated processes that can be directly correlated with the degree of adsorption-induced unfolding of the protein, which we measured by adsorbed-state circular dichroism (CD) spectropolarimetry.

CD spectropolarimetry was first used by McMillin *et al.* [128] to examine the adsorbed conformation of fibrinogen and factor XII on quartz substrates. Subsequent CD studies by Norde and Favier [205] showed that proteins tend to undergo a loss in α-helical content upon adsorption, with this effect being diminished with increasing protein solution concentration, which translated to higher protein surface coverage. As seen in Chapter 3, our investigations into the role of surface chemistry and protein solution concentration on the adsorbed conformation of fibrinogen (Fg) and Alb, showed that both these proteins underwent a greater degree of unfolding with increasing surface hydrophobicity and decreasing solution concentration, which is in agreement with the results obtained by Norde and Favier, as well other groups via grazing-angle infrared spectroscopy [33] and total internal reflectance fluorescence (TIRF) [34]. These studies have thus demonstrated that CD spectropolarimetry is a powerful technique for examining post-adsorptive conformational changes in proteins on biomaterial surfaces.

The role of the adsorbed conformation of the protein in mediating platelet interactions has come into prominence relatively recently [54, 55, 121], whereas previously the amount of adsorbed protein has generally been considered to be the primary determinant

of the hemocompatibility of biomaterials [65, 67]. Tanaka *et al.* [55] indicated that although poly(2-methoxyethylacrylate) (PMEA) and poly(2-hydroxyethylmethacrylate) (PHEMA) adsorbed similar amounts of Fg, the PHEMA surface exhibited higher platelet adhesion compared to PMEA, which was believed to be due to a higher degree of conformational change in the adsorbed Fg (as measured by the loss in α-helix using CD) on PHEMA. In support of the findings by Tanaka et al., a recent study by Hylton *et al.* [54] also showed a strong correlation between platelet adhesion and the adsorption-induced loss in percentage α-helix in adsorbed proteins, providing further evidence that conformation is a critical determinant of the ability of an adsorbed protein layer to mediate platelet adhesion. The fact that non-activated platelets do not become activated when they interact with proteins in their native state in the bloodstream, but readily bind and become activated when they interact with adsorbed proteins such as fibrinogen, vitronectin, and fibronectin [103], also strongly suggests that the adsorption process causes structural changes in the protein leading to the exposure, or possibly even the formation of platelet-binding sites which would otherwise have remained in a non-active form in their native state.

In order to further investigate the role of adsorption-induced conformational changes in mediating platelet adhesion and whether Alb itself can support platelet adhesion by specific mechanisms, we established test conditions to provide a broad range of conformational states of adsorbed Alb following which platelet adhesion studies were carried out, including the use of several different blocking agents to verify whether or not the platelet responses were indeed being mediated by specific interactions with the

adsorbed Alb. A broad range of conformational states of the adsorbed protein was obtained by using (*i*) a wide range of surface chemistries and (*ii*) varying the Alb solution concentrations to influence the degree of adsorption-induced protein unfolding. For our surfaces, we used alkanethiol self-assembled monolayers (SAMs) on gold-coated substrates functionalized with OH, COOH, NH_2, OCH_2CF_3, and CH_3 head-groups to provide a broad range of surface hydrophobicity. These types of surfaces have been widely used in previous studies dealing with both plasma protein adsorption [51, 94, 95] and platelet adhesion [84, 97]. Alb was adsorbed to each of these surfaces from three different solution concentrations (0.1, 1.0, and 10 mg/mL) to vary the rate of protein adsorption, following which the conformation of the adsorbed Alb was assessed by adsorbed-state CD spectropolarimetry. Platelet adhesion studies were then conducted and correlated with the degree of adsorption induce Alb unfolding, with the platelet adhesion response assessed by a lactate dehydrogenase (LDH) assay and scanning electron spectroscopy (SEM). Platelet blocking studies were performed using a set of antibody, soluble peptide, and protein side-chain modification studies.

6.2 Materials and Methods

6.2.1 Gold substrates

Quartz slides (0.375” x 1.625” x 0.0625”, Chemglass) were used for CD experiments, while 18 mm square cover glasses (VWR Scientific, Catalog No. 48368-040) were used as substrates for the platelet adhesion experiments. These substrates were cleaned as

previously described in Chapter 3, prior to the deposition of chromium and gold films via thermal vapor deposition. Briefly, the substrates were immersed in a piranha solution (7:3 v/v H_2SO_4:H_2O_2) at 50°C for 30 min, followed by an RCA basic wash (1:1:5 v/v NH_4OH:H_2O_2:H_2O), and this cleaning procedure was repeated twice. The cleaned substrates were then rinsed copiously with 100% ethanol (Pharmco-Aaper; Catalog No. 111000200) and nanopure water, and finally dried using a stream of nitrogen gas.

The cleaned cover glasses were coated with a 50 Å chromium adhesion layer and 1000 Å of gold, while the quartz slides for CD were coated with 30 Å of chromium and 100 Å of gold. The thicknesses of the gold and chromium layers were verified using a DekTak profilometer and a GES5 ellipsometry (Sopra, Inc., Palo Alto, CA).

6.2.2 Formation of self-assembled monolayers (SAMs) of alkanethiols

The following alkanethiols were prepared in 100% ethanol, and used for creating the SAM surfaces, as described previously in Chapters 4 and 5:

1-Dodecanethiol (SH-$(CH_2)_{11}CH_3$; Aldrich; CH_3),

11-(2,2,2-Trifuoroethoxy) undecane-1-thiol (SH-$(CH_2)_{11}OCH_2CF_3$; Asemblon; CF_3)

11-Amino-1-undecanethiol, hydrochloride (SH-$(CH_2)_{11}NH_2HCl$; Prochimia; NH_2)

11-Mercaptoundecanoic acid (SH-$(CH_2)_{11}COOH$; Aldrich; COOH), and

11-Mercapto-1-undecanol (SH-$(CH_2)_{11}OH$; Aldrich; OH).

The gold-coated substrates were cleaned by dipping them in a modified piranha wash (4:1 v/v H_2SO_4:H_2O_2), followed by an RCA basic wash, for 1 minute each and then

rinsed copiously with 100% ethanol, prior to incubating them in 1.0 mM alkanethiol solutions for 24 h, as per the established protocols [181, 182].

After SAM formation on the gold substrates, the SAM surfaces were cleaned to remove any traces of hydrophobic contaminants on their surface prior to surface characterization and protein adsorption [99]. The CH_3 and OCH_2CF_3 SAMs were cleaned by sonication in ethanol, hexane and ethanol, and then rinsed with nanopure water. The NH_2, COOH, and OH SAMs were sonicated in ethanol, and then incubated in a 25 mM potassium phosphate buffer containing 0.005 volume % Triton-X-100 (Sigma; Catalog No. T-9284), order to block off any hydrophobic defect sites (e.g. grain boundaries), and then rinsed thoroughly with acetone, ethanol and nanopure water to remove loosely-bound Triton.

6.2.3 Contact angle goniometry

Advancing contact angle measurements on the SAM surfaces were carried out using a CAM 200 Optical Contact Angle/Surface Tension Meter (KSV Instruments Ltd.) and the CAM 200 software, as described previously in Chapter 4, with the results presented in Table 4.1.

6.2.4 Buffers

Protein adsorption experiments were carried out using a 25 mM potassium phosphate buffer (pH 7.4), which was prepared by combining appropriate amounts of the mono- and dibasic salts (Sigma-Aldrich) to maintain the pH at 7.4. This buffer is recommended for protein structural determination by CD experiments [79, 132, 193] as it permits measurement of CD spectra with minimal noise below 200 nm, especially the positive CD peaks at 193 and 195 nm, which are critical in determining the α-helix and β-sheet content of the proteins, respectively.

The platelet suspension buffer (PSB, pH 7.4) contained 137 mM NaCl, 2.7 mM KCl, 5.5 mM Dextrose, 0.4 mM sodium phosphate monobasic, 10 mM HEPES and 0.1U/mL apyrase [201]. 2.5 mM $CaCl_2$ and 1.0 mM $MgCl_2$ was added to the PSB to give a platelet suspension buffer with metal ions (PSB+MI). It should be noted that bovine serum Alb (BSA) was not added to the platelet suspension buffer as a blocking agent, as is commonly used in platelet adhesion studies. Preliminary studies were also conducted, however, with 4 mg/mL BSA added to this buffer to assess the influence of this blocking agent on the platelet adhesion response, with the use of BSA not resulting in any significantly differences (see Supporting Information, Section 6.5).

6.2.5 Protein adsorption

Human Alb (Sigma, Catalog No. A9511) was dissolved in 25 mM phosphate buffer solution (pH 7.4), to prepare the protein stock solutions, and protein adsorption was carried out as described previously in Chapters 4 and 5, at three different protein concentrations of 0.1 mg/mL, 1.0 mg/mL, and 10.0 mg/mL, so as to obtain a broad range of conformations and surface coverages of adsorbed Alb.

The cleaned SAM surfaces were then incubated in 25 mM potassium phosphate buffer (pH 7.4) in a six-well-plate (Corning Costar, Catalog No. 3506), and a suitable amount of protein stock solution was added to give the desired bulk protein solution concentration, taking care to ensure that the tip of the pipette was held below the air-water interface to avoid denaturation of the protein at this interface. The SAM surfaces were incubated in the protein solution for 2 h, after which an infinite dilution step was carried out to wash away the bulk protein solution in addition to any loosely adherent protein. Following this infinite dilution step, the SAM surfaces were safely removed from the pure buffer solution without dragging the surfaces through the denatured protein film that can be expected to present at the liquid-air interface if the protein solution had not been replaced with pure buffer prior to surface removal.

At the end of the protein incubation step, the surfaces with preadsorbed protein were either used for CD studies to analyze the structure of the adsorbed layer, or the surfaces were incubated with the platelet suspension.

6.2.6 CD studies to quantify the conformational changes and total surface coverage of Alb on SAM surfaces

The native and adsorbed secondary structures of Alb, as well as the surface coverage of adsorbed Alb, was determined using a Jasco J-810 spectropolarimeter (Jasco, Inc., Easton, MD), as described earlier in as described earlier (in Section 4.2.6). Special high-transparency quartz cuvettes (Starna Cells, Inc., Atascadero, CA) were used for determining the native solution structure of Alb, while the adsorbed structure of Alb on the SAM surfaces was determined using a special custom-designed cuvette, which maximizes the signal-to-noise ratio (as seen in Fig. 4.1). The ellipticity of the samples (θ, in mdeg) was converted to molar ellipticity (designated as [θ], with standard units of deg·cm^2/dmol) using the following equation [132, 135]:

$$[\theta] = (\theta \cdot M_0)/(10{,}000 \cdot C_{soln} \cdot L), \qquad (6.1)$$

where θ is the molar ellipticity in mdeg, L is the path length of the cuvette in cm, C_{soln} is the solution concentration of the protein in g/mL, and M_0 is the mean residue molecular weight of 118 g/mol.

Since proteins exhibit an absorbance peak at 195 nm [184], we used the height of this absorbance peak (A_{195}) for constructing a calibration curve of A_{195} vs. C_{soln} for various known concentrations of Alb, as described in Section 4.2.6. The slope of this plot is "$\varepsilon_{protein} \cdot L$" from Beer's Law, which can be written as:

$$A_{195} = \varepsilon_{protein} \cdot C_{soln} \cdot L \qquad (6.2)$$

where $\varepsilon_{protein}$ is the extinction coefficient of the protein in $mL \cdot g^{-1} \cdot cm^{-1}$ (or cm^2/g) and L is the path length of the cuvette.

The term "$C_{soln} \cdot L$" in eq. 6.2 (above) has units of g/cm^2, which is equivalent to the amount of protein adsorbed per unit area. Assuming that the absorbance is dependent on the total amount of protein present per unit area through which the beam of light passes, irrespective of whether the protein is in the solution or the adsorbed state, the calibration curve of A_{195} vs. C_{soln} can also be used for calculating the amount of Fg adsorbed per unit area on the SAMs (i.e., Q_{ads}). The validity of this method for measuring the surface coverage of adsorbed protein has been confirmed by independent measurement of Q_{ads} from the thickness of the adsorbed protein film obtained by ellipsometry (see Section 4.5.S.2) using de Feijter's formula [198].

Hence, while calculating the molar ellipticity for the adsorbed Fg layer on the SAMs, the term "$C_{soln} \cdot L$" in eq. 6.1 can be replaced by the term Q_{ads} to give the following equation:

$$[\theta] = (\theta \cdot M_0)/(10{,}000 \cdot Q_{ads}), \qquad (6.3)$$

The CD spectra (molar ellipticity vs. wavelength) thus obtained were deconvoluted using the SP-22X algorithm and analyzed using the SELCON and CONTIN/LL software packages to quantify the percentage of α-helix and β-sheet content of the native/adsorbed protein [148].

6.2.7 Platelet adhesion

Platelet adhesion was carried out, using a suspension of washed platelets from human blood. Briefly, 25.0 mL of blood was collected from volunteers as per protocols approved by the Institutional Review Board (IRB) and Institutional Biosafety Committee (IBC) at Clemson University, in BD Vacutainer tubes (Becton-Dickinson, Catalog No. 364606) containing an acid-citrated dextrose (ACD) anti-coagulant. The first few mL of blood was discarded, as it is rich in clotting factors and then the 25 mL of blood was collected.

The ACD-anticoagulated blood was centrifuged (225g, 15 min, 25°C) to generate platelet rich plasma (PRP), and platelets were separated from PRP via a gel separation method [201], using a liquid chromatography column (Sigma-Aldrich, Catalog No. C4169) containing Sepharose 2B (Sigma-Aldrich, Catalog No. 2B-300). The Sepharose column was allowed to equilibrate with PSB, after which the PRP was carefully pipetted on to the column and allowed to pass into the column. PSB was then added to the column from a reservoir, while keeping the column running. Fractions were collected from the bottom of the column, with the platelets being identified by their increased turbidity. The platelet-rich fractions were pooled, and platelet concentration was measured using a Beckman Coulter Z2 Coulter Particle Count and Size Analyzer (Beckman Coulter, Fullerton, CA). The platelet count was adjusted to 10^8 platelets/mL with PSB, and $CaCl_2$ and $MgCl_2$ were added to give 2.5 mM and 1.0 mM concentrations of these salts, respectively. Platelet suspension was allowed to rest for 30 min, and the platelet adhesion step was carried out on the protein-coated SAMs for 1 h at 37°C.

The platelet suspension was then aspirated from each well at the end of the platelet adhesion step, and the non-adherent platelets were rinsed away by filling and aspirating the wells five times with PBS. The substrates were then removed to a fresh well-plate, for carrying out the lactate dehydrogenase (LDH) assay to quantify the platelet adhesion levels. Additionally, the morphology of the adherent platelets was visualized using scanning electron microscopy (SEM).

6.2.8 SDS-PAGE analysis of platelet suspension

The platelet suspensions obtained from two separate gel separation runs were centrifuged at 1200 rpm, 1500 rpm, and 1800 rpm, and the supernatant was aspirated and analyzed via sodium dodecyl sulfate polyacrylamide gel electrophoresis (SDS-PAGE) for any traces of residual plasma proteins. Silver staining was done using a Silver SNAP Stain Kit II (Pierce, Rockford, IL), which provides a highly sensitive detection system for sub-nanogram levels of proteins. This is essential in ensuring that the platelet suspension was free of any residual plasma proteins, which may potentially complicate our analysis by displacing the preadsorbed protein and then binding platelets.

6.2.9 Quantification of platelet adhesion using lactate dehydrogenase (LDH) assay

The platelet adhesion levels on the Alb-coated SAMs was quantified by measuring the lactate dehydrogenase (LDH) released when the adherent platelets were lysed with a

Triton-PSB buffer, (2% v/v Triton-X-100 in PSB) using a CytoTox96® Non-Radioactive Cytotoxicity Assay (Promega Corporation, Madison, WI), as indicated in Section 4.2.8. A calibration curve was constructed using a known number of platelets, counted using a Beckman Coulter Z2 Coulter Particle Count and Size Analyzer (Beckman Coulter, Fullerton, CA), and the platelet adhesion on the SAM surfaces was determined from this calibration curve.

6.2.10 Morphological analysis of adherent platelets using scanning electron microscopy (SEM)

The samples for SEM were fixed, as described in section 4.2.10. Briefly, the samples were immersed in a special fixing buffer (3% glutaraldehyde, 0.1 M sodium cacodylate, pH 7.4), for 30 min at room temperature, after which they were rinsed with PBS thrice. The fixed samples were then incubated in ascending ethanol:water mixtures (50%, 60%, 70%, 80%, 90% and 99% ethanol) for 10 min to dehydrate them. These samples were finally treated with 0.02 mL of hexamethyldisilazane (Sigma) and allowed to dry overnight. The morphology of the adherent platelets was examined using a FESEM-Hitachi S4800 scanning electron microscope (Electron Microscopy Facility, Advanced Materials Research Laboratory, Clemson University, Pendleton, SC).

6.2.11 Study using polyclonal antibodies against Alb

Polyclonal antibodies against human Alb (Anti-Alb Rabbit pAb; Calbiochem, La Jolla, CA) at a concentration of 4 µg/mL were incubated for 30 min at room temperature, on the Alb surfaces in order to inhibit Alb recognition by the platelet receptors. As a control, SAM surfaces coated with Fg (FIB 3; plasminogen, von Willebrand factor, and fibronectin depleted; Enzyme Research Laboratories, South Bend, IN) were incubated with 4 µg/mL of the anti-Alb polyclonal antibodies, and platelet adhesion was quantified using an LDH assay.

6.2.12 Study using polyclonal antibodies against Fg

Polyclonal antibodies against human Fg (Anti-fibrinogen Rabbit pAb; Calbiochem, La Jolla, CA) at a concentration of 4 µg/mL were incubated for 30 min at room temperature, on the Alb coated surfaces in order to verify whether the inhibition of platelet-Alb interactions was due to the effects of the anti-Alb polyclonal antibodies or the adsorption of these antibodies on bare surface exposed between the adsorbed Alb molecules. Platelet adhesion was characterized as described above.

6.2.13 Inhibition of platelet-protein interactions using Arg-Gly-Asp (RGD)-containing peptides

The platelet suspension was incubated with 300 μM of an Arg-Gly-Asp-Ser (RGDS) peptide (Calbiochem, La Jolla, CA) for 30 min at room temperature, in order to inhibit interactions between RGD-binding platelet receptors and Alb. These RGDS-treated platelets were then allowed to adhere on the Alb-coated SAM surfaces for 1h at 37°C, after which the platelet adhesion was quantified using an LDH assay and the morphology of the adherent platelets was examined using SEM.

Platelets incubated with 300 μM of a control Arg-Gly-Glu-Ser (RGES) peptide (American Peptide Company, Sunnyvale, CA) were allowed to adhere on the SAM surfaces preadsorbed with Alb.

6.2.14 Modification of Arg residues in Alb using 2,3-butanedione

Site-specific modification of R residues in Alb was carried out using 2,3-butanedione (Fluka), as described previously [177]. Briefly, an Alb solution was modified by addition of suitable amount of 2, 3-butanedione to borate buffer to give a final concentration of 50 mM of the modifying agent. The modified protein samples were dialyzed for 12 h against 25 mM phosphate buffer, and then analyzed for Arg modification via a protocol described previously [99], using electrospray ionization mass spectrometry (ESI-MS) performed at the Clemson University Genomics Institute. Additionally, we used CD

spectropolarimetry to analyze the secondary structure of the modified Alb in solution and compared it with that of unmodified Alb.

6.2.15 Platelet adhesion to SAM surfaces coated with Alb with modified arginine residues

Alb adsorption was carried out, after which the arginine residues exposed in the adsorbed Alb layer were neutralized by 2, 3-butanedione, using the protocol described above. After washing away the excess butanedione, the surfaces were incubated with platelets, and the platelet adhesion levels were quantified using an LDH assay, with the morphology of the being observed using SEM.

6.2.16 Statistical analysis

The results we present are the mean values with 95% confidence intervals (CI). Statistical significance of differences between mean values for different samples and conditions was evaluated using a Student's t-test, with $p \leq 0.05$ considered as statistically significant.

6.3 Results and Discussion

6.3.1 Circular dichroism studies on native and adsorbed Alb

The secondary structural content of native and adsorbed Alb on the SAM surfaces as a function of surface chemistry and solution concentration, determined via CD spectropolarimetry, are presented in Figure 6.1. These results clearly illustrate the higher degree of adsorption-induced conformational changes (i.e., loss of α-helix accompanied by increased β-sheet) as the surfaces became more hydrophobic and when the protein was absorbed from a lower solution concentration, with the combined variation of both surface chemistry and solution concentration effectively providing a wide range of conformational states of the adsorbed Alb.

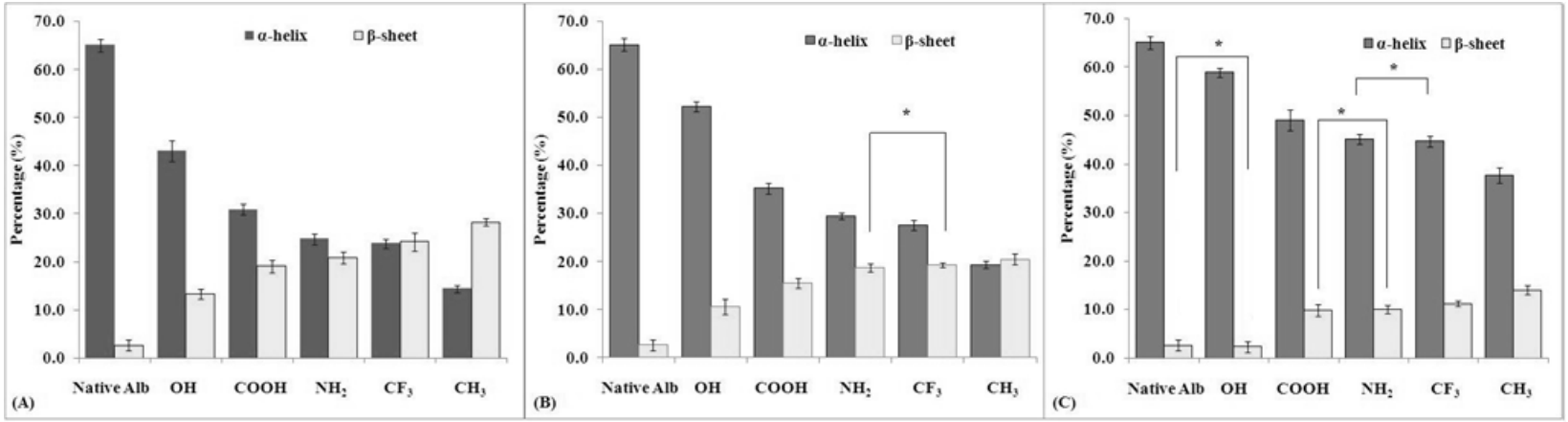

Figure 6.1. Secondary structure of adsorbed Alb on SAM surfaces at (A) 0.1 mg/mL, (B) 1.0 mg/mL and (C) 10.0 mg/mL bulk solution concentrations (n= 6, mean ± 95% CI). * denotes difference not statistically significant, $p > 0.05$.

The surface coverage of albumin adsorbed on the SAMs from the three different bulk concentrations was calculated using the height of the absorbance peak at 195 nm (A_{195}), and is shown in Table 6.1. The surface coverage at 0.1 and 1.0 mg/mL bulk Alb solution concentration lie between the theoretical monolayer surface coverage values of 0.72 $\mu g/cm^2$ for end-on adsorption and 0.21 $\mu g/cm^2$ for side-on adsorption [34], assuming that the Alb molecule has dimensions of 4.0 x 4.0 x 14 nm^3 [50]. The surface coverage at 10.0 mg/mL Alb solution concentration was well beyond the theoretical values for monolayer surface coverage, indicating multilayer adsorption. These results clearly indicate that the surfaces are saturated with Alb, and the amount of Alb adsorbed increases with increasing hydrophobicity of the SAM surfaces. Significantly greater Alb adsorption also occurred on a given SAM surface with increasing Alb solution concentration. This can be explained by the fact that the rate of transport of the protein molecules to the surface increases as solution concentration increases, as a result of which the molecules that adsorb from higher concentration have less time to unfold and spread before the surface becomes saturated with protein [31, 34, 39].

Table 6.1. Amounts of Alb adsorbed on SAM surfaces from 0.1, 1.0 and 10.0 mg/mL bulk solution concentrations (n= 6, mean ± 95% CI).

Albumin concentration [mg/mL]	OH [μg/cm^2]	COOH [μg/cm^2]	NH_2 [μg/cm^2]	CF_3 [μg/cm^2]	CH_3 [μg/cm^2]
0.1 mg/mL	0.25 ± 0.01	0.28 ± 0.01	0.46 ± 0.03	0.40 ± 0.02	0.54 ± 0.03
1.0 mg/mL	0.26 ± 0.01	0.29 ± 0.01	0.49 ± 0.02	0.44 ± 0.01	0.58 ± 0.01
10.0 mg/mL	1.77 ± 0.05	2.23 ± 0.09	2.26 ± 0.19	2.55 ± 0.24	2.71 ± 0.18

6.3.2 Platelet adhesion to adsorbed Alb

A suspension of washed platelets was used for the platelet adhesion runs. Prior to carrying out the platelet adhesion experiments, it was essential to check for traces of residual proteins that could potentially adsorb onto and/or displace the preadsorbed Alb from the SAM surfaces through the Vroman effect [204]. As was shown in Chapter 5 in Fig. 5.3, sodium dodecyl sulfate polyacrylamide gel electrophoresis (SDS-PAGE) analysis performed on supernatant fluid from centrifugation of the platelet suspensions showed no detectable levels of proteins in the suspensions centrifuged at 1200 rpm and 1500 rpm. Since activated platelets are likely to release proteins from their granules into the suspension, this also indicates that the platelets in suspension were not activated during the gel separation process through the Sepharose column, or during any handling prior to the platelet adhesion step.

Platelet adhesion levels on the SAM surfaces preadsorbed with Alb are shown in Figure 6.2. It is clearly evident that platelet adhesion did occur on these surfaces, with

platelet adhesion being strongly influenced by both surface chemistry and the solution concentration from which the Alb was adsorbed. Platelet adhesion levels followed the same general trends observed for the adsorption-induced conformational changes in Alb (Figure 6.1); i.e., increasing with increasing hydrophobicity of the surfaces and decreasing Alb solution concentration.

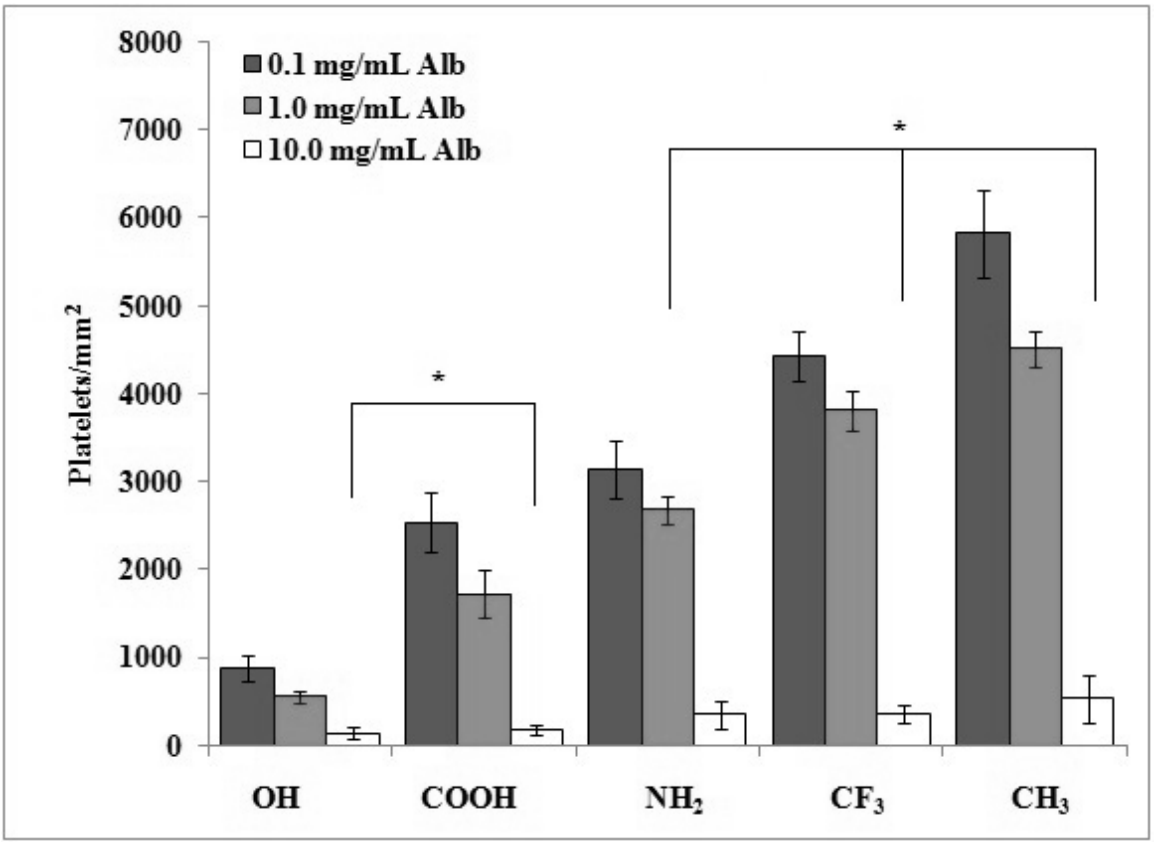

Figure 6.2. Platelet adhesion on SAM surfaces preadsorbed with Alb from bulk solutions of 0.1 mg/mL, 1.0 mg/mL and 10.0 mg/mL (n=6, mean ± 95% CI). * denotes no statistically significant difference, $p > 0.05$.

To investigate the relationship between platelet adhesion and the degree of adsorption-induced protein unfolding, the platelet adhesion levels (Figure 6.2) were plotted as a function of the extent of loss of α-helix in Alb measured on these surfaces, as presented in Figure 6.3A. As is clearly shown in this figure, the platelet adhesion response correlated strongly (r^2 = 0.92) with the degree of conformational change in adsorbed Alb when the percentage of α-helix loss was greater than about 34%. For levels of unfolding less than this threshold value, platelet adhesion was negligible, with the slope of the regression line for this region of the plot not being significantly different than zero (p = 0.60). Thus, below this critical level of unfolding, the layer of adsorbed Alb can be considered to be 'passive' in terms of its ability to adhere platelets, which supports the conventional understanding that Alb functions as a blocking agent for non-specific interactions [80]. However, once this critical level of unfolding was exceeded, platelets readily adhered to the adsorbed Alb, with the adhesion response increasing linearly as the degree of unfolding increased. Hence, this suggests that platelet binding domains in Alb are being exposed and/or formed beyond this critical level of unfolding, thereby inducing the platelet adhesion response.

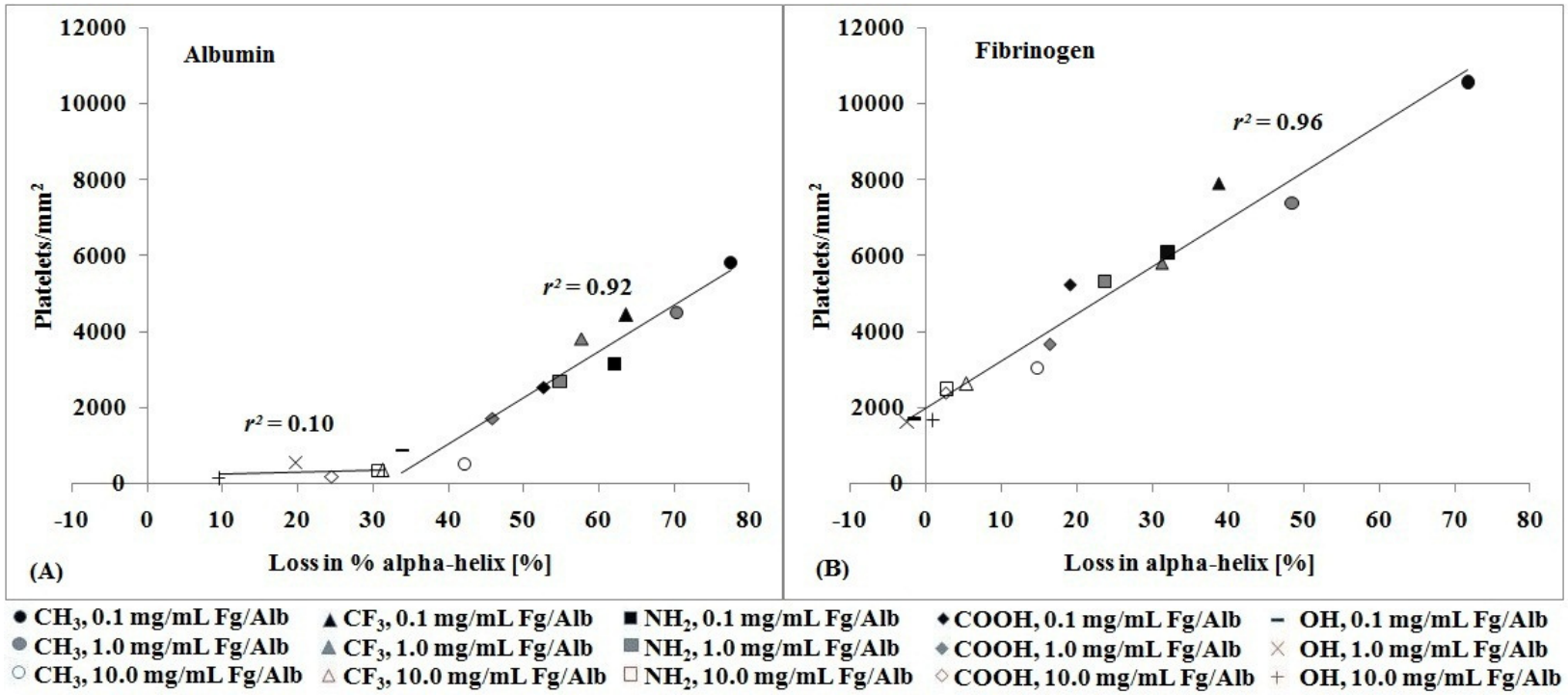

Figure 6.3. Platelet adhesion to (A) Alb and (B) Fg on the SAM surfaces as a function of the degree of loss in α-helix (Each point represents the mean of six values for each SAM surface). Fg data is provided for comparison to the Alb results and is reproduced from Fig. 5.5B.

A particularly intriguing result from this study is that, as seen in Figure 6.3, beyond this critical level of unfolding, the increase in platelet adhesion as a function of continued unfolding of the Alb (Fig. 6.3A) occurred in a manner very similar to Fg (Fig. 6.3B), which we measured in a related set of experiments listed in Chapter 5. This finding suggests that, beyond this critical level, platelet adhesion to both of these proteins as a function of the degree of adsorption-induced unfolding may be due to similar mechanisms. Given the fact that there are no known platelet binding sites in albumin, this similarity actually suggests that the platelet binding response to adsorbed Fg as it unfolds may be mediated by processes that are not associated with currently known platelet binding motifs in Fg, but rather are being driven by the exposure and/or formation of new platelet receptor recognition sites similar to the process that is occurring in Alb.

6.3.3 Delineating the role of RGD-specific receptors in platelet-Alb interactions

To probe the molecular mechanisms underlying the observed platelet adhesion response, four independent blocking studies were conducted for Alb adsorbed from the most dilute Alb solution (0.1 mg/mL) on the two SAM surfaces representing the extremes in hydrophobicity (OH and CH_3 SAMs).

First, in order to confirm that platelets were actually adhering to the adsorbed Alb and not to residual proteins that may have adsorbed from the platelet suspension during the platelet adhesion process (e.g., proteins released from the platelets granules), the adsorbed Alb layer was treated with polyclonal antibodies against human Alb (pAb-Alb)

prior to performing the platelet adhesion studies. These pAb-Alb were then also used to treat adsorbed Fg as a negative control. Secondly, to ensure that the effect of the pAb-Alb was due to their specificity towards Alb, and not due to minimization of interactions between platelets and bare SAMs as a result of the adhesion of these antibodies on the surface of the SAMs (i.e., in the gaps possibly present between adjacent adsorbed Alb molecules), the Alb-coated SAMs were treated with anti-Fg polyclonal antibodies (pAb-Fg) before exposure to the platelet suspension. Thirdly, the platelet suspensions were treated with RGDS peptides prior to exposure to the Alb-coated SAM surfaces, with RGES used as a control, to determine whether platelet adhesion was being mediated by RGD-specific receptors. Finally, the solvent-accessible arginine (R) residues in preadsorbed Alb were chemically modified using 2,3-butanedione [174, 175] prior to conducting the platelet adhesion studies, to determine if they were involved in the platelet binding motifs that were being exposed or formed as a function of the adsorption-induced Alb unfolding. Control studies were conducted by using 2,3-butanedione to modify the R residues in Alb in solution, followed by analysis via electrospray ionization mass spectrometry (ESI-MS) to confirm that the modification procedures actually caused the intended site-specific modification of the R residues. In addition, CD studies were conducted to determine the effect of this chemical modification process on the conformation of Alb in both its soluble and adsorbed states. The results of these four studies are shown in Figure 6.4.

As seen in Figure 6.4, the pAb-Alb nearly completely inhibited platelet adhesion to preadsorbed Alb on both the CH_3 and OH SAMs, while not significantly affecting

platelet adhesion to either the CH_3 or OH SAMs preadsorbed with Fg. Also, the pAb-Fg did not inhibit platelet adhesion to adsorbed Alb, providing further proof that the pAb-Alb were effective in blocking platelet adhesion to adsorbed Alb due to their specificity towards Alb and not due to their adsorption on bare surface exposed between the adsorbed Alb molecules on the SAMs.

Treatment of the platelets with the RGDS peptides resulted in a substantial decrease in platelet binding, with 60.2% and 48.0% reductions in platelet adhesion to the adsorbed Alb on the CH_3 and OH SAM surfaces, respectively; while the RGES peptides had no significant effect. These results indicate that non-RGD specific platelet receptors, which account for nearly 50% of the platelet response on both SAM surfaces, mediate the adhesion of RGDS-treated platelets to adsorbed Alb. When these results were compared with those obtained from our previous related study for RGDS-based inhibition of platelet adhesion to Fg (see Chapter 5, Section 5.3.4), it was surprising to find that for a given SAM surface, the levels of inhibition observed were nearly identical for both Alb and Fg (58.3% for Fg adsorbed on a CH_3 SAM, and 45.7% for Fg adsorbed on the OH SAM). These results further support the possibility of platelet adhesion to Fg and Alb as a function of their unfolded state is mediated by similar specific mechanisms.

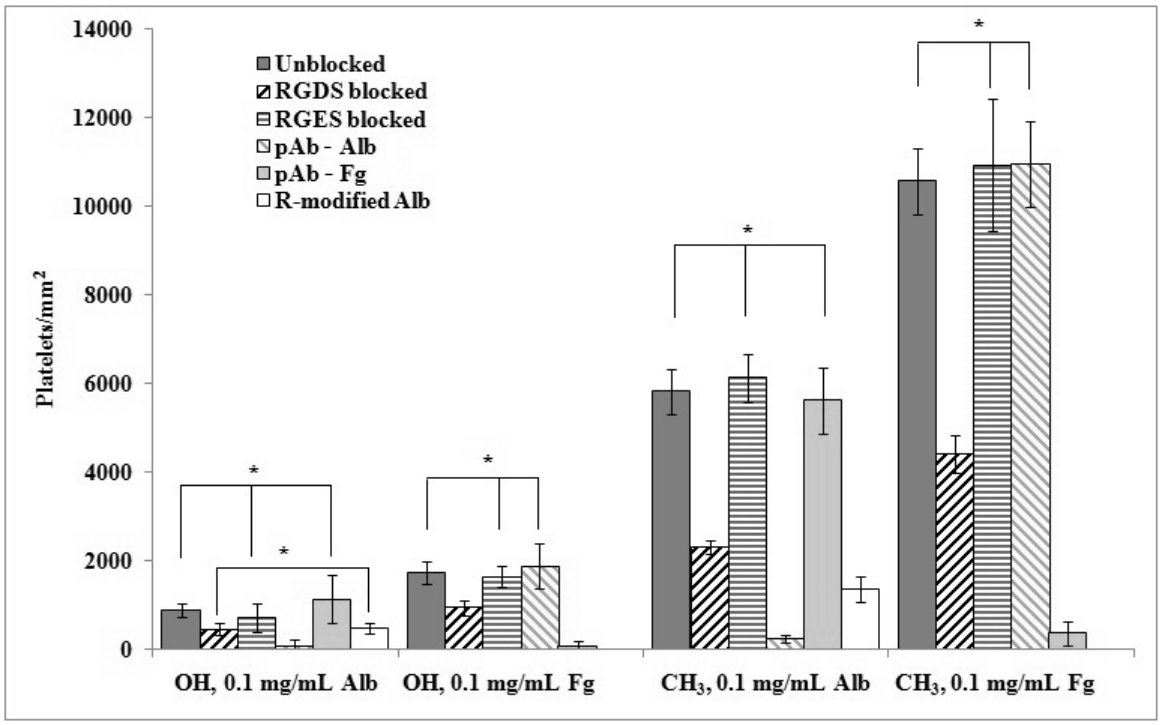

Figure 6.4. Platelet adhesion on SAM surfaces preadsorbed with Alb and Fg from 0.1 mg/mL solutions under various blocking conditions. The blocking treatments included RGDS and RGES peptides, as well as polyclonal antibodies against Alb (pAb vs. Alb) and Fg (pAb vs. Fg) (n=6, mean ± 95% CI). * denotes no statistically significant difference, $p > 0.05$. Fg data is provided for comparison to the Alb results and is reproduced from Fig. 5.6.

Chemical modification of R residues of the preadsorbed Alb also significantly reduced platelet adhesion, with the reduction on the OH SAMs not being significantly different ($p = 0.18$) than the response from the RGDS peptides, while the reduction on the CH_3 SAMs was significantly greater ($p < 0.05$) than the reduction from treatment with

RGDS. This may be due to the fact that R- modification is irreversible, while binding of the RGDS peptide by the platelet receptors represents a reversible, competitive binding situation, with some level of RGD-mediated platelet adhesion thus still being expected to occur in the presence of the RGDS peptide. The ESI-MS results confirmed that the chemical modification was specific to only the R residues, with all R residues in the Alb in its solution state being modified under the applied conditions. Table 6.2 presents the results from the CD analyses of Alb before and after R-modification, which confirms that this chemical treatment had minimal influence on the secondary structure of the Alb in either its solution or its adsorbed condition. CD spectra comparing the unmodified and R-modified Alb in solution are presented in Figure 6.5.

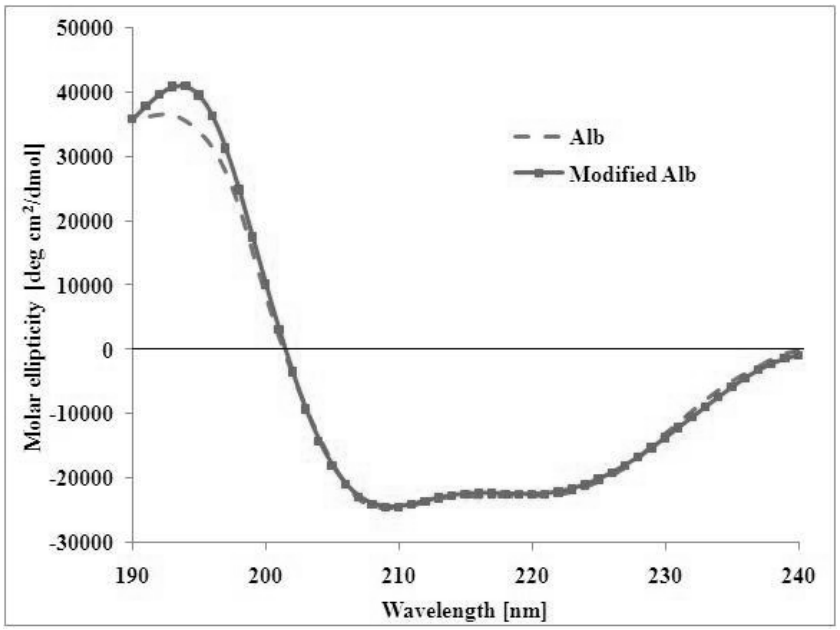

Figure 6.5. Representative CD spectra for solution structure of normal native Alb and Alb with modified arginine residues.

Table 6.2. Comparison of secondary structural composition of unmodified Alb and Alb with arginine residues modified using 2, 3-butanedione, in solution and after adsorption on the CH_3 and OH SAMs (n= 6, mean ± 95% CI).

Sample	α-helix (%)	β-sheet (%)
In solution		
Human Alb unmodified	66.5 ± 1.5	1.5 ± 0.7
Human Alb with R-modification	65.8 ± 0.9	0.9 ± 0.3
After adsorption		
CH_3, 0.1 mg/mL Alb-unmodified	14.4 ± 0.7	28.3 ± 0.7
CH_3, 0.1 mg/mL Alb-modified	15.7 ± 1.3	28.6 ± 1.5
OH, 0.1 mg/mL Alb-unmodified	43.1 ± 2.1	13.4 ± 1.1
OH, 0.1 mg/mL Alb-modified	42.6 ± 1.4	12.3 ± 0.5

Overall, these results indicate that platelets are able to adhere to adsorbed Alb and that adhesion is strongly correlated with the adsorption-induced loss of α-helix in Alb (Figure 6.4A). The adhesion is substantially due to a specific binding mechanism involving RGD-specific receptors on non-activated platelets that are able to recognize motifs involving R residues that are either exposed and/or formed in Alb after it undergoes a critical degree of adsorption-induced unfolding.

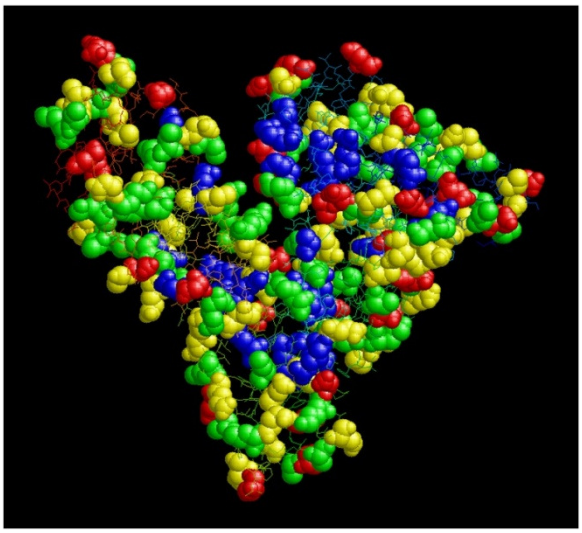

Figure 6.6. Molecular structure of human serum Alb (PDB ID: 1E7H) [78] with charged residues displayed in spacefill mode and all other residues displayed in wireframe. Arginine (blue), lysine (green), aspartic acid (red), and glutamic acid (yellow). Figure was generated using RASMOL.

The prominent role played by RGD-binding platelet receptors and the R residues of Alb in mediating platelet adhesion to adsorbed Alb is intriguing, considering the conventional view that Alb does not support platelet adhesion through specific binding mechanisms. As shown in Figure 6.6, Alb contains a large number of charged amino acids (24 arginine, 59 lysine, 35 aspartic acid, and 62 glutamic acid residues). We hypothesize that in its native state, these residues are not structured in a manner to be recognized by platelet receptors, but after undergoing a critical level of adsorption-induced unfolding, oppositely charged pairs of residues within this protein become spatially positioned such that they become recognizable to RGD-specific receptors in the platelets similar to an RGD motif. We further hypothesize that the incidence of this

increases with increased degree of conformational rearrangement, thus resulting in the linear relationship between platelet adhesion and the percent loss in α-helix, observed in Figure 6.4A.

Scanning electron microscopy (SEM) analyses were conducted to assess the effect of RGDS peptides and the R modification of adsorbed Alb on the morphology of adherent platelets on the OH and CH_3 SAMs with preadsorbed Alb. Figures 6.7A and 6.7D, show that the platelets adherent on the CH_3 and OH SAMs preadsorbed with Alb underwent a similar moderate degree of spreading and extension of filopodia on both surfaces, even though platelet adhesion on the CH_3 SAM was more than six times higher than on the OH SAM. These results indicate that the adhesion mechanisms were similar and induced a moderate level of platelet activation on both surfaces. However, when the platelets were treated with an RGDS peptide prior to the platelet adhesion (Figures 6.7B and 6.7E), which resulted in about 50-60% reduction in adhesion, they exhibited a distinctly different morphology, with much less spreading and minimal extension of filopodia. These results suggest that the mechanism of adhesion to RGDS-treated platelets was different from that of untreated platelets. As shown in Figures 6.7C and 6.7F, platelets adherent on the adsorbed Alb with R modification exhibited morphologies similar to the RGDS-treated platelets. This supports a hypothesis that R modification of adsorbed Alb results in blocking the same platelet receptors as those blocked by the RGDS peptides.

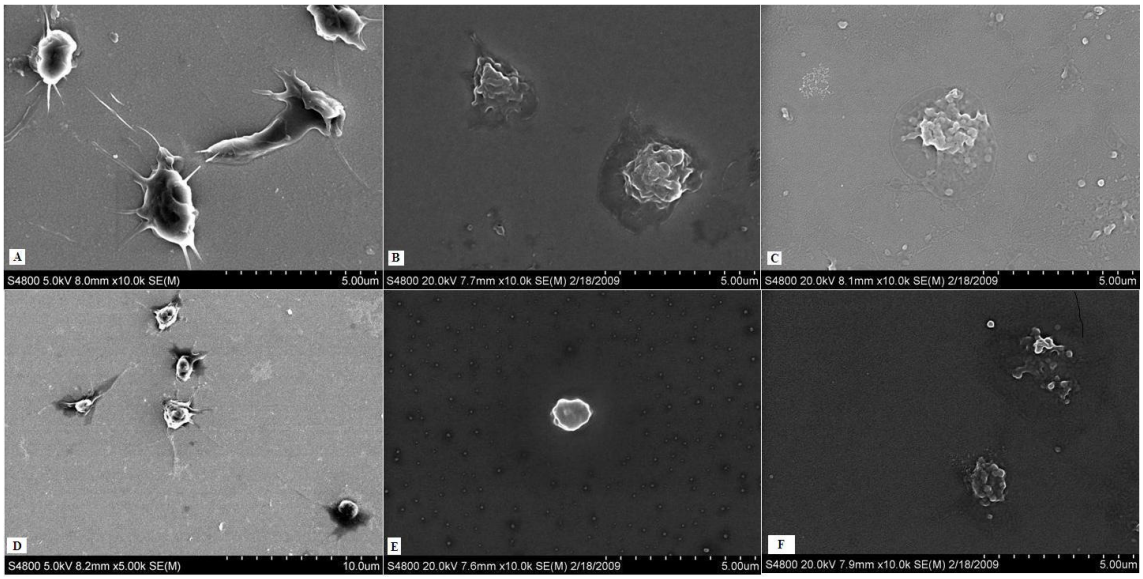

Figure 6.7. Platelet adhesion to the CH_3 (top row) and OH SAMs (bottom row) preadsorbed with 0.1 mg/mL Alb, under different blocking conditions: (A,D) unblocked Alb, (B,E) platelets treated with RGDS, and (C,F) adsorbed Alb layer treated with 2,3-butanedione to neutralize Arg.

The morphology of RGDS-treated platelets adherent to adsorbed Alb on the CH_3 and OH SAMs was strikingly similar to those observed to be adherent to Fg in the presence of RGDS on the same SAMs (see Section 5.3.5), as seen in Figure 6.8. This provides further evidence that similar adhesion mechanisms are involved in platelet adhesion to both Alb and Fg as a function of their degree of adsorption-induced unfolding on a surface.

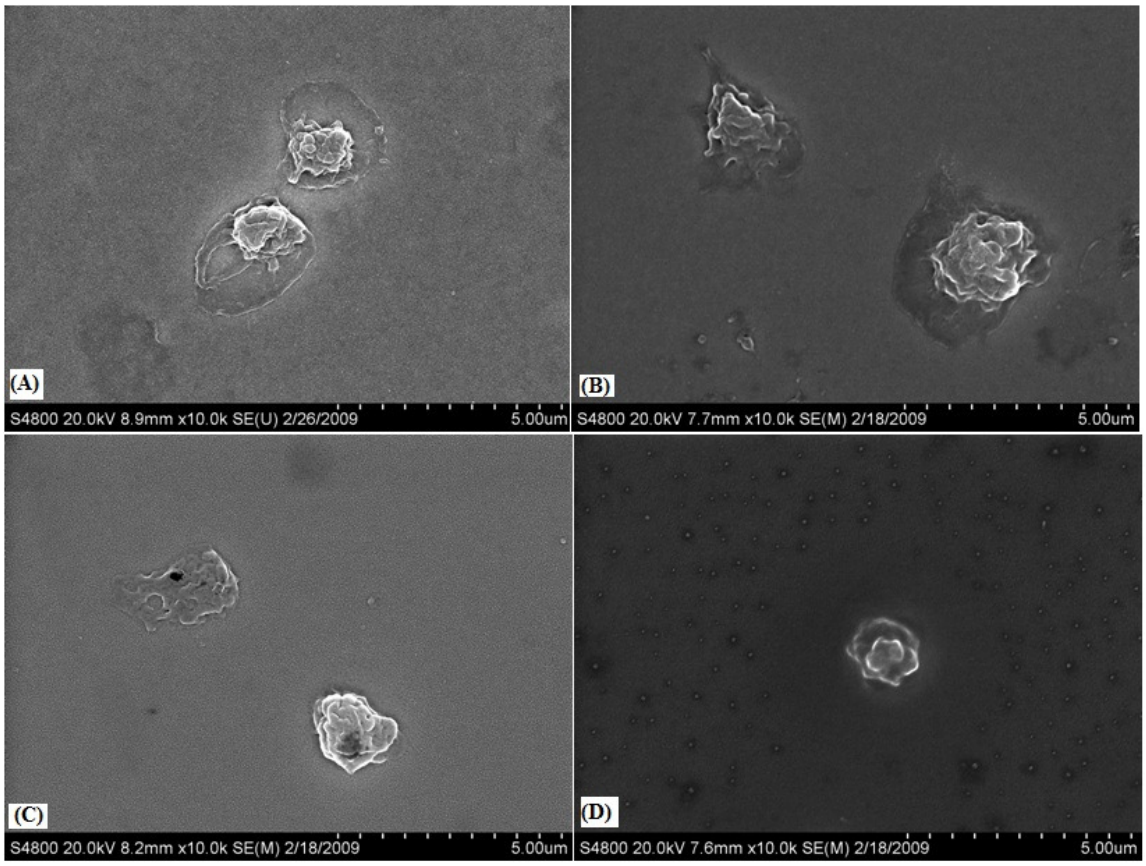

Figure 6.8. Morphology of RGDS-treated platelets adherent to CH_3 (top row) and OH SAMs (bottom row), preadsorbed with Fg (A,C) and Alb (B,D). Fg data is provided for comparison to the Alb results and is reproduced from Fig. 5.6.

Taken altogether, the SEM results strongly suggest that there are at least two distinct sets of receptors associated with platelet adhesion to sites in adsorbed Alb that are exposed and/or formed following adsorption-induced unfolding beyond a critical degree; one RGD-specific receptor that recognizes a protein motif involving R that mediates both adhesion along with a moderate degree of activation, and another that induces platelet

adhesion with minimal activation. We plan to attempt to identify these receptors and to further examine the mechanisms underlying their interactions with adsorbed Alb in future investigations.

6.4 Conclusions

The results from these studies conclusively demonstrate that platelets adhesion to adsorbed Alb is substantially mediated by interactions between RGD-specific platelet receptors and R residues in the adsorbed Alb, beyond a critical level of adsorption-induced protein unfolding. Additionally, we provide evidence that the mechanisms underlying platelet adhesion to Fg and Alb as a function of the degree of adsorption-induced unfolding are similar in nature, with platelet adhesion increasing as a function of the degree in adsorption-induced unfolding for both proteins (beyond a critical degree of unfolding of the Alb) and RGDS-treatment induced similar levels of inhibition of platelet adhesion to both proteins, with similar morphology of the adherent RGDS-treated platelets. Overall, these results suggest that platelet adhesion to adsorbed fibrinogen, and possibly many other adsorbed proteins, involves mechanisms that may be quite different than currently understood. Thus, there is still much to learn about the molecular mechanisms that mediate the interactions of platelets with adsorbed proteins and how to control these interactions to improve the blood compatibility of biomaterials used in cardiovascular applications.

6.5 Supporting Information

6.5.S.1 Platelet adhesion with bovine serum albumin (BSA) added to the platelet suspension buffer

Platelet adhesion was carried out on the CH_3 and OH SAMs preadsorbed with Alb from 0.1 mg/mL bulk solutions, using a platelet suspension supplemented with 4.0 mg/mL BSA. As seen in Figure 6.5.S.1, there was no significant change ($p > 0.05$) in the platelet adhesion levels, which concurred with the results obtained using polyclonal antibodies (Figure 6.4), confirming that non-specific interactions had minimal role in mediating platelet adhesion to Alb.

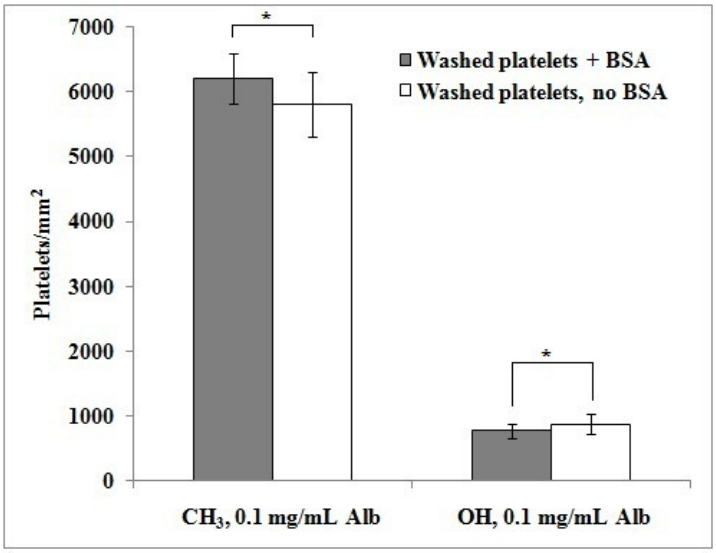

Figure 6.S.1. Adhesion of platelet suspensions supplemented with 4.0 mg/mL BSA (grey bars) and without BSA (white bars) to CH_3 and OH SAMs preadsorbed with 0.1 mg/mL Alb, assessed by LDH assay (n=6, mean ± 95% CI). * denotes no statistically significant difference, $p > 0.05$.

CHAPTER 7

DELINEATING THE ROLES OF THE $\alpha_{IIb}\beta_3$ AND GPIb-IX-V PLATELET RECEPTORS IN MEDIATING ADHESION TO ADSORBED FIBRINOGEN AND ALBUMIN

7.1 Introduction

Platelets respond to minimal stimuli, and adhere and activate upon contact with thrombogenic surfaces such as the exposed endothelium/subendothelium at vascular injury sites, as well as on synthetic surfaces [1]. These interactions involve the binding of platelet agonists to receptors on the surface of the platelet plasma membrane [206]. Agonists include plasma proteins (e.g., thrombin, fibrinogen and von Willebrand factor), components of the vascular wall (such as collagen), as well as molecules released by inflammatory cells and platelets (such as ADP and serotonin). In order to understand the factors underlying platelet interactions with adsorbed proteins, it is imperative to examine the role of the principal platelet receptors involved in adhesion and signaling. These receptors function in positive and negative feedback loops, playing critical roles in platelet function, thereby providing deeper insights into the mechanisms mediating the platelet response [207].

The $\alpha_{IIb}\beta_3$ integrin, which is also known as the GPIIb/IIIa receptor, is the most abundant platelet receptor with 60,000-80,000 copies per platelet [73], in addition to an

intracellular pool which becomes exposed on the platelet surface upon activation [208]. $\alpha_{IIb}\beta_3$ mediates the adhesion, aggregation and spreading of platelets at vascular injury sites upon activation, as well as during pathological thrombus formation [208, 209], as a result of which it is considered to be the main platelet receptor involved in regulating thrombosis and hemostasis [60]. Glanzmann's thrombasthenia is a blood disorder associated with impaired platelet adhesion and aggregation as a result of the lack or dysfunction of the $\alpha_{IIb}\beta_3$ platelet integrin [210], illustrating its critical role in mediating the platelet response.

$\alpha_{IIb}\beta_3$ binds several ligands, such as fibrin(ogen) (Fg), von Willebrand factor (vWf), fibronectin (Fn) and vitronectin (Vn), which contain the arginine-glycine-aspartic acid (RGD) amino acid sequence. In their resting, non-activated state, the $\alpha_{IIb}\beta_3$ receptor is in a 'low-affinity' state with its RGD-binding site hidden. Upon agonist-induced platelet activation, the receptor changes to its 'high-affinity' state as a result of 'inside-out' signaling events, leading to conformational changes in the platelet receptor which causes the unmasking of the RGD-binding site, thereby mediating platelet adhesion [73].

The GPIb-IX-V receptor complex (25,000 copies per platelet) mediates the initial adhesion of platelets to the vessel wall under conditions of high shear via interactions with the A1 domain of vWf in the exposed extracellular matrix at vascular injury sites [69, 71]. However, this interaction is insufficient for stable adhesion of the platelets and is characterized by its rapid dissociation rate, as a result of which they cause platelets to roll or translocate along the vessel wall under normal flow conditions [70]. Therefore, the

primary role of this receptor is to reduce the velocity of platelets in flowing blood and recruit them to vascular injury sites, thereby facilitating their interactions with the thrombogenic surface via other platelet receptors, notably $\alpha_{IIb}\beta_3$.

Although the exact nature of GPIb-vWf interactions remain to be completely elucidated, the process has been shown to involve conformational changes in the GPIb-IX-V receptor complex, as well as the vWf [72]. A recent study by Lecut *et al.* [111] showed that the GPIb-IX-V receptor complex does not have a role in platelet integrin activation, although it is critical for platelet adhesion to collagen, thereby illustrating its essential role as an adhesive, non-activation receptor. Studies using inhibitory antibodies have narrowed down the vWf binding epitopes on GPIb to amino acids 1-81 and 201-268 [165, 166]. Vanhoorelbeke *et al.* [211] recently reviewed the potential of GPIb-IX-V as an antithrombotic target, highlighting its role in binding other ligands such as α-thrombin, factor XII (FXII), factor XI (FXI), high molecular weight kininogen (HMWK), macrophage integrin Mac-1 and P-selectin. This suggests that GPIb-IX-V receptors may play a more important role in mediating platelet interactions than has been previously thought.

Our results (illustrated in Chapters 5 and 6) indicate that the platelet adhesion mechanisms to adsorbed Fg and more importantly albumin (Alb) are mediated by specific mechanisms involving RGD- and non-RGD-specific receptor sets. Using chemical modification of Arg residues in the adsorbed Alb layer, we have shown that the RGD-specific receptors interact with Arg residues, confirming the specific mode of platelet-Alb

interactions. This led us to hypothesize that since Alb contains a large number of charged residues (59 Lys, 24 Arg, 35 Asp and 62 Glu) [192], beyond a critical degree of adsorption-induced unfolding, oppositely-charged residues may become spatially oriented such that they form an RGD-like motif, which then becomes recognizable to the RGD-specific platelet receptors. We further hypothesized that the RGD-specific receptor set mediates the adhesion and activation of platelets, while the non-RGD-specific receptor set mediates adhesion with little/no platelet activation. The strong correlation between the platelet adhesion levels and the degree of protein unfolding as measured by the loss of α-helix (Fig. 6.3) also raised the question as to whether the platelet adhesion response as a function of post-adsorptive unfolding was mediated by the same adhesion mechanisms and/or platelet receptors.

Since the $\alpha_{IIb}\beta_3$ platelet receptor binds to ligands such as Fg, vWf, Fn and Vn, which contain the RGD sequence, we hypothesized that it likely plays the role of the RGD-specific receptor set. The GPIb-IX-V receptor complex was likely the non-RGD-specific set, since it has been shown to mediate platelet adhesion without activation [111]. Aggrastat (trade name for tirofiban) is a peptidomimetic $\alpha_{IIb}\beta_3$ antagonist which has been shown to inhibit platelet binding to collagen, as well as platelet activation as measured by P-selectin exposure [157]. Studies using monoclonal antibodies 24G10 (targeting residues 1-81 of GPIb) and 6B4 (targeting residues residues 201-268 of GPIb) have shown that these antibodies are effective in inhibiting GPIb-vWf interactions [166]. A recent study that examined the joint inhibition of the $\alpha_{IIb}\beta_3$ platelet integrin and the GPIb-

IX-V receptor complex showed that this strategy was effective in preventing arterial thrombosis [169].

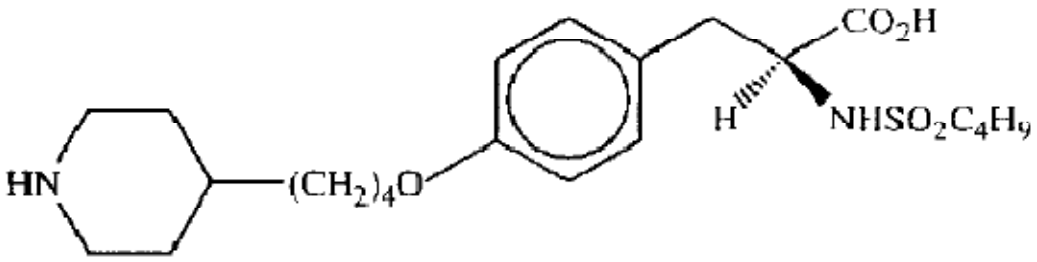

Figure 7.1. Chemical structure of Aggrastat. [212]

Hence, in order to analyze the potential roles of these two receptor sets in mediating platelet interactions with adsorbed Fg and Alb, we pretreated the washed platelet suspension with the different platelet antagonists (Aggrastat against $\alpha_{IIb}\beta_3$, and mAbs 6B4/24G10 against GPIb) prior to adhesion to the Fg- and Alb-coated SAM surfaces. Additionally, to delineate any potential role for GPIb as the non-RGD-specific receptor set involved in mediating the adhesion of RGDS-treated platelets, we treated the platelet suspension with RGDS followed by 6B4/24G10 anti-GPIb antibodies prior to the platelet adhesion step. Finally, in order to modify both Lys and Arg in Alb and thereby neutralize the positively charged residues in the adsorbed layer, we carried out the acetylation of these residues using acetic anhydride, which has been shown to be a potent strategy for chemical modification of the amino groups in proteins [171].

7.2 Materials and Methods

7.2.1 Gold substrates

1.0 cm x 1.0 cm silicon wafers (Silicon Quest, Inc.) were used as substrates for the platelet adhesion experiments, while quartz slides (0.375" x 1.625" x 0.0625", Chemglass) were used for CD experiments. These substrates were cleaned by immersing them in a piranha solution (7:3 v/v H_2SO_4:H_2O_2) at 50°C for 30 min, followed by an RCA basic wash (1:1:5 v/v NH_4OH:H_2O_2:H_2O), and this cleaning procedure was repeated twice, as described previously in Chapter 3. The cleaned substrates were rinsed with 100% ethanol (Pharmco-Aaper; Catalog No. 111000200) and nanopure water, and then dried using a stream of nitrogen gas.

The cleaned silicon wafers were coated with a 50 Å chromium adhesion layer and 1,000 Å of gold, while the quartz slides for CD were coated with 30 Å of chromium and 100 Å of gold, via a thermal vapor deposition process. The thicknesses of the gold and chromium layers were verified using a DekTak profilometer and a GES5 ellipsometer (Sopra, Inc., Palo Alto, CA).

7.2.2 Formation of self-assembled monolayers (SAMs) of alkanethiols

The gold-coated substrates were cleaned by dipping them in a modified piranha wash (4:1 v/v H_2SO_4:H_2O_2), followed by an RCA basic wash, for 1 minute each and then

rinsed with 100% ethanol, prior to incubation in 1.0 mM alkanethiol solutions for 24 h, as per the standard protocols [181, 182].

The following alkanethiols were used for creating the SAM surfaces, and were prepared in 100% ethanol, as described previously in Chapter 4:

1-Dodecanethiol ($SH-(CH_2)_{11}CH_3$; Aldrich; CH_3), and

11-Mercapto-1-undecanol ($SH-(CH_2)_{11}OH$; Aldrich; OH).

The SAM surfaces were cleaned to remove any traces of hydrophobic contaminants on their surface prior to surface characterization and protein adsorption [99]. The CH_3 SAM surfaces were cleaned by sonication in ethanol, hexane and ethanol, and then rinsed with nanopure water. The OH SAMs were sonicated in ethanol, and then incubated in a 25 mM potassium phosphate buffer containing 0.005 volume % Triton-X-100 (Sigma; Catalog No. T-9284), in order to block off any hydrophobic defect sites (e.g. grain boundaries), and then rinsed thoroughly with acetone, ethanol and nanopure water to remove loosely-bound Triton.

7.2.3 Surface characterization of SAM surfaces

The SAM surfaces were characterized using contact angle goniometry, ellipsometry and XPS, and the results are listed in Chapter 4.

7.2.4 Buffers

Protein adsorption was carried out in a 25 mM potassium phosphate buffer (pH 7.4), which was made by combining suitable amounts of the mono- and dibasic salts (Sigma-Aldrich), in order to maintain the pH at 7.4. This buffer is recommended for CD experiments for determining the structure of native/adsorbed proteins [79, 132, 193] as it permits measurement of CD spectra with minimal noise below 200 nm, especially the positive CD peaks at 193 and 195 nm, which are critical in determining the α-helix and β-sheet content of the proteins, respectively.

The platelet suspension buffer (PSB, pH 7.4) contained 137 mM NaCl, 2.7 mM KCl, 5.5 mM Dextrose, 0.4 mM sodium phosphate monobasic, 10 mM HEPES and 0.1U/mL apyrase [201]. 2.5 mM $CaCl_2$ and 1.0 mM $MgCl_2$ was added to the PSB to give a platelet suspension buffer with metal ions (PSB+MI). It should be noted that bovine serum Alb (BSA) was not added to the platelet suspension buffer as a blocking agent, as is commonly used in platelet adhesion studies.

7.2.5 Protein adsorption

Human Fg (FIB3, plasminogen, von Willebrand factor and fibronectin depleted, Enzyme Research Laboratories) and Alb (Sigma, Catalog No. A9511) was dissolved in 25 mM phosphate buffer solution (pH 7.4), to prepare the protein stock solutions, and

protein adsorption was carried out as described previously in Chapters 5 and 6, at a protein concentration of 0.1 mg/mL.

The cleaned SAM surfaces were incubated in 25 mM potassium phosphate buffer (pH 7.4) in a Pyrex petridish, and a suitable amount of protein stock solution was added to give the 0.1 mg/mL bulk protein solution concentration, taking care to ensure that the tip of the pipette was held below the air-water interface to avoid denaturation of the protein at this interface. The protein adsorption step lasted 2 h, after which an infinite dilution step was carried out to wash away the bulk protein solution in addition to any loosely adherent protein on the SAM surfaces. The SAM surfaces with preadsorbed protein were then incubated with the platelet suspension in a well-plate.

7.2.6 Preparation of washed platelet suspension

Platelet adhesion was carried out, using a suspension of washed platelets from human blood, as described in Chapters 5 and 6, in a well plate (Corning Costar, Catalog No. 3527). 25.0 mL of blood was collected from healthy volunteers as per research protocols approved by the Institutional Review Board (IRB) and Institutional Biosafety Committee (IBC) at Clemson University. The first few mL of blood was discarded, as it is rich in clotting factors, and then 25 mL of blood was collected in BD Vacutainer tubes (Becton-Dickinson, Catalog No. 364606) containing an acid-citrated dextrose (ACD) anti-coagulant.

The ACD-anticoagulated blood was centrifuged (225g, 15 min, 25°C) to generate platelet rich plasma (PRP), and platelets were separated from PRP via a gel separation method [201], using a liquid chromatography column (Sigma-Aldrich, Catalog No. C4169) containing Sepharose 2B (Sigma-Aldrich, Catalog No. 2B-300). The Sepharose column was first equilibrated with PSB, after which the PRP was carefully pipetted on to the column and allowed to pass into the column. PSB was then added to the column from a reservoir, while keeping the column running. Fractions were collected from the bottom of the column, with the platelet-rich fractions being identified by their increased turbidity. These fractions were pooled, and platelet concentration was measured using a Beckman Coulter Z2 Coulter Particle Count and Size Analyzer (Beckman Coulter, Fullerton, CA). The platelet count was adjusted to the desired concentration with PSB, and $CaCl_2$ and $MgCl_2$ were added to give 2.5 mM and 1.0 mM concentrations of these salts, respectively. Platelet suspension was allowed to rest for 30 min, and the platelet adhesion step was carried out on the protein-coated SAMs for 1 h at 37°C.

At the end of the platelet adhesion step, the platelet suspension was aspirated from each well, and the non-adherent platelets were rinsed away by filling and aspirating the wells five times with PBS. The substrates were transferred to a fresh well-plate, and the adhesion levels were quantified using a lactate dehydrogenase (LDH) assay.

7.2.7 Measurement of platelet adhesion using lactate dehydrogenase (LDH) assay

The platelets adherent on the Fg- and Alb-coated SAMs were lysed with a Triton-PSB buffer, (2% v/v Triton-X-100 in PSB), and the platelet adhesion levels on the SAMs was quantified by measuring the lactate dehydrogenase (LDH) released from these lysed adherent platelets using a CytoTox96® Non-Radioactive Cytotoxicity Assay (Promega Corporation, Madison, WI), as indicated in Section 5.2.8. A calibration curve was constructed using a known number of platelets, counted using a Beckman Coulter Z2 Coulter Particle Count and Size Analyzer, and the platelet adhesion on the SAM surfaces was determined from this calibration curve.

7.2.8 Inhibition of platelet-protein interactions using anti-GPIb antibodies 6B4 and 24G10

Monoclonal antibodies 6B4 and 24G10 against the GPIb platelet receptor were generously provided by Dr. Hans Deckmyn (Laboratory for Thrombosis Research, Katholieke Universiteit, Leuven, Belgium). The platelet suspension was incubated first with 300 µM of an Arg-Gly-Asp-Ser (RGDS) peptide (Calbiochem, La Jolla, CA) for 30 min at room temperature, in order to inhibit interactions between RGD-binding platelet receptors and adsorbed protein, followed by a similar incubation with 5 µg/mL of the anti-GPIb antibody for 30 min at room temperature, in order to inhibit any potential interactions between the GPIb platelet receptors and the adsorbed Fg/Alb. These platelets were then allowed to adhere on the Fg- and Alb-coated SAM surfaces for 1h at

37°C, after which the platelet adhesion was quantified using an LDH assay and the morphology of the adherent platelets was examined using SEM.

Control experiments were also carried out with a washed platelet suspension without blocking with RGDS prior to treatment with the anti-GPIb antibodies.

7.2.9 Aggrastat treatment of platelets

Aggrastat, which is a trade-name for the generic drug called tirofiban, is a potent $\alpha_{IIb}\beta_3$ antagonist, and has been shown to inhibit platelet adhesion and activation on collagen [158]. The washed platelet suspension was treated with 5 µg/mL of Aggrastat (Baxter Healthcare, Product Code 2J1400) for 30 min at room temperature prior to the platelet adhesion step. The Aggrastat-treated platelets were then allowed to adhere to the Fg- and Alb-coated SAMs for 1h at 37°C, with the platelet adhesion levels being quantified using the LDH assay, and the adherent morphology of the platelets being examined via SEM. A platelet suspension without Aggrastat pre-treatment was used as a control in the platelet adhesion experiments.

7.2.10 Acetylation of Arg and Lys residues in Alb using acetic anhydride

Acetylation of proteins using acetic anhydride is one of the oldest and most extensively used methods for chemical modification of proteins [171]. Acetylation of Arg and Lys residues in Alb was carried out using acetic anhydride (Sigma-Aldrich), as

described previously [176, 178]. Briefly, an Alb solution was modified by the addition of 10% acetic anhydride. The modification step lasted 2 h, after which modified protein samples were dialyzed for 12 h against 25 mM phosphate buffer, and then analyzed for Arg and Lys modification via a protocol described previously [99] using electrospray ionization mass spectrometry (ESI-MS) performed at the Clemson University Genomics Institute, to confirm that the chemical reaction caused the modification of Arg and Lys residues. Additionally, acetylation of Alb on the CH_3 and OH SAMs preadsorbed from 0.1 mg/mL bulk solution concentration was carried out, as described above.

7.2.11 CD studies to quantify the adsorption-induced conformational changes and total surface coverage of Alb on SAM surfaces

The secondary structures of acetylated Alb in the solution and adsorbed states, along with the surface coverage of adsorbed Alb, was determined using a Jasco J-810 spectropolarimeter (Jasco, Inc., Easton, MD), as described earlier (in Section 4.2.6). The solution structure was determined using a special high-transparency quartz cuvette (Starna Cells, Inc., Atascadero, CA), while the adsorbed structure of Alb on the SAM surfaces was determined using a special custom-designed cuvette, which maximizes the signal-to-noise ratio (as seen in Fig. 4.1). The ellipticity of the samples (θ, in mdeg) was converted to molar ellipticity (designated as [θ], with standard units of deg·cm^2/dmol) using the following equation [132, 135]:

$$[\theta] = (\theta \cdot M_0)/(10{,}000 \cdot C_{soln} \cdot L), \qquad (7.1)$$

where θ is the ellipticity in mdeg, L is the path length of the cuvette in cm, C_{soln} is the solution concentration of the protein in g/mL, and M_0 is the mean residue molecular weight of 118 g/mol.

Since proteins exhibit an absorbance peak at 195 nm [184], we used the height of this absorbance peak (A_{195}) for constructing a calibration curve of A_{195} vs. C_{soln} for various known concentrations of Alb, as described in Section 4.2.6. The slope of this plot is "$\varepsilon_{protein} \cdot L$" from Beer's Law, which can be written as:

$$A_{195} = \varepsilon_{protein} \cdot C_{soln} \cdot L \qquad (7.2)$$

where $\varepsilon_{protein}$ is the extinction coefficient of the protein in $mL \cdot g^{-1} \cdot cm^{-1}$ (or cm^2/g) and L is the path length of the cuvette.

The term "$C_{soln} \cdot L$" in eq. 7.2 (above) has units of g/cm^2, which is equivalent to the amount of protein adsorbed per unit area. Assuming that the absorbance is dependent on the total amount of protein present per unit area through which the beam of light passes, irrespective of whether the protein is in the solution or the adsorbed state, the calibration curve of A_{195} vs. C_{soln} can also be used for calculating the amount of Alb adsorbed per unit area on the SAMs (i.e., Q_{ads}). The validity of this method for measuring the surface coverage of adsorbed protein has been confirmed by independent measurement of Q_{ads} from the thickness of the adsorbed protein film obtained by ellipsometry (see Section 4.5) using de Feijter's formula [198].

Hence, while calculating the molar ellipticity for the adsorbed Alb layer on the SAMs, the term "$C_{soln} \cdot L$" in eq. 7.1 can be replaced by the term Q_{ads} to give the following equation:

$$[\theta] = (\theta \cdot M_0)/(10{,}000 \cdot Q_{ads}), \qquad (7.3)$$

The CD spectra (molar ellipticity vs. wavelength) thus obtained were deconvoluted using the SP-22X algorithm and analyzed using the CONTIN/LL software package to quantify the percentage of α-helix and β-sheet content of the Alb in the solution and adsorbed states [148].

7.2.12 Effect of acetylation of the adsorbed Alb layer on platelet adhesion

The CH_3 and OH SAM surfaces were preadsorbed with Alb at 0.1 mg/mL bulk solution concentration, and acetylation of the adsorbed Alb was carried out, using the protocol described in Section 7.2.11. After washing away the excess acetic anhydride, the surfaces were incubated with platelets, and the platelet adhesion levels were quantified using an LDH assay, with the morphology of the being observed using SEM.

7.2.13 Statistical analysis

The results we present are the mean values with 95% confidence intervals (CI). Statistical significance of differences between mean values for different samples and

conditions was evaluated using a Student's t-test, with $p \leq 0.05$ considered as statistically significant.

7.3 Results and Discussion

7.3.1 Effect of anti-GPIb antibodies on platelet adhesion to adsorbed Fg and Alb

Our platelet adhesion results (shown in Chapters 5 and 6) indicated that platelet adhesion to adsorbed Fg and Alb was potentially mediated by a non-RGD-specific receptor set, in addition to an RGD-specific receptor set. As seen in the adherent morphology of the RGDS-treated platelets in Fig. 6.8, the platelets were moderately spread with little or no filopodia, suggesting that this non-RGD-specific receptor set mediated adhesion without activation. Since the GPIb-IX-V receptor complex is the second most abundant receptor complex on platelets [73], and has been shown to mediate adhesion without activation on collagen [111], we examined its role as the non-RGD-specific platelet receptor set mediating adhesion to adsorbed Fg and Alb. Since studies [165, 166] have implicated two vWf-binding domains in platelet GPIbα spanning amino acid residues 1-81 and 201-268, we used monoclonal antibodies 24G10 and 6B4 against these domains, respectively, in delineating the interactions of this receptor complex with adsorbed Fg and Alb.

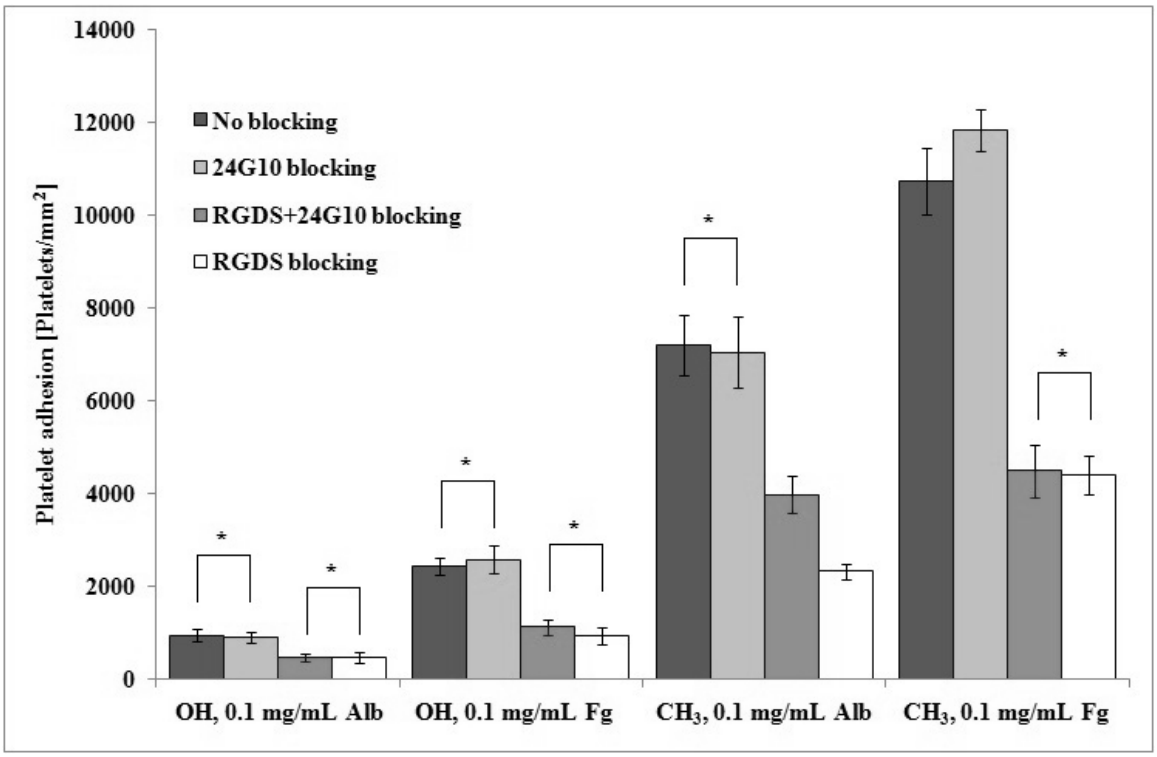

Figure 7.2. Platelet adhesion on SAM surfaces preadsorbed with Alb and Fg from 0.1 mg/mL solutions under various blocking conditions. The blocking treatments on the platelet suspension included the anti-GPIb antibody 24G10, as well as pretreatment of the platelets with an RGDS peptide prior to incubation with 24G10 (n=6, mean ± 95% CI). * denotes no statistically significant difference, $p > 0.05$.

As shown in Fig. 7.2, the addition of 24G10 did not lead to a significant reduction of platelet adhesion levels on the CH_3 and OH SAMs preadsorbed with Fg and Alb. Although we cannot explain the statistically significant higher adhesion levels for (RGDS+24G10)-treated platelets compared to the RGDS-treated platelets on the CH_3

SAM preadsorbed with Alb in Fig. 7.2, this result indicates that the addition of 24G10 did not cause any additional inhibition of the adhesion of the RGDS-treated platelets on this surface. Similarly, on the CH_3 SAM preadsorbed with Fg, the addition of the 24G10 anti-GPIb antibody did not lead to a decrease in platelet adhesion levels compared to the corresponding unblocked control. These results suggest that the amino acid residues 1-81 in GPIbα do not mediate platelet attachment to adsorbed Fg and Alb, as seen by the inability of 24G10 to inhibit the adhesion of untreated and RGDS-treated platelets to the adsorbed proteins.

Further analysis of the adhesion data for platelet adhesion to adsorbed Fg and Alb on these SAMs yielded the observation that although the extent of Fg and Alb unfolding was vastly different on the OH and CH_3 SAMs (~0% Fg unfolding on OH and 72% Fg unfolding on CH_3; ~34% Alb unfolding on OH and 77% Alb unfolding on CH_3), the extents of RGDS inhibition were similar (~50%). This suggests that the process of adsorption-induced unfolding does not change the basic mechanism that is mediating platelet adhesion to the adsorbed Fg and Alb.

The addition of 6B4, like 24G10, did not lead to an increased inhibition of platelet adhesion to adsorbed Fg or Alb, as seen in Fig. 7.3. There was no statistically significant difference between the platelet adhesion levels of untreated and 24G10-treated platelets on the CH_3 and OH SAMs preadsorbed with Fg and Alb. The increased adhesion of the (RGDS+6B4)-treated platelets compared to RGDS-treated platelets on the CH_3 SAM

preadsorbed with Alb confirms that the addition of 6B4 did not cause any further inhibition of the adhesion of these RGDS-blocked platelets.

These combined results for 24G10 and 6B4 indicate that the GPIb-IX-V complex does not play a role in mediating platelet adhesion to adsorbed Fg and Alb as the non-RGD-specific receptor set.

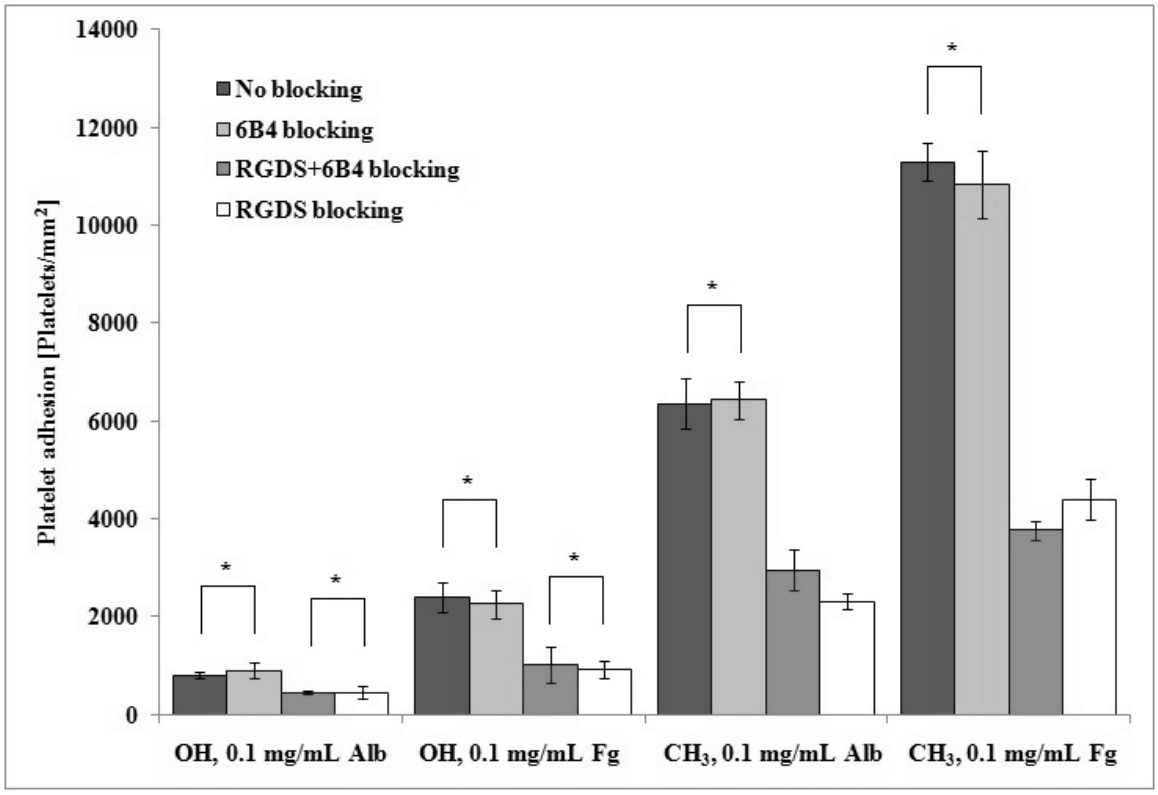

Figure 7.3. Platelet adhesion on SAM surfaces preadsorbed with Alb and Fg from 0.1 mg/mL solutions under various blocking conditions. The blocking treatments on the platelet suspension included the anti-GPIb antibody 6B4, as well as pretreatment of the platelets with an RGDS peptide prior to incubation with 6B4 (n=6, mean ± 95% CI). * denotes no statistically significant difference, $p > 0.05$.

7.3.2 Effect of Aggrastat-pretreatment on platelet adhesion to adsorbed Fg and Alb

Platelet adhesion and activation on collagen has been shown to be inhibited by the $\alpha_{IIb}\beta_3$ antagonist Aggrastat [158]. This is a potent, small molecule RGD-mimetic drug, which utilizes the separation distance between the Arg and Asp residues as a key determinant of its potency [212]. We therefore examined the ability of Aggrastat to inhibit interactions with adsorbed Fg and Alb, which, based on literature reports, should occur by blocking the $\alpha_{IIb}\beta_3$ platelet receptor.

The addition of Aggrastat to the washed platelet suspension prior to the platelet adhesion step led to a strong inhibition of platelet adhesion to adsorbed Fg and Alb, compared to the untreated and RGDS-treated platelet suspensions, as indicated in Fig. 7.4. The CH_3 SAM surfaces preadsorbed with Fg and Alb still exhibited low levels of platelet adhesion despite Aggrastat-pretreatment, and this could potentially be attributed to the inability of Aggrastat to inhibit the $\alpha_V\beta_3$ integrin [213], which belongs to the β_3 family of integrins like $\alpha_{IIb}\beta_3$, and is present on platelets with several hundred copies per platelet [207]. Thus, Aggrastat is clearly a more potent inhibitor of platelet interactions with the adsorbed proteins than the RGDS peptide.

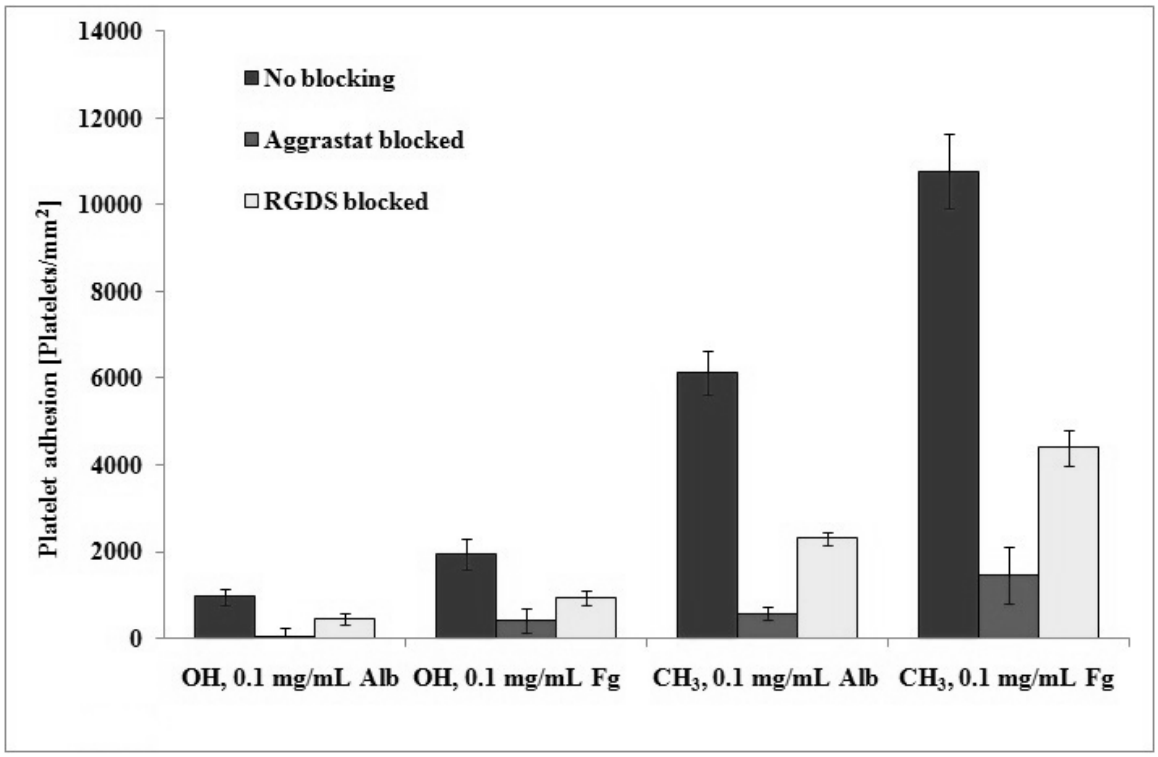

Figure 7.4. Adhesion of Aggrastat-treated platelets on SAM surfaces preadsorbed with Alb and Fg from 0.1 mg/mL solutions, compared to untreated and RGDS-treated platelets. (n=6, mean ± 95% CI). * denotes no statistically significant difference, $p > 0.05$.

The results obtained in Chapters 5 and 6 with RGDS-pretreatment of the washed platelet suspension suggested that the remaining adhesion observed for RGDS-treated platelets may either be mediated by the $\alpha_{IIb}\beta_3$ receptor in its RGD-bound 'low-affinity' state, or potentially by another receptor set which may become active upon addition of RGDS, as RGD-containing peptides have been shown to activate $\alpha_{IIb}\beta_3$ and other platelet

receptors [155, 158]. However, the ability of Aggrastat to function as a near-complete inhibitor of platelet adhesion to adsorbed Fg and Alb (as seen in Fig. 7.4), clearly illustrates the critical role played by the $\alpha_{IIb}\beta_3$ receptor in accounting for approximately 90% of the platelet adhesion response.

Studies have shown that the activation of $\alpha_{IIb}\beta_3$ due to inside-out platelet signaling or ligand binding (Fg, Fn, vWf, Vn) leads to conformational alterations in $\alpha_{IIb}\beta_3$ [105, 208]. These changes induce outside-in platelet signaling, leading to intraplatelet cytoplasmic changes including increased tyrosine kinase activity, cytoskeletal changes and platelet spreading [214]. Changes in the cytoplasmic domain of the β_3 sub-unit of $\alpha_{IIb}\beta_3$ have been shown to be a critical determinant of $\alpha_{IIb}\beta_3$-mediated outside-in signaling [160, 161, 215]. RGDS binding induces changes in both the α_{IIb} and β_3 sub-units of the $\alpha_{IIb}\beta_3$ platelet integrin, leading to outside-in platelet signaling which causes platelet adhesion and activation, thereby explaining the ability of RGDS-treated platelets to adhere to adsorbed Fg and Alb. Aggrastat, on the other hand, induces conformational changes only in the α_{IIb} sub-unit but not the β_3 sub-unit of $\alpha_{IIb}\beta_3$ [156, 157], which does not induce outside-in signaling, thus explaining the strong inhibitory effect that we observed on platelet interactions with adsorbed Fg and Alb.

7.3.3 Effect of acetylation of Arg and Lys residues in adsorbed Alb on platelet adhesion

Our preliminary results (listed in Chapter 6) showed that the site-specific chemical modification of Arg residues led to a significant decrease in platelet adhesion, indicating that these residues play a critical role in the adhesion process. However, platelet adhesion to Fg has also been shown to be mediated by Lys residues in certain domains, such as in the dodecapeptide sequence (HHLGGAKQAGDV) in the C-terminus of the γ-chain segment of Fg. Since the Alb molecule contains 59 Lys residues, as compared to 24 Arg residues, we also examined chemical modification of both Lys and Arg residues in the adsorbed Alb layer as a potential strategy to determine if Lys residues also play a role in platelet attachment to the adsorption-induced unfolded state of Alb.

The ESI-MS results confirmed that all 24 Arg residues were modified, while 52 out of 58 Lys residues were modified, under the applied conditions, thus confirming that the applied treatment modified these residues with high efficiency. It is assumed that the Lys residues that were not modified were not solvent accessible. The acetylation process had minimal effect on the secondary structural content of Alb in its solution and adsorbed state, as seen in Table 7.1 and in Fig 7.5.

Table 7.1. Comparison of secondary structural composition of unmodified Alb and Alb with Arg and Lys residues acetylated using acetic anhydride, in solution and after adsorption on the CH_3 and OH SAMs (n= 6, mean ± 95% CI).

Sample	α-helix (%)	β-sheet (%)
In solution		
Human Alb unmodified	68.8 ± 2.3	0.1 ± 0.1
Human Alb-acetylated	66.4 ± 0.7	0.8 ± 0.4
After adsorption		
CH_3, 0.1 mg/mL Alb-unmodified	14.4 ± 0.7	28.3 ± 0.7
CH_3, 0.1 mg/mL Alb-acetylated	15.0 ± 2.2	27.4 ± 1.8
OH, 0.1 mg/mL Alb-unmodified	43.1 ± 2.1	13.4 ± 1.1
OH, 0.1 mg/mL Alb-acetylated	41.1 ± 2.4	13.4 ± 2.0

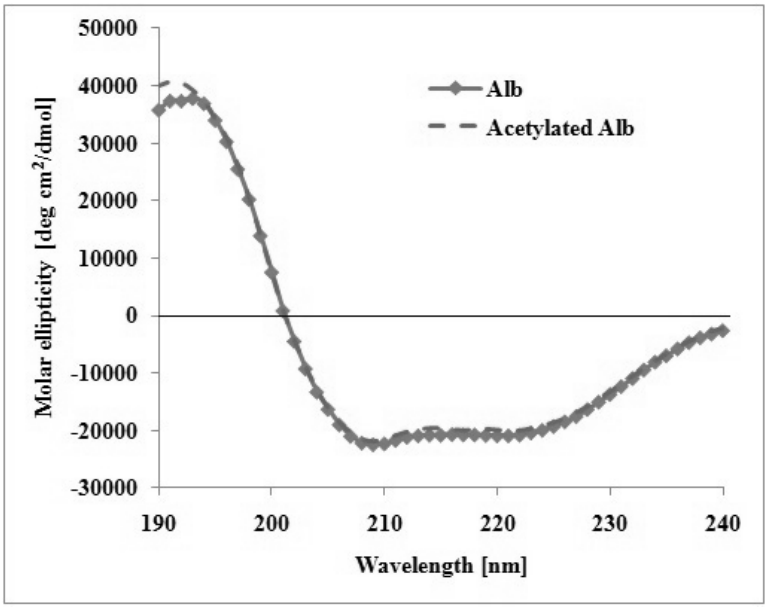

Figure 7.5. Representative CD spectra for solution structure of normal native Alb and acetylated Alb with modified Arg and Lys residues.

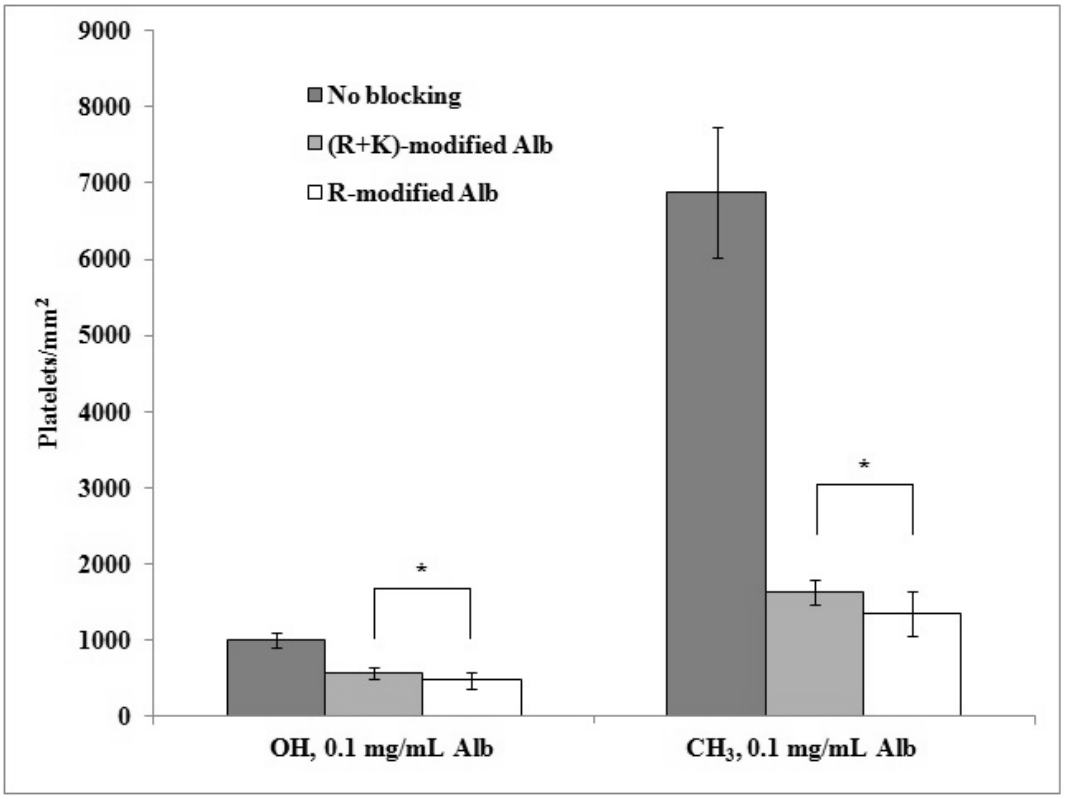

Figure 7.6. Platelet adhesion to SAM surfaces preadsorbed with Alb from 0.1 mg/mL solution, for unblocked and acetylated (R+K modified) conditions. Data for R-modified Alb is reproduced for comparison from Chapter 6. (n=6, mean ± 95% CI). * denotes no statistically significant difference, $p > 0.05$.

The acetylation of adsorbed Alb led to a significant decrease in platelet adhesion, as observed in Fig. 7.6. However, the reduction in adhesion levels was not significantly different (p = 0.12 for CH_3, p = 0.18 for OH) from those obtained for the site-specific modification of the Arg residues in adsorbed Alb via butanedione treatment. These results suggest that the Lys residues in adsorbed Alb likely do not play a role in

mediating platelet binding, and that the Arg residues in Alb are the only positive charged amino acid residues which are involved in platelet binding.

Coupled with the results obtained from the pretreatment of platelets with Aggrastat (Fig. 7.4), which suggest that the platelet adhesion to Alb is mediated by the RGD-specific $\alpha_{IIb}\beta_3$ receptor, this confirms the critical role played by the Arg residues in adsorbed Alb in mediating platelet adhesion. These combined results indicate that the residual platelet adhesion that occurred on acetylated Alb must be attributed to amino acid residues in Alb other than Arg or Lys, with further studies being necessary to determine which other amino acid residues are involved.

7.4 Conclusions

These studies were primarily aimed at delineating the roles of the GPIb-IX-V and $\alpha_{IIb}\beta_3$ platelet receptors in mediating platelet adhesion to adsorbed Fg and Alb. Although we had initially hypothesized that the former receptor set likely mediated adhesion with little/no activation as the non-RGD-specific receptor, our studies showed that anti-GPIb antibodies 6B4 and 24G10 were unable to inhibit the adhesion of untreated as well as RGDS-treated platelets to the adsorbed Fg and Alb layers. Furthermore, the fact that the anti-$\alpha_{IIb}\beta_3$ platelet antagonist drug Aggrastat nearly completely inhibited platelet adhesion indicates that the $\alpha_{IIb}\beta_3$ platelet integrin is the primary receptor involved in about 90% of the platelet binding to adsorbed Fg and Alb.

Chemical modification studies of amino acid residues provide information on the role of specific amino acids in mediating platelet attachment. Platelet adhesion studies to acetylated Alb yielded results that indicated that the Arg residues play a critical role in platelet binding to Alb, while the Lys residues likely had no role in this process. Further chemical modification studies are necessary to determine which other amino acid residues are involved in mediating platelet adhesion to Alb other than Arg.

Overall, these studies provide new insights into the molecular-level mechanisms mediating the interactions of platelets with adsorbed plasma proteins. This level of understanding is needed by biomaterials field to support its efforts to develop potent strategies to inhibit platelet adhesion to adsorbed proteins for the design of more hemocompatible biomaterials for cardiovascular applications.

CHAPTER 8

TIME-DEPENDENT CONFORMATIONAL CHANGES IN ADSORBED ALBUMIN, AND ITS SUBSEQUENT EFFECT ON PLATELET ADHESION

8.1 Introduction

The layer of adsorbed proteins on a material surface is a critical determinant of the bioactivity of the tissue-biomaterial interface [1, 31], affecting blood coagulation, complement activation and subsequent cell adhesion. It is a well known fact that proteins undergo some degree of structural changes when they come into contact with solid substrates. Conformational changes in the adsorbed protein molecules leads to stronger protein-surface interactions, which can lead to greater surface activity [31]. Additionally, hydrophobic regions which are generally located in the interior of the protein may become exposed upon protein unfolding.

The adsorption-induced conformational changes in the protein layer have been shown to mediate the subsequent cellular response to the biomaterial [1, 33]. Additionally, these structural alterations in adsorbed plasma proteins play a critical role in the ability of non-activated platelets to bind to the adsorbed protein layer [54, 55, 116] and mediate the thrombotic response, as shown in our experiments with adsorbed fibrinogen (Fg) and albumin (Alb), in Chapters 5 and 6, respectively.

According to Dee *et al.* [31], proteins can undergo conformational changes in two ways. One mode results from changes in the bulk protein solution concentration, while

the other involves time-dependent protein unfolding. In the former, the bulk solution concentration of the protein influences the rate of transport of protein molecules to the surface. Thus, at lower bulk protein solution concentrations, the protein molecules arrive at the surface at a slower rate compared to higher bulk concentrations, as a result of which they have more surface area over which they can spread (and form contacts), before they come into contact with neighboring protein molecules [31, 39]. Hence, the adsorption-induced conformational changes in proteins would be expected to be more pronounced, while the surface coverage would be lower, when the protein is adsorbed from lower bulk protein solution concentrations. This effect was clearly shown in our preliminary results in Chapter 4. On the other hand, as the residence time (i.e., the time the protein molecule resides on the surface) increases, the protein may unfold and expose functional residues in its interior which can potentially interact with the surface, as well as alter the bioactivity of the protein.

Fibrinogen (Fg) has been shown to undergo increased conformational changes with increasing residence time, which render it potentially less recognizable by platelets [37, 38]. However, these results represent the ability of anti-Fg antibodies to recognize Fg and may not accurately represent Fg recognition by platelets. Studies done by Balasubramanian *et al.* [36] on the effect of residence time on Fg adsorption and platelet adhesion to polytetrafluoroethylene (PTFE), polyethylene (PE) and silicone rubber (SR) showed that there was a very minimal decrease in platelet adhesion levels with increasing Fg residence time, which was not statistically significant. Additionally, the binding of the monoclonal antibody (mAb) 4A5 against the γC terminal dodecapeptide sequence (γ400-

411) of Fg, which is considered to be the primary platelet binding sequence in Fg [58], has been shown to be independent of the residence time of Fg for time periods up to 2 h following adsorption [36, 216]. mAb binding against the RGDF sequence (α95-98) was shown to be low initially, but increased with residence time [216], which may suggest that this amino acid sequence may become exposed as the adsorbed Fg unfolds with time. More recent studies [217, 218] have examined time-dependent conformational changes in Fg via atomic force microscopy (AFM), and its subsequent effect on platelet adhesion [218]. Platelet adhesion to adsorbed Fg was found to correlate well with the functional activity of the adsorbed Fg, peaking at 45 min of residence time and gradually decreasing with further increase in residence time [218].

These studies [36-38, 216-218] were done using low bulk Fg solution concentrations for short adsorption times (less than 15 min), after which the protein-coated substrates were rinsed and immersed in PBS for relatively short residence times of up to 2 h. The biomaterials field has yet to examine the potential conformational changes in an irreversibly adsorbed, tightly packed layer of plasma protein(s) on material surfaces over long residence times (of the order of weeks to months), and its effect (if any) on subsequent platelet adhesion and the blood compatibility of the biomaterial.

Alb is the most abundant plasma protein [77], and has been shown to be one of the first proteins to adsorb on implant surfaces [79]. Studies have shown minimal desorption of adsorbed Alb by other more surface-active proteins such as IgG and Fg [34, 219] on hydrophilic and hydrophobic surfaces, suggesting that adsorbed Alb may be a major component of the protein layer adsorbed on biomaterial implants. Additionally, the

inability of Fg to displace adsorbed Alb was found to be more prominent for longer Alb aging times on hydrophobic surfaces [34].

Our results listed in Chapter 6 indicated that platelet adhesion can occur on adsorbed Alb, but only if the adsorbed Alb underwent structural unfolding beyond a critical degree (i.e., unfolding resulting in about 34% loss in its α-helical structure). When Alb was preadsorbed from 10.0 mg/mL bulk solution concentration on SAM surfaces, minimal loss in the protein's structure was found to occur. This effect was attributed to the Alb not having sufficient time following adsorption to undergo surface-induced unfolding before neighboring proteins adsorbed and inhibited its ability to spread out on the surface. Therefore, when Alb is adsorbed from a solution concentration of 10.0 mg/mL or higher, it is expected that it will adsorb as an irreversibly bound, tightly packed layer that largely retains its native-state structure, thus being unable to mediate platelet adhesion. Because Alb is present at even higher concentrations in blood plasma (about 40 mg/mL), these results suggest that under clinical conditions, Alb will adsorb to an implant's surface with a minimal degree of unfolding, with negligible subsequent ability to support platelet adhesion. If this is the case, then our previous findings regarding platelet adhesion to unfolded Alb, while academically interesting, is of little clinical significance. However, the findings that Alb mediates platelet adhesion beyond a critical degree of unfolding (as shown in Fig. 6.3A) and generally adsorbs in an irreversible manner to surfaces, raise the question whether Alb that retains its native-state structure after adsorbing on an implant surface will undergo structural changes over time, and if so, whether this will lead to

platelet adhesion if the adsorbed Alb unfolds beyond our previously determined critical level.

The objectives of the studies presented in this chapter were to investigate if time-dependent conformational changes occur in an irreversibly adsorbed, tightly packed Alb layer that initially retains its native-state structure, and if this aging-induced unfolding process causes the adsorbed Alb to begin to support platelet adhesion if unfolding occurs beyond the previously determined critical degree of unfolding. In these studies, we used circular dichroism (CD) spectropolarimetry to monitor the structural state of adsorbed Alb that was preadsorbed from 10.0 mg/mL bulk solution concentration on CH_3 and OH SAMs and aged over a six month period of time, with the platelet adhesion response to this adsorbed Alb layer quantified at selected time points via a lactate dehydrogenase (LDH) assay.

8.2 Materials and Methods

8.2.1 Gold substrates

Quartz slides (0.375" x 1.625" x 0.0625", Chemglass) were used for CD experiments, while 18 mm square cover glasses (VWR Scientific, Catalog No. 48368-040) were used as substrates for the platelet adhesion experiments. These substrates were cleaned as described in Chapter 3. The substrates were incubated in a piranha solution (7:3 v/v H_2SO_4:H_2O_2) at 50°C for 30 min, followed by an RCA basic wash (1:1:5 v/v NH_4OH:H_2O_2:H_2O), and this cleaning procedure was repeated twice. These cleaned

substrates were then rinsed copiously with 100% ethanol (Pharmco-Aaper; Catalog No. 111000200) and nanopure water, and finally dried using a stream of nitrogen gas.

The cleaned substrates were coated with a chromium adhesion layer followed by a gold layer via a thermal vapor deposition method. A 50 Å chromium adhesion layer and 1,000 Å of gold were deposited on the cover glasses, while the quartz slides for CD were coated with 30 Å of chromium and 100 Å of gold. The thicknesses of the gold and chromium layers were also verified using a DekTak profilometer and a GES5 ellipsometer (Sopra, Inc., Palo Alto, CA).

8.2.2 Formation of self-assembled monolayers (SAMs) of alkanethiols

1-Dodecanethiol ($SH\text{-}(CH_2)_{11}CH_3$; Aldrich; CH_3) and 11-Mercapto-1-undecanol ($SH\text{-}(CH_2)_{11}OH$; Aldrich; OH) in 100% ethanol were used as the alkanethiols for creating the SAM surfaces, as described previously in Chapter 4.

The gold-coated substrates were dipped in a modified piranha wash (4:1 v/v H_2SO_4:H_2O_2), followed by an RCA basic wash, for 1 minute each and then rinsed copiously with 100% ethanol, to clean them. The cleaned gold substrates were then incubated in 1.0 mM alkanethiol solutions for 24 h, as per the established protocols described previously [181, 182].

Prior to the protein adsorption step, the SAM surfaces were cleaned to remove any traces of hydrophobic contaminants on their surface [99]. The CH_3 SAMs were sonicated

in ethanol, hexane and ethanol, and then rinsed with nanopure water. The OH SAMs were sonicated in ethanol, and then incubated in a 25 mM potassium phosphate buffer containing 0.005 volume % Triton-X-100 (Sigma; Catalog No. T-9284) in order to block off hydrophobic defect sites (e.g. grain boundaries), and then rinsed thoroughly with acetone, ethanol and nanopure water to remove loosely-bound Triton.

8.2.3 Buffers

25 mM potassium phosphate buffer (pH 7.4), prepared by combining appropriate amounts of the mono- and dibasic salts (Sigma-Aldrich) to maintain the pH at 7.4, was used for all adsorption experiments. This buffer is recommended for CD experiments to determine the secondary structure of proteins [79, 132, 193] as it permits measurement of CD spectra with minimal noise below 200 nm, especially the positive CD peaks at 193 and 195 nm, which are critical in determining the α-helix and β-sheet content of the proteins, respectively.

The platelet suspension buffer (PSB, pH 7.4) contained 137 mM NaCl, 2.7 mM KCl, 5.5 mM Dextrose, 0.4 mM sodium phosphate monobasic, 10 mM HEPES and 0.1 U/mL apyrase [201]. 2.5 mM $CaCl_2$ and 1.0 mM $MgCl_2$ was added to the PSB to give a platelet suspension buffer with metal ions (PSB+MI).

8.2.4 Protein adsorption

The Alb stock solution was prepared by dissolving human Alb (Sigma, Catalog No. A9511) in 25 mM phosphate buffer solution (pH 7.4), and protein adsorption was carried out as described previously in Chapters 4 and 6, at a bulk solution concentration of 10.0 mg/mL, so as to obtain an irreversibly adsorbed, tightly packed layer(s) of adsorbed Alb.

The cleaned SAM surfaces were incubated in 25 mM potassium phosphate buffer (pH 7.4), and then a suitable amount of Alb stock solution was added to give the desired bulk protein solution concentration. Special care was taken to ensure that the tip of the pipette was held below the air-water interface to avoid denaturation of the protein at this interface. The protein adsorption step lasted for 2 h, after which an infinite dilution step was carried out to wash away the bulk protein solution as well as any loosely adherent protein.

8.2.5 CD studies to quantify the adsorption-induced conformational changes and total surface coverage of Alb on SAM surfaces

A Jasco J-810 spectropolarimeter (Jasco, Inc., Easton, MD) was used to determine the native and adsorbed secondary structures of Alb, as well as the surface coverage of adsorbed Alb, as described earlier in Section 4.2.6. The native solution structure of Alb was determined using a high-transparency quartz cuvette (Starna Cells, Inc., Atascadero, CA), while the adsorbed structure of Alb on the SAM surfaces was determined using a

special custom-designed cuvette (as seen in Fig. 4.1), which maximizes the signal-to-noise ratio. The ellipticity of the samples (θ, in mdeg) was converted to molar ellipticity (designated as [θ], with standard units of deg·cm^2/dmol) using the following equation [132, 135]:

$$[\theta] = (\theta \cdot M_0)/(10{,}000 \cdot C_{soln} \cdot L), \qquad (8.1)$$

where θ is the ellipticity in mdeg, L is the path length of the cuvette in cm, C_{soln} is the solution concentration of the protein in g/mL, and M_0 is the mean residue molecular weight of 118 g/mol.

Since proteins exhibit an absorbance peak at 195 nm [184], a calibration curve plotting the height of this peak (A_{195}) as a function of C_{soln} for various known concentrations of Alb was created, as described in Section 4.2.6. The slope of this plot is "$\varepsilon_{protein} \cdot L$" from Beer's Law, which can be written as:

$$A_{195} = \varepsilon_{protein} \cdot C_{soln} \cdot L \qquad (8.2)$$

where $\varepsilon_{protein}$ is the extinction coefficient of the protein in mL · g^{-1} · cm^{-1} (or cm^2/g) and L is the path length of the cuvette.

The term "$C_{soln} \cdot L$" in eq. 8.2 has units of g/cm^2, which is equivalent to the amount of protein adsorbed per unit area. Assuming that the absorbance is dependent on the total amount of protein present per unit area through which the light beam passes, irrespective of whether the protein is in the solution or the adsorbed state, the calibration curve of A_{195} vs. C_{soln} can also be used for calculating the surface coverage of adsorbed Alb on the SAMs (i.e., Q_{ads}). The validity of this method for measuring the amount of adsorbed protein has been confirmed by independent measurement of Q_{ads} from the thickness of

the adsorbed protein film obtained by ellipsometry (see Section 4.5.S.2) using de Feijter's formula [198].

Hence, in the calculation for the molar ellipticity of the adsorbed Alb layer on the SAMs, the term "$C_{soln} \cdot L$" in eq. 8.1 can be replaced by the term Q_{ads} to give the following equation:

$$[\theta] = (\theta \cdot M_0)/(10{,}000 \cdot Q_{ads}), \qquad (8.3)$$

The CD spectra (molar ellipticity vs. wavelength) thus obtained were deconvoluted using the SP-22X algorithm and analyzed using the CONTIN/LL software packages to quantify the percentage of α-helix and β-sheet content of the native/adsorbed Alb [148].

8.2.6 Platelet adhesion

The platelet adhesion experiments were carried out using a suspension of washed human platelets. Briefly, 25.0 mL of blood was collected from volunteers in BD Vacutainer tubes (Becton-Dickinson, Catalog No. 364606) containing an acid-citrated dextrose (ACD) anti-coagulant, as per protocols approved by the Institutional Review Board (IRB) and Institutional Biosafety Committee (IBC) at Clemson University. It is important to note that the first few mL of blood was discarded, as it is rich in clotting factors and then 25 mL of blood was collected.

The blood collected was then centrifuged (225g, 15 min, 25°C) to generate platelet rich plasma (PRP), and platelets were separated from the PRP via a gel separation

method [201], using a liquid chromatography column (Sigma-Aldrich, Catalog No. C4169) containing Sepharose 2B (Sigma-Aldrich, Catalog No. 2B-300). The Sepharose column was equilibrated with PSB, prior to layering the PRP on the column. PSB was then added to the column from a reservoir, with the column running. Fractions were collected from the bottom of the column, with the platelets being identified by their increased turbidity, and the platelet-rich fractions were pooled. Platelet concentration was measured using a Beckman Coulter Z2 Coulter Particle Count and Size Analyzer (Beckman Coulter, Fullerton, CA), and the platelet count was adjusted to 10^8 platelets/mL with PSB. $CaCl_2$ and $MgCl_2$ were added to give 2.5 mM and 1.0 mM concentrations of these salts, respectively. The washed platelet suspension was allowed to rest for 30 min, and the platelet adhesion step was carried out on the protein-coated SAMs for 1 h at 37°C.

At the end of the platelet adhesion step, the platelet suspension was aspirated from each well, and the non-adherent platelets on the Alb-coated surfaces were rinsed away by filling and aspirating the wells five times with PBS. The substrates were then removed to a fresh well-plate, for carrying out the lactate dehydrogenase (LDH) assay to quantify the platelet adhesion levels.

8.2.7 Measurement of platelet adhesion using lactate dehydrogenase (LDH) assay

A CytoTox96® Non-Radioactive Cytotoxicity Assay (Promega Corporation, Madison, WI), was used for quantification of the platelet adhesion levels on the Alb-coated SAMs

by measuring the lactate dehydrogenase (LDH) released when the adherent platelets were lysed with a Triton-PSB buffer, (2% v/v Triton-X-100 in PSB), as indicated in Section 5.2.9. A calibration curve was constructed by concurrent measurement of the LDH released from a known number of platelets, and the platelet adhesion on the SAM surfaces was determined from this calibration curve.

8.2.8 Aging studies for adsorbed Alb on SAM surfaces

CD and platelet adhesion studies were performed to measure the conformation of the adsorbed Alb layers on the SAM surfaces and the platelet adhesion response to the adsorbed Alb at day 0. The Alb-coated SAMs were then re-immersed in fresh 25 mM potassium phosphate buffer, supplemented with 0.1% cellgro antibiotic/antimycotic solution (Mediatech Inc., Catalog No. MT30-004-CI). These substrates were then incubated for up to 6 months at 37°C in an incubator, with the buffer (supplemented with antibiotic/antimycotic solution) being replenished regularly at 2 week intervals. CD and platelet adhesion analyses were then performed after aging the adsorbed Alb layers at 3 month and 6 month time points following initial Alb adsorption. Prior to conducting the CD and platelet adhesion studies, the protein-coated aged samples were infinitely diluted and rinsed copiously with nanopure water, to remove all traces of the antibiotic/antimycotic solution.

8.2.9 Statistical analysis

The results we present are the mean values with 95% confidence intervals (CI). Statistical significance of differences between mean values for different samples and conditions was evaluated using a Student's t-test, with $p \leq 0.05$ considered as statistically significant.

8.3 Results and Discussion

8.3.1 Time-dependent conformational changes in adsorbed Alb on SAM surfaces

The percentage α-helix and β-sheet content of Alb adsorbed on the CH_3 and OH SAMs from 10.0 mg/mL bulk Alb solution concentration, determined using adsorbed-state CD spectropolarimetry, is presented in Fig. 8.1.

As seen in Fig. 8.1, there was a distinct loss in α-helix of adsorbed Alb with increasing residence time over the 6 month duration of the study for both the OH and CH_3 SAMs, indicating that the adsorbed Alb layer underwent a significant degree of structural unfolding over the 6-month time period. This is in agreement with previous studies which have pointed to the fact that proteins undergo time-dependent conformational changes [31, 37, 38]. Additionally, the decrease in α-helix of adsorbed Alb was more pronounced on the CH_3 SAM compared to the OH SAM, which is in agreement with observations from studies done by other groups [33, 35] as well as our preliminary CD results listed in Chapter 4. This increased extent of unfolding on the hydrophobic CH_3 SAM as compared

to the hydrophilic OH SAM may be attributed to the strong thermodynamic driving force on hydrophobic surfaces which induces protein unfolding in order to minimize the overall solvent-accessible surface area of the system.

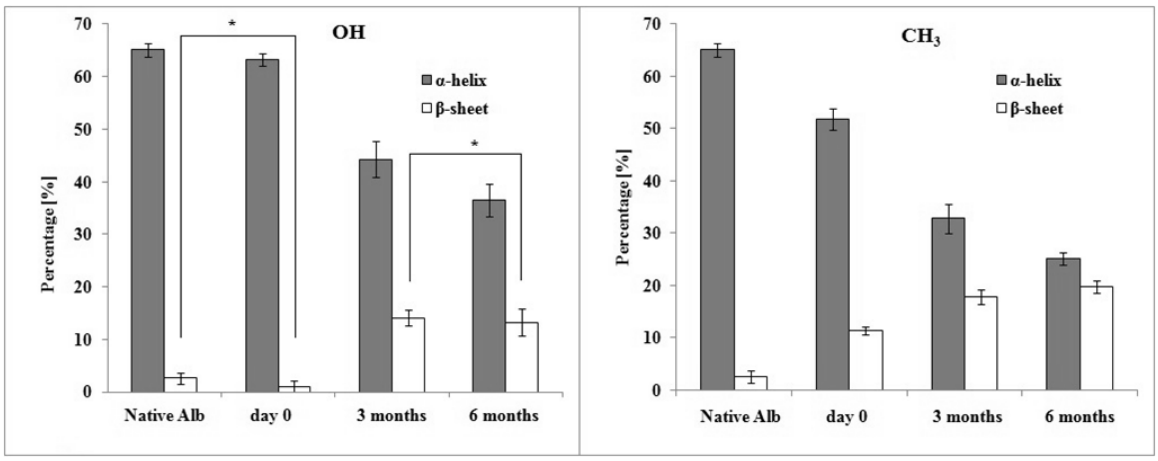

Figure 8.1. Secondary structural changes in Alb adsorbed on OH (left) and CH_3 (right) SAMs, from 10.0 mg/mL bulk solution concentration for time points of 0, 3, and 6 months (n=10, mean ± 95% CI). The native solution structure of Alb is included for comparison. * denotes no statistically significant difference, $p > 0.05$.

Table 8.1. Amounts of Alb adsorbed on CH_3 and OH SAM surfaces from 10.0 mg/mL bulk solution concentrations, for 3 and 6 month residence times. Initial values of surface coverage at day 0 are included for comparison (n= 6, mean ± 95% CI).

Surface	Day 0 [μg/cm^2]	3 months [μg/cm^2]	6 months [μg/cm^2]
CH_3	2.65 ± 0.24	2.63 ± 0.30	2.83 ± 0.18
OH	1.63 ± 0.23	1.64 ± 0.19	1.73 ± 0.16

8.3.2 Surface coverage of adsorbed Alb over residence times up to six months

In addition to the percentages of α-helix and β-sheet of the adsorbed Alb, the surface coverages on the CH_3 and OH SAMs were also calculated at day 0, 3 months, and 6 months, with the results listed in Table 8.1. The values for the amount of Alb adsorbed were comparable to those obtained in our earlier studies listed in Chapter 6 (2.71 ± 0.18 μg/cm^2 for the CH_3 SAM, 1.77 ± 0.49 μg/cm^2 for the OH SAM). Additionally, the surface coverage values remained consistent over the six month residence time, suggesting that the adsorbed Alb layer did not desorb over this period of time.

8.3.3 Effect of residence-time dependent changes in adsorbed Alb on platelet adhesion

Our previous results indicated that platelet adhesion to adsorbed Alb on SAM surfaces was significantly reduced for preadsorption from 10.0 mg/mL bulk solution concentration

compared to those for preadsorption from 0.1 and 1.0 mg/mL bulk solution concentrations, as presented in Chapters 5 and 6. This was attributed to the relatively minimal conformational changes undergone by the adsorbed Alb layer under these conditions. Our primary aim was to examine whether this adsorbed Alb layer on an implant surface underwent any structural changes for residence times of up to six months, and if so, whether this would enable and enhance platelet adhesion, an issue which has not been previously addressed by the biomaterials field.

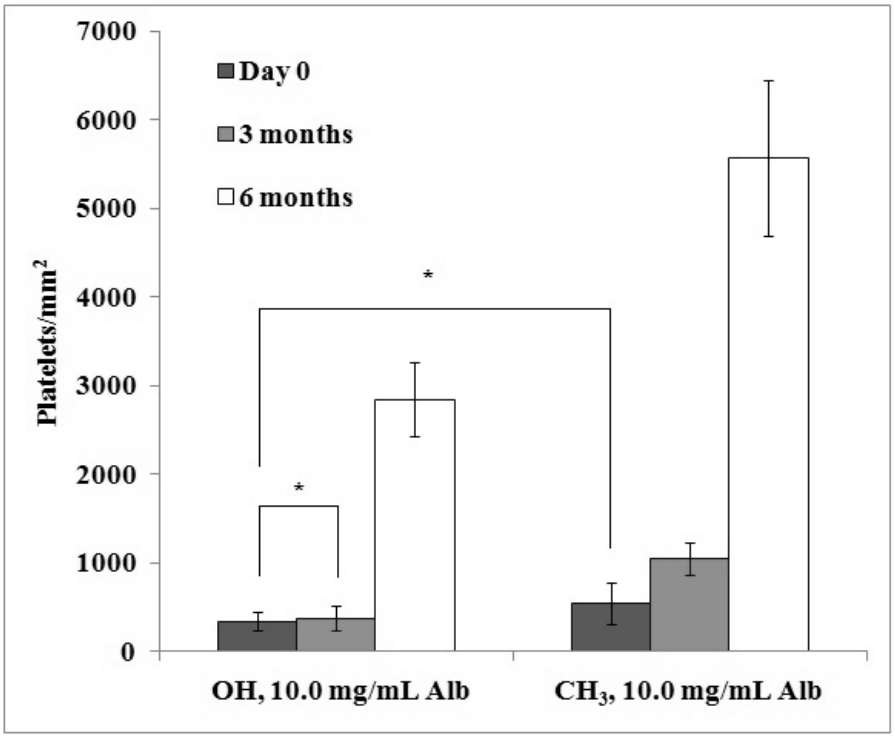

Figure 8.2. Platelet adhesion to OH and CH_3 SAMs preadsorbed with Alb from 10.0 mg/mL bulk solution concentration, for residence times of 0, 3, 6 months (n=6, mean ± 95% CI). * denotes no statistically significant difference, $p > 0.05$.

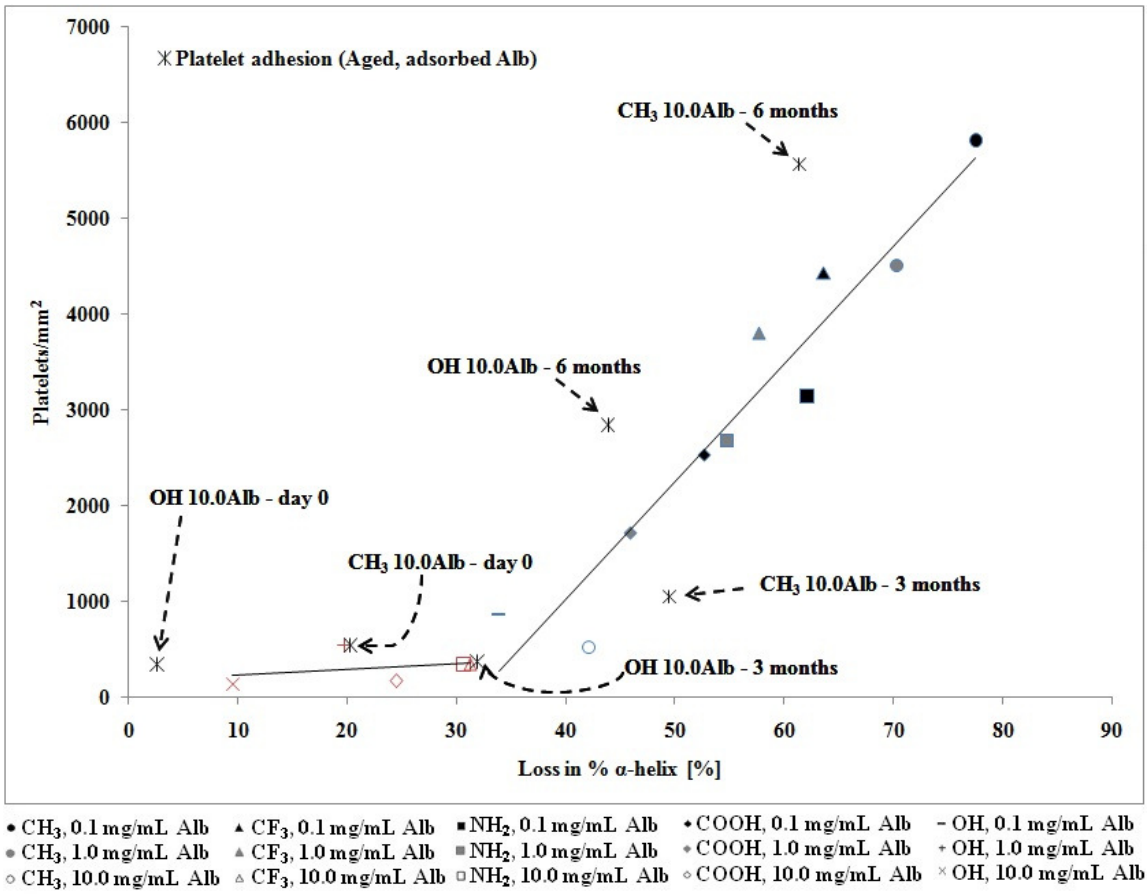

Figure 8.3. Platelet adhesion to adsorbed Alb aged on the OH and CH_3 SAM surfaces for 'aging' times of 0, 3, and 6 months, as a function of the degree of unfolding, as measured by the percentage loss in α-helix. These data points are overlaid on Fig. 6.3A for purposes of comparison. (Each point represents the mean of six values for each SAM surface).

The platelet adhesion levels on the OH and CH_3 SAMs preadsorbed with Alb from 10.0 mg/mL bulk solutions for residence times of 0, 3, and 6 months are shown in Fig. 8.2. Although there was no statistically significant difference in the platelet adhesion

levels on the OH and CH_3 SAMs at day 0, the difference in the adhesion levels on the two SAMs became apparent after 3 and 6 months of aging, following the same general trend observed for the aging-induced conformational changes in the adsorbed Alb layer (as seen in Fig. 8.1); i.e., more pronounced on the hydrophobic CH_3 SAM compared to the hydrophilic OH SAM for both 3 and 6 months of aging. Additionally, the platelet adhesion response on the OH SAM preadsorbed with Alb and aged over 6 months showed a significant increase compared to the two earlier time points (which were not statistically significantly different from each other). Similarly, there was a strong increase in the platelet response at the 6 month time point compared to the values at 3 months and day 0 on both SAMs. Coupled with the information on the conformational state of the adsorbed Alb layer on the SAM surfaces from Fig. 8.1, these results suggest that platelet adhesion to the adsorbed Alb layers over increasing residence times is driven by the time-dependent conformational changes in the adsorbed Alb layer.

The platelet adhesion levels on these aged Alb layers as a function of the degree of time-dependent unfolding, as measured by the percentage loss of α-helix, was overlaid on Figure 6.3A in which we had previously plotted the platelet adhesion levels on the different SAM surfaces at the three different Alb preadsorption conditions as a function of the percentage α-helix loss. As seen in Fig. 8.3, the large increase in the platelet adhesion levels on the OH SAM after 6 months of residence time can be attributed to the fact that the degree of unfolding at this time-point was greater than the critical degree of unfolding (~34% loss in α-helix) required for an adsorbed Alb layer to mediate platelet attachment, with platelet adhesion being even greater than that which was found for the

same degree of unfolding without aging. Although the CH_3 SAM aged over a 3 month period exhibited platelet adhesion levels which were somewhat lower than anticipated as per Fig. 8.3, the platelet adhesion response on the same SAM surface after 6 months of aging was found to be significantly greater than that which occurred for the same degree of unfolding without aging.

8.4 Conclusions

This study is the first study to our knowledge to examine long-term, aging-induced conformational changes in an adsorbed plasma protein, and its potential effect on platelet adhesion. The results conclusively illustrate that an irreversibly adsorbed, tightly packed layer of Alb is structurally altered with increasing residence time, and this leads to an enhanced platelet adhesion response. The platelet adhesion levels on the CH_3 and OH SAMs agree well with the results presented in Chapter 6, which suggest that Alb is capable of mediating platelet adhesion only beyond a critical degree of adsorption-induced unfolding. Since Alb is the most abundant plasma protein [77], and has been shown to only exhibit minimal to modest desorption by more surface-active plasma proteins, such as Fg and IgG, these results have critical implications in the development of a more comprehensive understanding of the factors associated with the hemocompatibility of biomaterials used for cardiovascular applications. Further studies are needed to examine residence time-dependent conformational changes in Fg and other

plasma proteins, and their influence (if any) on potentially mediating platelet adhesion responses to biomaterial surfaces.

CHAPTER 9

CONCLUSIONS AND RECOMMENDATIONS

9.1 Conclusions

The layer of adsorbed plasma proteins on the surface of a biomaterial is a critical determinant of its hemocompatibility due to the ability of cells such as platelets and leukocytes to recognize specific amino acid sequences, adhere and become activated, thereby triggering the deleterious thrombotic and inflammatory response(s) to the biomaterial. In addition to Fg, the role of which is well known in thrombosis, we also delineated the role of Alb in mediating platelet adhesion. Based on the results from this project, the following conclusions can be drawn regarding the role of plasma protein adsorption and the mechanisms of platelet adhesion to these adsorbed plasma proteins:

- Using a broad range of surface chemistries and protein solution concentrations, it was possible to independently vary the conformation of the adsorbed Fg layers from its surface coverage.
- With the ability to differentiate the adsorbed conformation from the amount of adsorbed Fg, we proved that the conformation of the adsorbed Fg layer plays a more critical role in mediating platelet adhesion than simply the amount of Fg adsorbed.
- We conclusively demonstrated that platelets can adhere to adsorbed Alb, beyond a critical degree of adsorption-induced unfolding.

- Pretreatment of the platelet suspension with an Arg-Gly-Asp-Ser (RGDS) peptide led to a partial inhibition (~50%) of platelet adhesion due to its inhibition of RGD-specific platelet receptors, which are hypothesized to mediate both adhesion and activation. However, this pretreatment also likely led to the activation of a non-RGD-specific receptor set(s), which mediates adhesion with little or no platelet activation.
- Anti-GPIb antibodies were found to be unable to inhibit the adhesion of RGDS-treated platelets to adsorbed Fg and Alb, indicating that this receptor set was not the non-RGD-specific receptor set that mediated the amount of platelet adhesion that occurred with RGDS-blocking.
- Blockade of the GPIIb/IIIa receptors by a peptidomimetic platelet antagonist Aggrastat led to a near complete inhibition of platelet adhesion to both adsorbed Fg and Alb, thus illustrating the critical role played by this receptor set in mediating platelet interactions with adsorbed proteins.
- Site-specific chemical modification of amino acids represents a powerful technique to examine their roles in mediating platelet binding. This technique was used to show that platelet adhesion to adsorbed Alb is largely mediated by Arg amino acid residues in Alb and that Lys amino acid residues did not play a significant role in the platelet adhesion response to adsorbed Alb.
- Additionally, we also showed that an irreversibly adsorbed, tightly packed layer of Alb undergoes residence time-dependent structural changes over a 6-month

time period, leading to a greater amount of platelet adhesion to the adsorbed Alb than that which occurs due to the unfolding process alone.

In conclusion, although our results show that the conformation of the adsorbed protein is a critical determinant of its ability to adhere platelets, we have also conclusively demonstrated that an irreversibly adsorbed, tightly packed Alb layer with near native structure undergoes time-dependent structural changes which enables and enhances platelet adhesion. Hence, this suggests that the optimal hemocompatible biomaterial would be one which adsorbs plasma protein(s) reversibly, without causing any adsorption-induced unfolding. This would represent a significant shift from the current design strategy of developing protein-resistant materials for cardiovascular applications.

9.2 Recommendations for future studies

The studies done as part of this project were aimed at delineating the molecular-level mechanisms of single-component protein adsorption on biomaterial surfaces, and subsequent platelet adhesion on this layer of adsorbed protein. However, blood-biomaterial interactions are highly complex, involving a variety of other proteins and cells including the complement system as well as leukocytes which mediates the inflammatory response. Additionally, the inflammatory and thrombotic responses are also highly interlinked.

Hence, the following studies are proposed for future studies to further the understanding of the factors underlying biomaterial-associated thrombosis:

- The studies must be extended to include other proteins including vWf, Fn and Vn. Additionally, competitive protein adsorption studies involving Fg and Alb as well as the proteins listed above would also help build a more comprehensive understanding of the interplay of these proteins both in the adsorption process, and also in mediating platelet adhesion.
- Although SAM surfaces are very useful in delineating the influence of specific surface chemistries on protein adsorption and subsequent platelet adhesion, they are not generally implanted in vivo. Hence, methods developed in this research need to be applied to study the relationships between adsorbed protein structure and platelet adhesion on more clinically relevant polymers, metals, and ceramic surfaces.
- Carrying out the protein adsorption and platelet adhesion experiments in a flow system is needed to more closely simulate in vivo conditions.
- In addition to the adhesion of platelets to adsorbed proteins on biomaterials, their activation and subsequent aggregation also play a critical role in biomaterial-associated thrombosis. Hence, it would be important to address this by carrying out assays to examine the activation state of the adherent platelets via a suitable method, such as a platelet factor 4 (PF4) assay.
- Extending our work with Alb, it would be important to examine whether the relationship between adsorption-induced conformational changes in proteins and

platelet adhesion is universal to all types of proteins. This could be addressed by extending these investigations to include non-plasma proteins (e.g., hemoglobin), which are not known to be unable to bind platelets.

- Since leukocytes and macrophages have been found to bind to adsorbed plasma proteins, understanding the mechanisms mediating the response of these cells on a protein layer as a function of its adsorption-induced conformational states would provide insights into the inflammatory response as well.
- Chemical modification of amino acid residues in proteins represents a powerful technique to examine the role of specific residues in mediating cell attachment, and our present work can be extended to potentially include other proteins, as well as other amino acid targets as an investigative tool to determine the types of amino acid residues that are involved in cellular responses to adsorbed proteins.
- Investigation of the GPVI and $\alpha_2\beta_1$ collagen receptors, among other platelet receptors as the non-RGD specific receptor set would provide deeper insight into platelet-protein interactions.

CHAPTER 10

APPENDICES

A. PROTOCOL FOR SAM FORMATION AND CHARACTERIZATION

A.1. Cleaning procedures for bare substrates

All cleaning procedures are to be carried out in the chemical hood, and all wash solutions must be freshly prepared.

1. The following wash solutions were prepared first:
    a. 'Piranha' wash: (7:3 v/v H_2SO_4:H_2O_2). (Note: The hydrogen peroxide used is purchased from VWR, Catalog No. VW3742-1).

       NOTE: It is very important to note that the sulfuric acid is added to the hydrogen peroxide, and not vice versa. This reaction is highly exothermic, with the temperature of the solution reaching up to 100°C. While handling this solution, suitable precautions (gloves, safety glasses and lab coat) must be taken, as the solution is highly corrosive. It may also be advisable to use a face-shield as well.
    b. RCA basic wash: (1:1:5 v/v H_2O_2:NH_4OH:H_2O).
2. The bare substrates (quartz slides or cover glasses or silicon chips) are removed from their packaging and placed in a Pyrex petridish containing the 'piranha' wash, and then incubated in an oven at 50°C for at least 30 minutes.

3. The petridish containing the substrates in ‘piranha’ wash is kept under distilled water for 2 minutes. The slides are removed and rinsed thoroughly with distilled water.
4. The slides/cover glasses are then transferred to another petridish containing RCA basic wash, and kept in the oven at 50°C for at least 30 minutes.
5. The petridish is removed from the oven and placed under distilled water for 5 minutes. The substrates are transferred to a petridish containing ‘piranha’ wash, and the process is repeated twice starting from step 2.
6. After going through the ‘piranha’ and RCA basic washes twice, the substrates are rinsed with nanopure water, 100% ethanol (Pharmco-Aaper, Catalog No. 11100200; obtained from Mr. Michael Moore in Jordan Hall at Clemson University) and then dried under a stream of nitrogen gas.

   Note: It is essential that 100% ethanol is used, as commercial sources of ethanol contain impurities which lead to the presence of undesirable contaminants on the surface.
7. The cleaned, dry bare substrates are kept in a clean, dry plastic petridish and taken for gold coating to Dr. James Harriss at the Microstructures Laboratory in the Department of Electrical Engineering in 22-B Riggs Hall.
8. Thermal vapor deposition of gold and chromium (which serves as an adhesive layer for the overlaying gold layer) is carried out.
   a. Substrates are generally coated with 50 Å of chromium and 1000 Å of gold.

b. For circular dichroism experiments, the quartz slides are coated with 30 Å of chromium and 100 Å of gold, to ensure optical transparency of these substrates.

A.2 Cleaning protocol for gold-coated substrates

The cleaning procedures for the gold coated substrates are similar to those used for bare substrates, but are less aggressive to avoid etching and pitting of the gold coating. Special caution must be exercised while cleaning the gold-coated quartz slides used for CD experiments, which have a thin layer of gold.

1. The gold-coated substrates are dipped in a modified 'piranha' wash (8:2 v/v H_2SO_4:H_2O_2) for about 15 sec, and then rinsed thoroughly with nanopure water.
2. The RCA basic wash is prepared and heated on a hot-plate. The substrates were then dipped in the RCA basic wash for about 15 sec, and then rinsed copiously with nanopure water.
3. The cleaned gold substrates are rinsed with 100% ethanol and either stored in a petridish filled with ethanol until needed, or directly immersed in a petridish containing alkanethiol solution for surface modification.

A.3 Formation of self-assembled monolayers (SAMs) of alkanethiols

1. 1.0 mM solutions of the following alkanethiols were prepared in 50 mL of 100% ethanol:
    a. 1-dodecanethiol (CH_3, Sigma #471364, 12.0 μL),

b. 11-(2,2,2-Trifuoroethoxy) undecane-1-thiol (CF_3, custom-synthesized by Asemblon Inc., 5 mL of 10X CF_3 solution in 45 mL of 100% ethanol)

c. 1-mercaptoundecanylamine (NH_2, Prochimia #FT 02A.11-1, 10.6 mg),

d. 12-mercaptododecanoic acid (COOH, Prochimia #FT 01.11-1, 11.6 mg), and

e. 11-mercapto-1-undecanol (OH, Sigma #447528, 10.22 mg).

NOTE: 3% v/v triethylamine must be added to the ethanol prior to the addition of the 1-mercaptoundecanylamine while preparing the NH_2 SAM solution, so as to prevent the thiol from adsorbing in an inverted fashion and thereby avoid a double layer formation.

2. The gold-coated substrates are incubated in the alkanethiol solutions overnight (for at least 16 hours) in the dark, to avoid/reduce oxidation of the thiol groups.

A.4 Cleaning the SAM surfaces

1. The substrates are removed from the alkanethiol solutions, rinsed with ethanol and sonicated in ethanol for 1 minute to displace any multilayers which may have formed.
2. The SAM surfaces are then cleaned to removed any traces of hydrophobic contaminants

    a. CH_3 and CF_3 SAMs are sonicated sequentially in ethanol, hexane and ethanol for 5 minutes each.

b. NH_2, COOH and OH SAMs are incubated in 25 mM phosphate buffer containing 0.005% v/v Triton-X-100 for 5 minutes to block off any hydrophobic defect sites (e.g., grain boundaries). These SAMs were then sonicated in acetone and ethanol for 5 minutes each, to remove any traces of loosely-bound Triton-X-100.

3. The cleaned SAM surfaces are then rinsed with ethanol and nanopure water, and stored in a petridish until further use.

A.5 Contact angle measurements

1. The slides are removed from the petridish, sonicated in ethanol for 10 minutes, rinsed with nanopure water and dried under a nitrogen gas stream, prior to being mounted on the sample stage of the CAM 200 Optical Contact Angle/Surface Tension Meter (KSV Instruments Ltd.).
2. Six drops of nanopure water (volume of each drop = 3.0 μL) is pipetted on to the surface. (Multiple drops are pipetted onto the surface to speed up the analysis).
3. The camera of the instruments is carefully focused on each drop individually, and then snapshot is captured using the CAM 200 software. The camera is then moved to the next drop, and the process is repeated until images of all drops have been captured.
4. The slides are then rinsed with nanopure water and then ethanol, and finally stored in ethanol until further use.

A.6 Ellipsometry

1. The cleaned SAM surface is rinsed with ethanol and dried under a stream of nitrogen gas, prior to being placed on the ellipsometry stage for analysis. If the liquid cell is being used, the sample must be placed in the cell, which is filled with buffer or nanopure water.
2. The position of the slide on the stage is adjusted to ensure that the spot (from the laser) falls on the desired region of the surface for analysis.
3. Start-up the computer, open the GESPACQ software, and click on "Show".
4. In the window which opens, set the following parameters:
    a. Wavelength = 0.45 μm,
    b. Analyzer angle = 0˚, and
    c. Incidence angle = 90˚.
5. Then click "Run".
6. After a pause of about 15 seconds, the instruments will start.
7. Lower the stage of the ellipsometer until the sample is out of the light beam.
8. Adjust the slit using the gold knob located under the ellipsometer table-top, until the counts value is approximately 20,000,0000.
9. Raise the stage until the counts value is half the original value, i.e., 10,000,000 counts.
10. Change the incidence angle to 70° (the general angle used for analysis of SAMs and protein layers). Higher incidence angles can be used for reducing noise and large variations in the measured thicknesses of rougher surfaces.

Note: The liquid cell can only be used at an incidence angle of 70°.

11. Ensure that the laser beam is hitting the desired location for analysis. If not, then the slide will have to be moved, and redo steps 7-11.
12. The sample is then leveled by adjusting two of the three screws located at the corners underneath the stage.
    a. The screw located on the left front side of the stage must not be touched.
    b. The back screw is adjusted until the counts are maximized, and then repeat with the right screw until the counts are maximized.
    c. Adjust the screws again, if necessary, until the symmetry is as close to zero as is possible (± 0.2).
13. Click on "Stop" and then exit "Show" mode.
14. Click on "Settings" and ensure that the incidence angle is set at the desired value for ellipsometric analysis. Then click on "Ok" to confirm the settings and close the "Settings" window.
15. Now click on the "Measurement" button, and then "Run".
16. Once the data has been collected, save the .dat and .mse files.
17. Close the GESPACQ program, and open the WINELLI software, which is used for calculating the thickness of the layer(s).
18. Open the .dat file.
19. In the "Analysis" tab, choose the "Regression" option.
20. For measuring the thickness of the alkanethiol layer, set the following parameters:
    a. Layer type of Layer 1 = Dispersion Law.

i. Double-click on Layer 1 and set Dispersion Law Type = Standard Dielectric Function,
ii. Selected Term = UV Term,
iii. Selected Law = Cauchy (nk), and
iv. A = 1.5.

b. Layer 2 is the gold layer. Browse and find the required .nk file (Au.nk).
   i. Set Layer Type = Materials,
   ii. Set Layer Thickness = 0.1 µm.

c. Layer 3 is the chromium layer. Browse and find the required .nk file (Cr.nk)
   i. Set Layer Type = Materials,
   ii. Set Layer Thickness = 0.005 µm.

d. The Substrate Layer is Quartz. Browse and find the required .nk file (SiO2.nk)
   i. Set Layer Type = Materials.

e. If the measurement is being carried out in air, the void.nk file is set for the ambient, and layer type is set as Materials. For samples analyzed under aqueous conditions (say, in the liquid cell), the suitable .nk file for the solution must be used. Usually, the measurements are generally carried out in buffer or nanopure water.

21. Click “Run”, and then click “Run” again to determine the thickness of the layer.

B. PROTOCOL FOR CIRCULAR DICHROISM SPECTROPOLARIMETRY

B.1 Buffer used for circular dichroism spectropolarimetry

1. Stock solutions of 25 mM monobasic and dibasic potassium phosphate are prepared.
2. Equal amounts of the two buffers mixed together yield a 25 mM potassium phosphate buffer with a pH close to 7.4, which generally needs minimal adjustment.

B.2 Circular dichroism measurements

1. The nitrogen gas flow rate is set to between 6-7 liters/min, and the nitrogen gas is allowed to flow for about 1 minute before the CD spectropolarimeter is switched on.
2. The instrument is left on for about 10 minutes, and then the Spectra Manager program is opened on the computer.
3. Open the "Spectrum Measurement" tool. A timer will count down for 5 minutes before the lamp gets turned on.
4. At the end of this, diagnostics will run. Errors may occur under the Amp and HT checks, and the "Ignore" box should be clicked, should they occur. The instrument will now be ready for use.
5. It is important to calibrate the instrument using the standard CD calibration solution of (1S)-(+)-10-camphorsulfonic acid (Sigma-Aldrich, Catalog No. C2107-5G), to ensure that the instrument does not have any true errors.

a. A 0.06% aqueous solution of this salt (30 mg of salt in 50 mL nanopure water) in a 1.0 cm quartz cuvette is used for calibration.
b. The CD value at a wavelength of 350 nm should be 0 mdeg. If this value is off, then it can be adjusted using the CD offset screw located on the back of the instrumentation circuit board observed when you take the top panel off the instrument.
c. Similarly, the CD value at a wavelength of 291 nm should be adjusted to 190.4 mdeg.

6. Before carrying out a CD scan, it is important to ensure that the scan parameters are set.
    a. The normal parameters used for CD scans on protein in solution are:
        i. Sensitivity = Standard (100 mdeg)
        ii. Starting wavelength = 300 nm
        iii. End wavelength = 190 nm
        iv. Data Pitch = 0.1 nm
        v. Scan mode = Continuous
        vi. Scan speed = 50 nm/min
        vii. Response = 0.25 sec
        viii. Bandwidth = 1.0 nm
        ix. Accumulations = 6
    b. The parameters used for high resolution scans (i.e., for adsorption studies) are:

i. Sensitivity = Standard (100 mdeg)
ii. Starting wavelength = 300 nm
iii. End wavelength = 190 nm
iv. Data Pitch = 0.1 nm
v. Scan mode = Continuous
vi. Scan speed = 5 nm/min
vii. Response = 16 sec
viii. Bandwidth = 1.0 nm
ix. Accumulations = 3

7. Background spectra are collected first. For protein solution studies this will be of the buffer in the cuvette, while for adsorption studies this will be of the buffer plus the alkanethiol-modified gold substrates in the custom-designed cuvette (see Fig. 4.1).
8. The 0.1 mm quartz cuvette (with removable windows) is typically used for CD studies on the native/solution structure of proteins.
    a. The protein solutions analyzed in these cuvettes typically have a concentration of approximately 2.0 mg/mL.
    b. The CD response is a function of both the concentration of the protein solution and the path-length of the cuvette, and the signal is based on the total number of molecules in the path of the light beam. Hence, a 0.2 mg/mL protein solution in a 1 mm cuvette would give an identical spectrum as a 2.0 mg/mL protein solution in a 0.1 mm cuvette.

c. If the protein concentration is too high in a cuvette with a given path-length, the absorbance may spike at wavelengths below 200 nm and yield a very noisy CD spectrum. In this case, it would be advisable to dilute the protein solution and then re-run the CD scan.

   Note: It is very important to ensure that the absorbance of the samples does not exceed a value of ~4.0, as the high tension (HT) voltage at this absorbance would be in the range of 800 V, and voltages above this can potentially damage the instrument.

d. If the characteristic CD minima for proteins do not appear in the 208-225 nm range, this likely implies that the concentration of protein is too low. This issue can be overcome by using a cuvette with longer path-length or using a more concentrated protein solution.

9. The custom-designed cuvette (shown in Fig. 4.1) was used for CD studies on the structure of adsorbed proteins on the SAM surfaces.

   a. The cleaned SAM surfaces were incubated in a petridish filled with 25 mM potassium phosphate buffer.

   b. Stock solutions of proteins were prepared in 25 mM phosphate buffer, and a suitable amount of stock protein was added to the SAM surfaces in the petridish to give the desired bulk solution concentration, taking care to ensure that the tip of the pipette is held below the air-water interface to avoid protein denaturation at this interface.

c. The protein adsorption step was carried out for the required duration (2 hours, in our case). For smaller proteins, the protein adsorption step may last even as long as 24 hours.

d. At the completion of protein adsorption, the petridish containing the protein-coated SAM surfaces in protein solution was infinitely diluted with buffer (or nanopure water) to wash away the protein solution as well as any loosely adherent protein.

e. This infinite dilution step gets rid of the layer the denatured protein which would have been present at the air-water interface and potentially contaminated the adsorbed protein layer, thereby permitting the removal of the SAM surfaces from the petridish without dragging it through this layer.

f. The custom-designed cuvette is filled with 1.0 mL of phosphate buffer, and then protein-coated SAM surfaces are then loaded into this cuvette. Any buffer overflowing from the cuvette is wiped off with a KimWipe, and once the cuvette has been wiped dry, it is loaded into the CD spectropolarimeter and scanned.

10. The spectrum obtained from the CD scans consists of the CD (in mdeg) and the absorbance values over the wavelength range scanned, and the .jws file is saved.
11. The CD spectra obtained are analyzed using the "Spectrum Analysis" program, which is part of the Spectrum Manager software package, and the percentage

composition of the secondary structural components of the native/adsorbed protein is calculated using the CDPro software package.

a. The .jws file is opened, to load the CD and absorbance spectra.

b. The spectra can be smoothed by using the "Data Cut" function (Processing → Correction → Data Cut), and adjusting the data pitch from 0.1 nm to either 0.5 nm or 1.0 nm. Further smoothing can also be done using the Savitzky-Golay algorithm under the curve smoothing option (Processing → Correction → Smoothing).

c. The data dump option (Processing → Common Options →Data Dump) is then used to copy the raw CD and absorbance data as a function of wavelength to a Microsoft Excel spreadsheet for further data analysis, taking care to ensure that the "thin out" (i.e., data pitch) is set to 1.0 nm. Additionally, the data dump option can also be used to choose CD and absorbance values for the wavelength range of 190 nm – 240 nm.

d. The ellipticity (θ, in mdeg) is converted to molar ellipticity ($[\theta]$, in deg·cm^2/dmol) using the following formulae:

$$[\theta] = (\theta \cdot M_0) / (10{,}000 \cdot C_{soln} \cdot L) \qquad (A.1)$$

$$[\theta] = (\theta \cdot M_0) / (10{,}000 \cdot Q_{ads}) \qquad (A.2)$$

where M_0 is the mean residue molecular weight (118 g/mol), C_{soln} is the protein solution concentration (g/mL), Q_{ads} is the protein surface concentration (g/cm^2), and L is the path-length of the cuvette (cm).

e. The concentrations of the protein in solution (C_{soln}) and adsorbed on the SAM surfaces (Q_{ads}) is determined from the height of the peptide absorbance peak at 195 nm (A_{195}).

   i. Using a reference wavelength of 300 nm, the height of the absorbance peaks ($A_{195} = Abs_{195nm} - Abs_{300nm}$) for serial dilutions of 2.0 mg/mL protein stock solutions are determined at 195 nm, with the actual concentrations of these solutions being determined using a bicinchoninic acid assay (BCA, Pierce Biotechnology).

   ii. Calibration curves of A_{195} vs. C_{soln} were plotted for both Fg and Alb, with the slope of these plots representing the term "$\varepsilon_{protein} \cdot L$" from Beer's Law, which can be written as:

$$A_{195} = \varepsilon_{protein} \cdot C_{soln} \cdot L \qquad (A.3)$$

   where $\varepsilon_{protein}$ is the extinction coefficient of the protein (which has units of $mL \cdot g^{-1} \cdot cm^{-1}$ or cm^2/g)

   iii. The terms "$C_{soln} \cdot L$" in equation A.3 has units of g/cm^2, which is equivalent to the units of surface coverage of the adsorbed protein. Hence this explains the equivalency of the "$C_{soln} \cdot L$" term in equation A.1 being replaced by Q_{ads} in equation A.2.

f. The wavelength and molar ellipticity values are copied to a text document "s.txt" in the CDPro folder.

g. Double-click/run the crdata.exe file in the CDPro folder, and enter the following parameters:

i. Type ‘0” for a new input file and hit the enter key.

ii. Enter a suitable name for the data and hit the enter key.

iii. Since the data has wavelength intervals (i.e., data pitch) of 1.0 nm, choose number 1.

iv. Input the initial and final wavelengths of 240 nm and 190 nm.

v. When prompted, enter the number 1 to indicate that the data is in units of molar ellipticity.

vi. Enter s.txt as the name of the file which contains the CD data.

vii. The next screen will ask the user to choose a reference set of proteins for deconvolution of the CD spectra. Choose option 2 (i.e., SP-22X algorithm), which generally has been found to be suitable for fibrinogen and albumin.

viii. Now go to the CDPro folder and run the CONTINLL.exe and SELCON3.exe files to get the values of the various secondary structural components in the native/adsorbed protein.

ix. It is advisable to note these values in the research lab notebook immediately, although they are stored the file protss.out, and may be accessed later if required. However, the data in this file does not have any date/time stamp, but has the name entered for the data in step (ii) above.

C. PROTOCOL FOR PLATELET ADHESION ASSAYS

C.1 Buffers used in platelet adhesion assays

1. The platelet suspension buffer (PSB, pH 7.4) contained 137 mM NaCl, 2.7 mM KCl, 5.5 mM Dextrose, 0.4 mM sodium phosphate (monobasic), 10 mM HEPES and 0.1 U/mL apyrase.
2. PSB was supplemented with 2.5 mM $CaCl_2$ and 1.0 mM $MgCl_2$ to give a platelet suspension with metal ions (PSB + MI).
3. Phosphate buffered saline (PBS) was made by dissolving 9.9 g of PBS powder (Fisher, Catalog No. BP661-10) in 1.0 L of nanopure water.

C.2 Protocol for obtaining whole blood from human volunteers

1. The use of human blood for research projects requires approval of the Institutional Review Board (IRB) and the Institutional Biosafety Committee (IBC) at Clemson University. The following protocols were approved by the IRB and IBC: IRB#2007-140 and IBC# 2009-39.
2. In addition to the main IRB and IBC protocol forms, two keys documents are the IRB-approved consent form and the IRB-approved questionnaire, for volunteers who consent to donate blood.
    a. The consent form, which is renewed annually by the IRB, will be filled in by the donor and signed at any time, indicating their consent to donate blood for our research project. It also outlines the risks associated with the

blood-draw process and suggests suitable steps, should a medical emergency arise due to the blood donation process.

b. The questionnaire on the other hand, is filled in by the donor on the day of the blood draw process, and is renewed annually by the IRB. It asks the donor some simple questions to assess whether (s)he is fit for donating blood on that day.

3. The blood is drawn from the volunteers by trained nurses at the Redfern Health Center in Clemson University. The student in charge of the project always accompanies the volunteer to and from the Redfern Health Center.

    a. The student generally picks up the ice chest, which is used to transport the blood samples from Redfern to the laboratory in Rhodes, from 202 Rhodes and fills the chest with 2-3 scoops of ice from the ice-making machine in the Histology Lab in 418 Rhodes.

    b. Approximately 30.0 mL of blood is collected per draw per donor into four BD Vacutainer tubes (Becton-Dickinson, Catalog No. 364606) containing an acid-citrated dextrose (ACD) anticoagulant. Note: These Vacutainer tubes are purchased by our laboratory and are generally kept in the laboratory at Redfern.

    c. Since the first few mL of blood is rich in coagulation factors, the first tube is always discarded, and remaining three Vacutainer tubes are put into a biohazard Ziploc bag, and transported back to the BSL-2 laboratory in 202 Rhodes on ice in an ice chest.

C.3 Protocol for processing whole blood to obtain washed platelets

While handling blood and platelets, it is essential to observe all safety precautions and wear a lab coat and safety glasses. A face mask may also be used, if the student deems it necessary.

1. The Vacutainer tubes are carefully removed from the Ziploc bag and the blood is transferred into 15.0 mL centrifuge tubes. The blood is centrifuged at 225g (i.e., 1190 rpm) for 15 minutes at 20°C in a Beckman Coulter Allegra 6R centrifuge located in 202 Rhodes to generate a yellowish supernatant which is platelet rich plasma (PRP).
2. The PRP is carefully aspirated out of each centrifuge tube and transferred to a fresh centrifuge tube using a transfer pipette, taking care not to disturb/touch the layer below the supernatant.
3. The used centrifuge and Vacutainer tubes are closed tightly and carefully put into the biohazard Ziploc bag, for disposal at the end of the experiment.
4. Washed platelets are separated from PRP by a gel separation method.
    a. Sepharose 2B (Sigma, Catalog No. 2B-300) is poured into a measuring cylinder and allowed to stand for about 2 hours, after which the supernatant is discarded and replaced with PSB. This process is repeated thrice, and the Sepharose suspension is finally poured into a liquid chromatography column (Sigma, Catalog No. C4169).

b. The Sepharose suspension is allowed to settle in the column for about 1 hour, with additional Sepharose added, if necessary. The level of Sepharose in the column should be visible, and should ideally be around the “Sigma” etching near the top of the column. The column can be kept running, with the addition of a suitable amount of PSB, to speed up the settling process, ensuring that the column does not run dry.

c. The remainder of the liquid column above the Sepharose layer is filled with PSB using a Pasteur pipette or transfer pipette and the column is connected to the reservoir containing PSB.

d. The system is allowed to run until about 100 mL of PSB has flowed through the column, to ensure optimal settling of the column.

e. The column is now ready for use.

   Note: It is ideal to complete steps (a-e) before going to Redfern to collect blood, so that the washed platelets can be separated from the PRP as soon as possible.

f. Once the PRP is ready, the flow of PSB from the reservoir to the column is stopped, and the PSB in the column is allowed to drain until its level is just above the top edge of the Sepharose. At this point, the bottom outlet of the column is closed.

g. The top of the column is then opened and the PRP is carefully layered on to the Sepharose using a transfer pipette, and allowed to pass into the main column. The remainder of the column is then filled carefully with PSB,

and the top of the column is closed and the flow of PSB from the reservoir to the column is restarted after re-opening the bottom outlet of the column.

h. Fractions are collected from the column in 1.7 or 2.0 mL centrifuge tubes. Buffer from the column elutes first, followed by the platelets and then the plasma proteins.

i. About 2 minutes after restarting flow from the column, the platelets will start exiting the column and are identified by their increased turbidity (compared to the buffer). The platelet-rich fractions with maximum turbidity are pooled and their concentration is measured using a Beckman Coulter Z2 Particle Counter and Size Analyzer (in the common cell culture laboratory in 416 Rhodes).

j. After the platelets have been collected from the column, the plasma proteins are collected (for disposal) in a 15 mL centrifuge tube, and the column is allowed to run until all the proteins have eluted from the column.

k. All biohazard waste from the blood collection and processing steps are packed in the biohazard Ziploc bag, sealed and disposed in the red biohazard bucket in 202 Rhodes.

C.3 Platelet adhesion experiments

1. The typical platelet count we generally get in the washed platelet suspension is 2-3 x 10^8 platelets/mL, which is adjusted to 10^8 platelets/mL with PSB, and then

supplemented with $CaCl_2$ and $MgCl_2$ to give final salt concentrations of 2.5 mM and 1.0 mM, respectively.

2. The platelet suspension is allowed to rest for 30 min at 37°C, after which it is added to the protein-coated SAMs in the 6- or 24-well plate and allowed to adhere for 1 hour at 37°C.
3. Six serial dilutions of the platelet suspension are made in PSB + MI in 1.7 mL centrifuge tubes, which are used for constructing the calibration curve used for quantifying the platelet adhesion levels. A seventh (control) centrifuge tube containing only PSB + MI is also used as part of the calibration curve samples. The samples for the calibration curve are incubated for 1 hour at 37°C, along with platelet-SAM samples.
5. At the end of the platelet adhesion step, the platelet suspension is aspirated from the wells into a centrifuge tube (which is later disposed in the biohazard disposal bin), and the SAM surfaces are rinsed five times with PBS to remove any non-adherent platelets.
6. The samples for SEM are processed via the following steps:
    a. A special buffer (3% glutaraldehyde + 0.1 M sodium cacodylate, pH 7.4) was used for fixing the samples for SEM for 30 minutes at room temperature, after which the fixed samples are rinsed with PBS thrice.
    b. The fixed samples are then incubated in ascending ethanol:water mixtures (50%, 60%, 70%, 80%, 90% and 99%) for 10 minutes each, to dehydrate them.

c. Finally, the samples are treated with 0.02 mL of hexamethyldisilazane (Sigma; obtained from Dr. Ken Webb's laboratory) and allowed to dry overnight in a laminar flow hood.

d. The next day, the samples are taken to the Microscopy Facility at the Advanced Materials Research Laboratory (AMRL, Clemson University, Pendleton, SC) to examine the morphology of the adherent platelets.

7. The platelet adhesion was quantified using a lactate dehydrogenase (LDH) assay. The kit we used as a Cytotox96® non-radioactive cytotoxicity assay (Promega).

   a. After the rinsing step (step 5), the samples are transferred to a fresh well-plate filled with PSB+MI, and the adherent platelets as well as the platelets for the calibration curve are lysed with a Triton-PSB buffer (2% v/v Triton-x-100 in PSB). 100 µL lysing buffer is used per 1 mL of PSB+MI in well-plate/centrifuge tube. The samples are then incubated at 37°C for 45 minutes (in 502 Rhodes).

   b. While this lysing step is running, we prepare the chromogenic substrate mix for the assay.

      i. Assay buffer from the kit is warmed to room temperature taking precautions to protect it from light), and 12 mL of this buffer is added to a bottle of the substrate mix (part of the kit).

      ii. Invert the bottle and shake gently until the substrate mix has dissolved in the assay buffer. One bottle of the reconstituted

substrate mix generally supplies enough chromogenic substrate for two 96-well plates, as per the suppliers instructions.

iii. It is important to always protect the reconstituted substrate mix from strong direct light. The unused portion of this mix can be stored for ≤ 6-8 weeks at -20°C.

c. After the cell lysis step is complete, 50 µL aliquots from all wells and tubes are transferred to a 96-well plate.

d. 50 µL of the reconstituted substrate mix is then added to each well of the 96-well plate. The plate is covered with foil/opaque box to protect it from direct light, and is incubated at room temperature for 30 minutes.

e. At the end of this incubation step, 50 µL of stop solution from the kit is added to each well, and the plate should be read within one hour of addition of the stop solution.

f. Prior to reading the plate, a syringe is used to pop any bubbles in the wells.

g. The plate is read at 492 nm and 600 nm (reference wavelength) and the values of the difference in absorbance at the two wavelengths for the samples are used to quantify the platelet adhesion.

h. A calibration curve of absorbance vs. platelet number is constructed, and the number of platelets adherent on the SAM surfaces can be read off this curve. This number is then divided by the surface area of the substrate to give the platelet adhesion per unit area.

D. PROTOCOL FOR MODIFICATION OF ARGININE RESIDUES IN ALBUMIN

D.1. Chemical modification of Arg and Lys in Alb solution

1. Prepare about 5.0 mL of 2.0 mg/mL Alb solution in 25 mM potassium phosphate buffer.
2. 2, 3-butanedione was used for the site-specific modification of Arg residues in Alb, while acetic anhydride was used for the acetylation of Alb.
    a. Prepare a 50 mM borate buffer, and add a suitable amount of 2, 3-butanedione to give a 50 mM final concentration of the butanedione.
    b. Prepare a 10% acetic anhydride solution in 25 mM phosphate buffer.
3. The modification reaction was carried out by mixing the protein and the modifying agents using the appropriate reaction conditions.
    a. Mix the Alb solution and the butanedione solution, and allow the modification reaction to proceed for 2 h at room temperature.
    b. For acetylation of the Alb solution, 100 µL aliquots of the acetic anhydride is added to the protein solution at 15 min intervals, over a 2 h period, with the reaction being carried out on ice.
4. At the end of the modification reaction, the modified protein solution was dialyzed against 25 mM phosphate buffer for at least 12 h, with the buffer being changed every 4 h.

5. The modified protein samples are then taken to the Clemson University Genomics Institute to analyze for Arg and Lys modification via electrospray ionization mass spectrometry (ESI-MS).

D.2. Chemical modification of Arg and Lys in adsorbed Alb on SAM surfaces

1. All substrates are cleaned with the wash solutions, coated with chromium and gold, and surface functionalized with alkanethiols, as described earlier in Section A of this appendix.
2. These cleaned SAM surfaces are incubated in the 25 mM phosphate buffer, and the Alb adsorption experiments are carried out on the SAM surfaces, as described in Section B.9 (a-e) of this appendix.
3. After the infinite dilution step is carried out, the Alb-coated SAM surfaces are incubated in 25 mM phosphate buffer, and the chemical modification of the adsorbed Alb on the SAM surfaces is carried out by the addition of the butanedione or acetic anhydride, as described in Section D.3 of this appendix.
4. At the end of the chemical modification step, an infinite dilution step is carried out to remove all traces of the modifying agent, and the surfaces are rinsed with nanopure water.
5. Further experimental analyses are carried out on the surfaces with adsorbed, modified Alb.

a. CD analysis was performed as described in Section B of this appendix, to examine the conformation of the modified protein layer.
b. The protein-coated SAMs are incubated with a washed platelet suspension, and the platelet adhesion levels are quantified by an LDH assay, as listed in Section C.3.

E. PROTOCOL FOR RESIDENCE TIME DEPENDENT STUDIES ON ADSORBED ALB ON SAM SURFACES

1. CH_3 and OH SAMs are prepared, as described in Section A of this appendix.
    a. 18 mm cover glasses are used for the platelet adhesion experiments.
    b. Standard quartz slides designed to fit our customized cuvette are used for CD studies.
2. These SAM surfaces are preadsorbed with 10.0 mg/mL bulk Alb solution concentration for 2 h, as described in Section B.9, so as to obtain an irreversibly adsorbed, tightly packed Alb layer.
3. These Alb-coated SAMs are analyzed via CD spectropolarimetry to evaluate the adsorbed conformation of the Alb layer, as listed in Section B of the appendix.
4. These surfaces are then immersed in 25 mM potassium phosphate buffer supplemented with 0.1% cellgro antibiotic/antimycotic solution (Mediatech Inc., Catalog No. MT30-004-CI), and incubated for 6 months at 37°C in an incubator (located in Room 416 Rhodes).
5. The buffer (with 0.1% antibiotic/antimycotic agent) is replenished every 2 weeks.
6. The samples are withdrawn at the 3 month and 6 month time-points for CD and platelet adhesion experiments.
    a. CD analysis is performed as described in Section B of this appendix, to examine the conformation of the modified protein layer, as well quantifying the surface coverage of the adsorbed Alb.

b. The protein-coated SAMs are incubated with a washed platelet suspension, and the platelet adhesion levels are quantified by an LDH assay, as listed in Section C.3.

REFERENCES

1. Gorbet MB, Sefton MV. Biomaterial-associated thrombosis: roles of coagulation factors, complement, platelets and leukocytes. Biomaterials 2004;25(26):5681-5703.

2. Horbett TA. The Role of Adsorbed Proteins in Tissue Response to Biomaterials. In: Ratner BD, Hoffman AS, Schoen FJ, Lemons JA, editors. Biomaterials Science: An Introduction to Materials in Medicine. New York: Elsevier Academic Press, 2004. p. 237-246.

3. Hanson SR. Blood Coagulation and Blood-Materials Interactions. In: Ratner BD, Hoffman AS, Schoen FJ, Lemons JA, editors. Biomaterials Science: An Introduction to Materials in Medicine. New York: Elsevier Academic Press, 2004. p. 332-338.

4. Schmaier AH. Contact activation: A revision. Thromb Haemost 1997;78(1):101-107.

5. Chatterjee K, Thornton JL, Bauer JW, Vogler EA, Siedlecki CA. Moderation of prekallkrein-factor XII interactions in surface activation of coagulation by protein-adsorption competition. Biomaterials 2009;30(28):4915-4920.

6. Vogler EA, Siedlecki CA. Contact activation of blood-plasma coagulation. Biomaterials 2009;30(10):1857-1869.

7. Hanson SR. Device Thrombosis and Thromboembolism. Cardiovasc Pathol 1993;2(3):S157-S165.

8. Kleinschnitz C, Stoll G, Bendszus M, Schuh K, Pauer HU, Burfeind P, et al. Targeting coagulation factor XII provides protection from pathological thrombosis in cerebral ischemia without interfering with hemostasis. J Exp Med 2006;203(3):513-518.

9. Renne T, Pozgajova M, Gruner S, Schuh K, Pauer HU, Burfeind P, et al. Defective thrombus formation in mice lacking coagulation factor XII. J Exp Med 2005;202(2):271-281.

10. Ziats NP, Pankowsky DA, Tierney BP, Ratnoff OD, Anderson JM. Adsorption of Hageman-Factor (Factor-XII) and Other Human Plasma-Proteins to Bio-Medical Polymers. J Lab Clin Med 1990;116(5):687-696.

11. Mulzer SR, Brash JL. Identification of Plasma-Proteins Adsorbed to Hemodialyzers During Clinical Use. J Biomed Mater Res 1989;23(12):1483-1504.

12. Cornelius RM, Brash JL. Identification of Proteins Adsorbed to Hemodialyzer Membranes from Heparinized Plasma. J Biomater Sci Polym Ed 1993;4(3):291-304.

13. Boisclair MD, Philippou H, Lane DA. Thrombogenic Mechanisms in the Human - Fresh Insights Obtained by Immunodiagnostic Studies of Coagulation Markers. Blood Coagul Fibrinolysis 1993;4(6):1007-1021.

14. Boisclair MD, Lane DA, Philippou H, Esnouf MP, Sheikh S, Hunt B, et al. Mechanisms of Thrombin Generation During Surgery and Cardiopulmonary Bypass. Blood 1993;82(11):3350-3357.

15. Chung JH, Gikakis N, Rao AK, Drake TA, Colman RW, Edmunds LH. Pericardial blood activates the extrinsic coagulation pathway during clinical cardiopulmonary bypass. Circulation 1996;93(11):2014-2018.

16. Ernofsson M, Thelin S, Siegbahn A. Monocyte tissue factor expression, cell activation, and thrombin formation during cardiopulmonary bypass: A clinical study. J Thorac Cardiovasc Surg 1997;113(3):576-584.

17. Wilhelm CR, Ristich J, Kormos RL, Wagner WR. Monocyte tissue factor expression and ongoing complement generation in ventricular assist device patients. Ann Thorac Surg 1998;65(4):1071-1076.

18. Hong J, Ekdahl KN, Reynolds H, Larsson R, Nilsson B. A new in vitro model to study interaction between whole blood and biomaterials. Studies of platelet and coagulation activation acid the effect of aspirin. Biomaterials 1999;20(7):603-611.

19. Schoen FJ. Host Reactions to Biomaterials and Their Evaluation: An Introduction. In: Ratner BD, Hoffman AS, Schoen FJ, Lemons JA, editors. Biomaterials Science: An Introduction to Materials in Medicine. New York: Elsevier Academic Press, 2004. p. 293-296.

20. Anderson JM, Schoen FJ. Interactions of blood with artificial surfaces. In: Butchart EG, Bodnar E, editors. Current Issues in Heart Valve Disease: Thrombosis, Embolism and Bleeding: ICR Publishers, 1992. p. 160-171.

21. Ratner BD, Hoffman AS, Schoen FJ, Lemons JE. Biomaterials Science: An Introduction to Materials in Medicine. 2nd. ed: Elsevier Academic Press, 2004.

22. Misoph M, Schwender S, Babin-Ebell J. Response of the cellular immune system to cardiopulmonary bypass is independent of the applied pump type and of the use of heparin-coated surfaces. Thorac Cardiovasc Surg 1998;46(4):222-227.

23. Bittl JA. Coronary stent occlusion: Thrombus horribilis. J Am Coll Cardiol 1996;28(2):368-370.

24. Hakim RM. Complement Activation by Biomaterials. Cardiovasc Pathol 1993;2(3):S187-S197.

25. Johnson RJ. Complement Activation During Extracorporeal Therapy - Biochemistry, Cell Biology and Clinical Relevance. Nephrology Dialysis Transplantation 1994;9:36-45.

26. Anderson JM. Mechanisms of Inflammation and Infection with Implanted Devices. Cardiovasc Pathol 1993;2(3):S33-S41.

27. Gorbet MB, Yeo EL, Sefton MV. Flow cytometric study of in vitro neutrophil activation by biomaterials. J Biomed Mater Res 1999;44(3):289-297.

28. Kao WJ, Sapatnekar S, Hiltner A, Anderson JM. Complement-mediated leukocyte adhesion on poly(etherurethane ureas) under shear stress in vitro. J Biomed Mater Res 1996;32(1):99-109.

29. McNally AK, Anderson JM. Complement C3 Participation in Monocyte Adhesion to Different Surfaces. Proc Natl Acad Sci USA 1994;91(21):10119-10123.

30. Mickelson JK, Lakkis NM, VillarrealLevy G, Hughes BJ, Smith CW. Leukocyte activation with platelet adhesion after coronary angioplasty: A mechanism for recurrent disease? J Am Coll Cardiol 1996;28(2):345-353.

31. Dee KC, Puleo DA, Bizios R. Protein-Surface Interactions. In: Dee KC, Puleo DA, Bizios R, editors. An Introduction to Tissue-Biomaterial Interactions: John Wiley, 2002. p. 37-52.

32. Horbett TA, Brash JL. Proteins At Interfaces - Current Issues And Future-Prospects. Acs Symposium Series 1987;343:1-33.

33. Roach P, Farrar D, Perry CC. Interpretation of protein adsorption: Surface-induced conformational changes. J Am Chem Soc 2005;127(22):8168-8173.

34. Wertz CF, Santore MM. Effect of surface hydrophobicity on adsorption and relaxation kinetics of albumin and fibrinogen: Single-species and competitive behavior. Langmuir 2001;17(10):3006-3016.

35. Andrade JD, Hlady V. Protein Adsorption And Materials Biocompatibility - A Tutorial Review And Suggested Hypotheses. Adv Polym Sci 1986;79:1-63.

36. Balasubramanian V, Grusin NK, Bucher RW, Turitto VT, Slack SM. Residence-time dependent changes in fibrinogen adsorbed to polymeric biomaterials. J Biomed Mater Res 1999;44(3):253-260.

37. Chinn JA, Posso SE, Horbett TA, Ratner BD. Postadsorptive Transitions in Fibrinogen Adsorbed to Biomer - Changes in Baboon Platelet-Adhesion, Antibody-Binding, and Sodium Dodecyl-Sulfate Elutability. J Biomed Mater Res 1991;25(4):535-555.

38. Chinn JA, Posso SE, Horbett TA, Ratner BD. Postadsorptive Transitions in Fibrinogen Adsorbed to Polyurethanes - Changes in Antibody-Binding and Sodium Dodecyl-Sulfate Elutability. J Biomed Mater Res 1992;26(6):757-778.

39. Latour RA. Biomaterials: Protein-Surface Interactions. In: Wnek GE, Bowlin GL, editors. The Encyclopedia of Biomaterials and Bioengineering: Informa Healthcare, 2008. p. 270-284.

40. Vroman L, Adams AL. Findings with Recording Ellipsometer Suggesting Rapid Exchange of Specific Plasma Proteins at Liquid/Solid Interfaces. Surf Sci 1969;16:438-&.

41. Evans-Nguyen KM, Tolles LR, Gorkun OV, Lord ST, Schoenfisch MH. Interactions of thrombin with fibrinogen adsorbed on methyl-, hydroxyl-, amine-, and carboxyl-terminated self-assembled monolayers. Biochemistry 2005;44(47):15561-15568.

42. Evans-Nguyen KM, Schoenfisch MH. Fibrin proliferation at model surfaces: Influence of surface properties. Langmuir 2005;21(5):1691-1694.

43. Elwing H. Protein absorption and ellipsometry in biomaterial research. Biomaterials 1998;19(4-5):397-406.

44. Stevens PW, Hansberry MR, Kelso DM. Assessment Of Adsorption And Adhesion Of Proteins To Polystyrene Microwells By Sequential Enzyme-Linked-Immunosorbent-Assay Analysis. Anal Biochem 1995;225(2):197-205.

45. Gorbet MB, Sefton MV. Complement inhibition reduces material-induced leukocyte activation with PEG modified polystyrene beads (Tentagel (TM)) but not polystyrene beads. J Biomed Mater Res 2005;74A(4):511-522.

46. Kidane A, Park K. Complement activation by PEO-grafted glass surfaces. J Biomed Mater Res 1999;48(5):640-647.

47. Caruso F, Furlong DN, Kingshott P. Characterization of ferritin adsorption onto gold. J Colloid Interface Sci 1997;186(1):129-140.

48. Hook F, Kasemo B, Nylander T, Fant C, Sott K, Elwing H. Variations in coupled water, viscoelastic properties, and film thickness of a Mefp-1 protein film during adsorption and cross-linking: A quartz crystal microbalance with dissipation monitoring, ellipsometry, and surface plasmon resonance study. Anal Chem 2001;73(24):5796-5804.

49. Hook F, Rodahl M, Brzezinski P, Kasemo B. Energy dissipation kinetics for protein and antibody-antigen adsorption under shear oscillation on a quartz crystal microbalance. Langmuir 1998;14(4):729-734.

50. Sigal GB, Mrksich M, Whitesides GM. Effect of surface wettability on the adsorption of proteins and detergents. J Am Chem Soc 1998;120(14):3464-3473.

51. Kidoaki S, Matsuda T. Adhesion forces of the blood plasma proteins on self-assembled monolayer surfaces of alkanethiolates with different functional groups measured by an atomic force microscope. Langmuir 1999;15(22):7639-7646.

52. Ta TC, McDermott MT. Mapping interfacial chemistry induced variations in protein adsorption with scanning force microscopy. Anal Chem 2000;72(11):2627-2634.

53. Taborelli M, Eng L, Descouts P, Ranieri JP, Bellamkonda R, Aebischer P. Bovine Serum-Albumin Conformation on Methyl and Amine Functionalized Surfaces Compared by Scanning Force Microscopy. J Biomed Mater Res 1995;29(6):707-714.

54. Hylton DM, Shalaby SW, Latour RA. Direct correlation between adsorption-induced changes in protein structure and platelet adhesion. J Biomed Mater Res Part A 2005;73A(3):349-358.

55. Tanaka M, Motomura T, Kawada M, Anzai T, Kasori Y, Shiroya T, et al. Blood compatible aspects of poly(2-methoxyethylacrylate) (PMEA) - relationship between protein adsorption and platelet adhesion on PMEA surface. Biomaterials 2000;21(14):1471-1481.

56. Tsai WB, Grunkemeier JM, McFarland CD, Horbett TA. Platelet adhesion to polystyrene-based surfaces preadsorbed with plasmas selectively depleted in fibrinogen, fibronectin, vitronectin, or von Willebrand's factor. J Biomed Mater Res A 2002;60(3):348-359.

57. Tsai WB, Shi Q, Grunkemeier JM, McFarland C, Horbett TA. Platelet adhesion to radiofrequency glow-discharge-deposited fluorocarbon polymers preadsorbed with selectively depleted plasmas show the primary role of fibrinogen. J Biomater Sci Polym Ed 2004;15(7):817-840.

58. Farrell DH, Thiagarajan P, Chung DW, Davie EW. Role of Fibrinogen Alpha-Chain and Gamma-Chain Sites in Platelet-Aggregation. Proc Natl Acad Sci USA 1992;89(22):10729-10732.

59. Savage B, Ruggeri ZM. Selective Recognition of Adhesive Sites in Surface-Bound Fibrinogen by Glycoprotein-IIb-IIIa on Nonactivated Platelets. J Biol Chem 1991;266(17):11227-11233.

60. Springer TA, Zhu JH, Xiao T. Structural basis for distinctive recognition of fibrinogen gamma C peptide by the platelet integrin alpha(IIb)beta(3). J Cell Biol 2008;182(4):791-800.

61. Remijn JA, Ijsseldijk MJW, van Hemel BM, Galanakis DK, Hogan KA, Lounes KC, et al. Reduced platelet adhesion in flowing blood to fibrinogen by alterations in segment gamma 316-322, part of the fibrin-specific region. Br J Haematol 2002;117(3):650-657.

62. Podolnikova NP, Yakubenko VP, Volkov GL, Plow EF, Ugarova TP. Identification of a novel binding site for platelet integrins alpha(IIb)beta(3) (GPIIbIIIa) and alpha(5)beta(1) in the gamma C-domain of fibrinogen. J Biol Chem 2003;278(34):32251-32258.

63. Podolnikova NP, Gorkun OV, Loreth RM, Yee VC, Lord ST, Ugarova TP. A cluster of basic amino acid residues in the gamma 370-381 sequence of fibrinogen comprises a binding site for platelet integrin alpha(IIb)beta(3) (glycoprotein IIb/IIIa). Biochemistry 2005;44(51):16920-16930.

64. Lishko VK, Kudryk B, Yakubenko VP, Yee VC, Ugarova TP. Regulated unmasking of the cryptic binding site for integrin alpha(M)beta(2) in the gamma C-domain of fibrinogen. Biochemistry 2002;41(43):12942-12951.

65. Ishihara K, Fukumoto K, Iwasaki Y, Nakabayashi N. Modification of polysulfone with phospholipid polymer for improvement of the blood compatibility. Part 2. Protein adsorption and platelet adhesion. Biomaterials 1999;20(17):1553-1559.

66. Iwasaki Y, Ishihara K. Phosphorylcholine-containing polymers for biomedical applications. Anal Bioanal Chem 2005;381(3):534-546.

67. Suhara H, Sawa Y, Nishimura M, Oshiyama H, Yokoyama K, Saito N, et al. Efficacy of a new coating material, PMEA, for cardiopulmonary bypass circuits in a porcine model. Ann Thorac Surg 2001;71(5):1603-1608.

68. Berndt MC, Shen Y, Dopheide SM, Gardiner EE, Andrews RK. The vascular biology of the glycoprotein Ib-IX-V complex. Thromb Haemost 2001;86(1):178-188.

69. Ruggeri ZM. Structure and function of von Willebrand factor. Thromb Haemost 1999;82(2):576-584.

70. Ruggeri ZM. von Willebrand factor. J Clin Invest 1997;99(4):559-564.

71. Savage B, Almus-Jacobs F, Ruggeri ZM. Specific synergy of multiple substrate-receptor interactions in platelet thrombus formation under flow. Cell 1998;94(5):657-666.

72. Andrews RK, Berndt MC. Platelet physiology and thrombosis. Thromb Res 2004;114(5-6):447-453.

73. Varga-Szabo D, Pleines I, Nieswandt B. Cell adhesion mechanisms in platelets. Arterioscler Thromb Vasc Biol 2008;28(3):403-412.

74. Ewenstein BM. Von Willebrand's disease. Annu Rev Med 1997;48:525-542.

75. Denis C, Methia N, Frenette PS, Rayburn H, Ullman-Cullere M, Hynes RO, et al. A mouse model of severe von Willebrand disease: Defects in hemostasis and thrombosis. Proc Natl Acad Sci USA 1998;95(16):9524-9529.

76. Jurk K, Clemetson KJ, de Groot PG, Brodde MF, Steiner M, Savion N, et al. Thrombospondin-1 mediates platelet adhesion at high shear via glycoprotein Ib (GPIb): an alternative/backup mechanism to von Willebrand factor. FASEB J 2003;17(9):1490-1492.

77. Curry S, Mandelkow H, Brick P, Franks N. Crystal structure of human serum albumin complexed with fatty acid reveals an asymmetric distribution of binding sites. Nat Struct Biol 1998;5(9):827-835.

78. Bhattacharya AA, Grune T, Curry S. Crystallographic analysis reveals common modes of binding of medium and long-chain fatty acids to human serum albumin. J Mol Biol 2000;303(5):721-732.

79. Coelho MAN, Vieira EP, Motschmann H, Mohwald H, Thunemann AF. Human serum albumin on fluorinated surfaces. Langmuir 2003;19(18):7544-7550.

80. Tsai WB, Grunkemeier JM, Horbett TA. Variations in the ability of adsorbed fibrinogen to mediate platelet adhesion to polystyrene-based materials: A multivariate statistical analysis of antibody binding to the platelet binding sites of fibrinogen. J Biomed Mater Res A 2003;67A(4):1255-1268.

81. Kottke-Marchant K, Anderson JM, Umemura Y, Marchant RE. Effect of albumin coating on the in vitro blood compatibility of Dacron arterial prostheses. Biomaterials 1989;10(3):147-155.

82. Marois Y, Chakfe N, Guidoin R, Duhamel RC, Roy R, Marois M, et al. An albumin-coated polyester arterial graft: In vivo assessment of biocompatibility and healing characteristics. Biomaterials 1996;17(1):3-14.

83. Ito Y, Sisido M, Imanishi Y. Adsorption of Plasma-Proteins and Adhesion of Platelets onto Novel Polyetherurethaneureas - Relationship between Denaturation of Adsorbed Proteins and Platelet-Adhesion. J Biomed Mater Res 1990;24(2):227-242.

84. Rodrigues SN, Goncalves IC, Martins MCL, Barbosa MA, Ratner BD. Fibrinogen adsorption, platelet adhesion and activation on mixed hydroxyl-/methyl-terminated self-assembled monolayers. Biomaterials 2006;27(31):5357-5367.

85. Weisiger R, Gollan J, Ockner R. Receptor for albumin on the liver-cell surface may mediate uptake of fatty-acids and other albumin-bound substances. Science 1981;211(4486):1048-1050.

86. Chaudhury C, Mehnaz S, Robinson JM, Hayton WL, Pearl DK, Roopenian DC, et al. The major histocompatibility complex-related Fc receptor for IgG (FcRn) binds albumin and prolongs its lifespan. J Exp Med 2003;197(3):315-322.

87. Davis GE. The Mac-1 and P150,95 Beta-2 Integrins Bind Denatured Proteins to Mediate Leukocyte Cell Substrate Adhesion. Exp Cell Res 1992;200(2):242-252.

88. Zhu XP, Meng G, Dickinson BL, Li XT, Mizoguchi E, Miao LL, et al. MHC class I-related neonatal Fc receptor for IgG is functionally expressed in monocytes, intestinal macrophages, and dendritic cells. J Immunol 2001;166(5):3266-3276.

89. Godek ML, Michel R, Chamberlain LM, Castner DG, Grainger DW. Adsorbed serum albumin is permissive to macrophage attachment to perfluorocarbon polymer surfaces in culture. J Biomed Mater Res A 2009;88A(2):503-519.

90. Dobson CM. Protein folding and misfolding. Nature 2003;426(6968):884-890.

91. Goncalves IC, Martins MCL, Barbosa MA, Ratner BD. Protein adsorption on 18-alkyl chains immobilized on hydroxyl-terminated self-assembled monolayers. Biomaterials 2005;26(18):3891-3899.

92. Margel S, Vogler EA, Firment L, Watt T, Haynie S, Sogah DY. Peptide, Protein, And Cellular Interactions With Self-Assembled Monolayer Model Surfaces. J Biomed Mater Res 1993;27(12):1463-1476.

93. Tidwell CD, Ertel SI, Ratner BD, Tarasevich BJ, Atre S, Allara DL. Endothelial cell growth and protein adsorption on terminally functionalized, self-assembled monolayers of alkanethiolates on gold. Langmuir 1997;13(13):3404-3413.

94. Hirata I, Hioko Y, Toda M, Kitazawa T, Murakami Y, Kitano E, et al. Deposition of complement protein C3b on mixed self-assembled monolayers carrying surface hydroxyl and methyl groups studied by surface plasmon resonance. J Biomed Mater Res Part A 2003;66A(3):669-676.

95. Martins MCL, Ratner BD, Barbosa MA. Protein adsorption on mixtures of hydroxyl- and methylterminated alkanethiols self-assembled monolavers. J Biomed Mater Res Part A 2003;67A(1):158-171.

96. Rixman MA, Dean D, Macias CE, Ortiz C. Nanoscale intermolecular interactions between human serum albumin and alkanethiol self-assembled monolayers. Langmuir 2003;19(15):6202-6218.

97. Sperling C, Schweiss RB, Streller U, Werner C. In vitro hemocompatibility of self-assembled monolayers displaying various functional groups. Biomaterials 2005;26(33):6547-6557.

98. Losic D, Shapter JG, Gooding JJ. Integrating polymers with alkanethiol self-assembled monolayers (SAMs): blocking SAM defects with electrochemical polymerisation of tyramine. Electrochem Commun 2002;4(12):953-958.

99. Fears KP, Sivaraman B, Powell GL, Wu Y, Latour RA. Probing the Conformation and Orientation of Adsorbed Enzymes Using Side-Chain Modification. Langmuir 2009;25(16):9319-9327.

100. Tegoulia VA, Cooper SL. Leukocyte adhesion on model surfaces under flow: Effects of surface chemistry, protein adsorption, and shear rate. J Biomed Mater Res 2000;50(3):291-301.

101. Wertz CF, Santore MM. Adsorption and relaxation kinetics of albumin and fibrinogen on hydrophobic surfaces: Single-species and competitive behavior. Langmuir 1999;15(26):8884-8894.

102. Tengvall P, Lundstrom I, Liedberg B. Protein adsorption studies on model organic surfaces: an ellipsometric and infrared spectroscopic approach. Biomaterials 1998;19(4-5):407-422.

103. Grunkemeier JM, Tsai WB, McFarland CD, Horbett TA. The effect of adsorbed fibrinogen, fibronectin, von Willebrand factor and vitronectin on the procoagulant state of adherent platelets. Biomaterials 2000;21(22):2243-2252.

104. Broberg M, Eriksson C, Nygren H. GPIIb/IIIa is the main receptor for initial platelet adhesion to glass and titanium surfaces in contact with whole blood. J Lab Clin Med 2002;139(3):163-172.

105. Shattil SJ, Newman PJ. Integrins: dynamic scaffolds for adhesion and signaling in platelets. Blood 2004;104(6):1606-1615.

106. Comfurius P, Williamson P, Smeets EF, Schlegel RA, Bevers EM, Zwaal RFA. Reconstitution of phospholipid scramblase activity from human blood platelets. Biochemistry 1996;35(24):7631-7634.

107. Gartner TK, Bennett JS. The Tetrapeptide Analog of the Cell Attachment Site of Fibronectin Inhibits Platelet-Aggregation and Fibrinogen Binding to Activated Platelets. J Biol Chem 1985;260(22):1891-1894.

108. Haverstick DM, Cowan JF, Yamada KM, Santoro SA. Inhibition of Platelet-Adhesion to Fibronectin, Fibrinogen, and Vonwillebrand-Factor Substrates by a Synthetic Tetrapeptide Derived from the Cell-Binding Domain of Fibronectin. Blood 1985;66(4):946-952.

109. Goldsmith HL, Turitto VT. Rheological Aspects of Thrombosis and Hemostasis - Basic Principles and Applications - ICTH Report - Subcommittee on Rheology of the International Committee on Thrombosis and Hemostasis. Thromb Haemost 1986;55(3):415-435.

110. Kroll MH, Hellums JD, McIntire LV, Schafer AI, Moake JL. Platelets and shear stress. Blood 1996;88(5):1525-1541.

111. Lecut C, Schoolmeester A, Kuijpers MJE, Broers JLV, van Zandvoort M, Vanhoorelbeke K, et al. Principal role of glycoprotein VI in alpha 2 beta 1 and alpha IIb beta 3 activation during collagen-induced thrombus formation. Arterioscler Thromb Vasc Biol 2004;24(9):1727-1733.

112. Frank RD, Dresbach H, Thelen H, Sieberth HG. Glutardialdehyde induced fluorescence technique (GIFT): A new method for the imaging of platelet adhesion on biomaterials. J Biomed Mater Res A 2000;52(2):374-381.

113. Jirouskova M, Jaiswal JK, Coller BS. Ligand density dramatically affects integrin alpha IIb beta 3-mediated platelet signaling and spreading. Blood 2007;109(12):5260-5269.

114. Patel D, Vaananen H, Jirouskova M, Hoffmann T, Bodian C, Coller BS. Dynamics of GPIIb/IIIa-mediated platelet-platelet interactions in platelet adhesion/thrombus formation on collagen in vitro as revealed by videomicroscopy. Blood 2003;101(3):929-936.

115. Shattil SJ, Cunningham M, Hoxie JA. Detection of Activated Platelets in Whole-Blood Using Activation-Dependent Monoclonal-Antibodies and Flow-Cytometry. Blood 1987;70(1):307-315.

116. Lindon JN, McManama G, Kushner L, Merrill EW, Salzman EW. Does the Conformation of Adsorbed Fibrinogen Dictate Platelet Interactions with Artificial Surfaces. Blood 1986;68(2):355-362.

117. Salzman EW, Lindon J, McManama G, Ware JA. Role of Fibrinogen in Activation of Platelets by Artificial Surfaces. Ann N Y Acad Sci 1987;516:184-195.

118. Shiba E, Lindon JN, Kushner L, Matsueda GR, Hawiger J, Kloczewiak M, et al. Antibody-Detectable Changes in Fibrinogen Adsorption Affecting Platelet Activation on Polymer Surfaces. Am J Physiol 1991;260(5):C965-C974.

119. Dyr JE, Tichy I, Jirouskova M, Tobiska P, Slavik R, Homola J, et al. Molecular arrangement of adsorbed fibrinogen molecules characterized by specific monoclonal antibodies and a surface plasmon resonance sensor. Sens Actuators B Chem 1998;51(1-3):268-272.

120. Jirouskova M, Dyr JE, Suttnar J, Holada K, Trnkova B. Platelet adhesion to fibrinogen, fibrin monomer, and fibrin protofibrils in flowing blood - The effect of fibrinogen immobilization and fibrin formation. Thromb Haemost 1997;78(3):1125-1131.

121. Moskowitz KA, Kudryk B, Coller BS. Fibrinogen coating density affects the conformation of immobilized fibrinogen: Implications for platelet adhesion and spreading. Thromb Haemost 1998;79(4):824-831.

122. Pelton JT, McLean LR. Spectroscopic methods for analysis of protein secondary structure. Anal Biochem 2000;277(2):167-176.

123. Chittur KK. FTIR/ATR for protein adsorption to biomaterial surfaces. Biomaterials 1998;19(4-5):357-369.

124. Haynes CA, Norde W. Structures And Stabilities Of Adsorbed Proteins. J Colloids Interface Sci 1995;169(2):313-328.

125. Baker BR, Garrell RL. g-Factor analysis of protein secondary structure in solutions and thin films. Faraday Discuss 2004;126:209-222.

126. Blondelle SE, Ostresh JM, Houghten RA, Perezpaya E. Induced Conformational States Of Amphipathic Peptides In Aqueous Lipid Environments. Biophys J 1995;68(1):351-359.

127. Herrick S, Blanc-Brude O, Gray A, Laurent G. Fibrinogen. Int J Biochem Cell B 1999;31(7):741-746.

128. McMillin CR, Walton AG. Circular-Dichroism Technique For Study Of Adsorbed Protein Structure. J Colloids Interface Sci 1974;48(2):345-349.

129. Layne E. Spectrophotometric and Turbidimetric Methods for Measuring Proteins. Meth Enzymol 1957;3:447-455.

130. Johnson CW. Circular Dichroism Instrumentation. In: Fasman GD, editor. Circular Dichroism and the Conformational Analysis of Biomolecules. New York: Plenum Press, 1996. p. 635-652.

131. Lowry TM. Optical Rotatory Power. New York: Dover Publications, 1964.

132. Greenfield NJ. Using circular dichroism spectra to estimate protein secondary structure. Nat Protoc 2006;1(6):2876-2890.

133. Snatzke G. Circular Dichroism: An Introduction. In: Nakanisha K, Berova N, Woody RW, editors. Circular Dichroism: Principles and Applications. New York: VCH Publishers, 1994.

134. Woody RW. Theory of Circular Dichroism of Proteins. In: Fasman GD, editor. Circular Dichroism and the Conformational Analysis of Biomolecules. New York: Plenum Press, 1996. p. 25-67.

135. Akaike T, Sakurai Y, Kosuge K, Senba Y, Kuwana K, Miyata S, et al. Study on the Interaction between Plasma-Proteins and Polyion Complex by Circular-Dichroism and Ultraviolet Spectroscopy. Kobunshi Ronbunshu 1979;36(4):217-222.

136. Lehrman SR. Protein Structure. In: Stein S, editor. Fundamentals of Protein Biotechnology. Boca Raton: CRC Press, 1990. p. 9-38.

137. Pauling L, Corey RB, Branson HR. The Structure of Proteins: Two Hydrogen Bonded Helical Configurations of the Polypeptide Chain. Proc Natl Acad Sci USA 1951;37(4):205-211.

138. Schulze GE, Schirmer RH. Patterns of Folding and Association of Polypeptide Chains. In: Cantor CR, editor. Principles of Protein Structure. New York: Springer-Verlag, 1990. p. 66-107.

139. Pauling L, Corey RB. Configurations of Polypeptide Chains with Favored Orientations Around Single Bonds: Two New Pleated Sheets. Proc Natl Acad Sci USA 1951;37(11):729-740.

140. Rose GD, Gierasch LM, Smith JA. Turns in Peptides and Proteins. Adv Protein Chem 1985;37:1-109.

141. Venkatachalam CM. Sterochemical Criteria for Polypeptides and Proteins. V. Conformation of a System of 3 Linked Peptide Units. Biopolymers 1968;6(10):1425-1436.

142. Sreerama N, Woody RW. Computation and analysis of protein circular dichroism spectra. Numerical Computer Methods, Pt D, 2004. p. 318-351.

143. Holzwarth G, Doty P. The Ultraviolet Circular Dichroism of Polypeptides. J Am Chem Soc 1965;87(2):218-228.

144. Greenfield NJ, Fasman GD. Computed circular dichroism spectra for the evaluation of protein conformation. Biochemistry 1969;8(10):4108-4116.

145. Venyaminov SY, Baikalov IA, Shen ZM, Wu CSC, Yang JT. Circular Dichroic Analysis of Denatured Proteins - Inclusion of Denatured Proteins in the Reference Set. Analytical Biochemistry 1993;214(1):17-24.

146. Sreerama N, Woody RW. Analysis of membrane protein CD spectra. Biophys J 2004;86(1):102A-102A.

147. Sreerama N, Woody RW. On the analysis of membrane protein circular dichroism spectra. Protein Sci 2004;13(1):100-112.

148. Sreerama N, Woody RW. Estimation of protein secondary structure from circular dichroism spectra: Comparison of CONTIN, SELCON, and CDSSTR methods with an expanded reference set. Anal Biochem 2000;287(2):252-260.

149. Quinn MJ, Byzova TV, Qin J, Topol EJ, Plow EF. Integrin alpha(IIb)beta(3) and its antagonism. Arterioscler Thromb Vasc Biol 2003;23(6):945-952.

150. Mustard JF, Kinlough-Rathbone RL, Packham MA, Perry DW, Harfenist EJ, Pai KRM. Comparison of Fibrinogen Association with Normal and Thrombasthenic Platelets on Exposure to ADP or Chymotrypsin. Blood 1979;54(5):987-993.

151. Jneid H, Bhatt DL. Advances in antiplatelet therapy. Expert Opin Emerg Drugs 2003;8(2):349-363.

152. Scarborough RM, Kleiman NS, Phillips DR. Platelet glycoprotein IIb/IIIa antagonists - What are the relevant issues concerning their pharmacology and clinical use? Circulation 1999;100(4):437-444.

153. Pierschbacher MD, Ruoslahti E. Cell Attachment Activity of Fibronectin Can Be Duplicated by Small Synthetic Fragments of the Molecule. Nature 1984;309(5963):30-33.

154. Pierschbacher MD, Ruoslahti E. Variants of the Cell Recognition Site of Fibronectin That Retain Attachment-Promoting Activity. Proc Natl Acad Sci USA 1984;81(19):5985-5988.

155. Du XP, Plow EF, Frelinger AL, Otoole TE, Loftus JC, Ginsberg MH. Ligands Activate Integrin Alpha-IIb-Beta-3 (Platelet GPIIb-IIIa). Cell 1991;65(3):409-416.

156. D'Souza SE, Ginsberg MH, Lam SCT, Plow EF. Chemical Cross-Linking of Arginyl-Glycyl-Aspartic Acid Peptides to an Adhesion Receptor on Platelets. J Biol Chem 1988;263(8):3943-3951.

157. Honda S, Tomiyama Y, Aoki T, Shiraga M, Kurata Y, Seki J, et al. Association between ligand-induced conformational changes of integrin alpha(IIb)beta(3) and alpha(IIb)beta(3)-mediated intracellular Ca2+ signaling. Blood 1998;92(10):3675-3683.

158. Van de Walle GR, Schoolmeester A, Iserbyt BF, Cosemans J, Heemskerk JWM, Hoylaerts MF, et al. Activation of alpha(IIb)beta(3) is a sufficient but also an imperative prerequisite for activation of alpha(2)beta(1) on platelets. Blood 2007;109(2):595-602.

159. Chen YP, O'Toole TE, Shipley T, Forsyth J, Laflamme SE, Yamada KM, et al. Inside-out Signal-Transduction Inhibited by Isolated Integrin Cytoplasmic Domains. J Biol Chem 1994;269(28):18307-18310.

160. Liu JL, Jackson CW, Gruppo RA, Jennings LK, Gartner TK. The beta 3 subunit of the integrin alpha IIb beta 3 regulates alpha IIb-mediated outside-in signaling. Blood 2005;105(11):4345-4352.

161. Ylanne J, Chen Y, Otoole TE, Loftus JC, Takada Y, Ginsberg MH. Distinct Functions of Integrin-Alpha and Integrin-Beta Subunit Cytoplasmic Domains in Cell Spreading and Formation of Focal Adhesions. J Cell Biol 1993;122(1):223-233.

162. Bavry AA, Bhatt DL, Topol EJ. Experimental Antiplatelet Therapy. In: Michelson AD, editor. Platelets. 2nd ed: Elsevier Science, 2007. p. 1193-1208.

163. Simon DI, Xu H, Ortlepp S, Rogers C, Rao NK. 7E3 monoclonal antibody directed against the platelet glycoprotein IIb/IIIa cross-reacts with the leukocyte integrin Mac-1 and blocks adhesion to fibrinogen and ICAM-1. Arterioscler Thromb Vasc Biol 1997;17(3):528-535.

164. Clemetson KJ, Clemetson JM. Platelet GPIb complex as a target for anti-thrombotic drug development. Thromb Haemost 2008;99(3):473-479.

165. Cauwenberghs N, Meiring M, Vauterin S, van Wyk V, Lamprecht S, Roodt JP, et al. Antithrombotic effect of platelet glycoprotein Ib-blocking monoclonal antibody Fab fragments in nonhuman primates. Arterioscler Thromb Vasc Biol 2000;20(5):1347-1353.

166. Cauwenberghs N, Vanhoorelbeke K, Vauterin S, Westra DF, Rome G, Huizinga EG, et al. Epitope mapping of inhibitory antibodies against platelet glycoprotein Ib alpha reveals interaction between the leucine-rich repeat N-terminal and C-terminal flanking domains of glycoprotein Ib alpha. Blood 2001;98(3):652-660.

167. Penz SM, Reininger AJ, Toth O, Deckmyn H, Brandl R, Siess W. Glycoprotein Ib alpha inhibition and ADP receptor antagonists, but not aspirin, reduce platelet thrombus formation in flowing blood exposed to atherosclerotic plaques. Thromb Haemost 2007;97(3):435-443.

168. Fontayne A, Meiring M, Lamprecht S, Roodt J, Demarsin E, Barbeaux P, et al. The humanized anti-glycoprotein Ib monoclonal antibody h6B4-Fab is a potent and safe antithrombotic in a high shear arterial thrombosis model in baboons. Thromb Haemost 2008;100(4):670-677.

169. Wu DM, Meiring M, Kotze HF, Deckmyn H, Cauwenberghs N. Inhibition of platelet glycoprotein Ib, glycoprotein IIb/IIIa, or both by monoclonal antibodies prevents arterial thrombosis in baboons. Arterioscler Thromb Vasc Biol 2002;22(2):323-328.

170. Hermanson GT. Bioconjugate Techniques. 2nd ed: Academic Press, 2008.

171. Lundblad RL. Chemical Reagents for Protein Modification. 3rd ed: CRC Press, 2005.

172. Fears KP. Adsorption-Induced Changes in Enzyme Bioactivity Correlated with Adsorbed Protein Orientation and Conformation. Clemson, SC: Clemson University; 2009.

173. Plow EF, Haas TK, Zhang L, Loftus J, Smith JW. Ligand binding to integrins. J Biol Chem 2000;275(29):21785-21788.

174. Riordan JF. Functional arginyl residues in carboxypeptidase A. Modification with butanedione. Biochemistry 1973;12(20):3915-3923.

175. Mahley RW, Innerarity TL, Pitas RE, Weisgraber KH, Brown JH, Gross E. Inhibition of Lipoprotein Binding to Cell-Surface Receptors of Fibroblasts Following Selective Modification of Arginyl Residues in Arginine-Rich and B-Apoproteins. J Biol Chem 1977;252(20):7279-7287.

176. Riordan JF, Vallee BL. Acetylation. Meth Enzymol 1967;11:565-570.

177. McTigue JJ, Vanetten RL. Essential Arginine Residue in Human Prostatic Acid-Phosphatase. Biochim Biophys Acta 1978;523(2):422-429.

178. Tayyab S, Haq SK, Sabeeha, Aziz MA, Khan MM, Muzammil S. Effect of lysine modification on the conformation and indomethacin binding properties of human serum albumin. Int J Biol Macromol 1999;26(2-3):173-180.

179. Greenfield N. Using circular dichroism collected as a function of temperature to determine the thermodynamics of protein unfolding and binding interactions. Nat Protoc 2006;1(6):2527-2535.

180. Sreerama N, Venyaminov SY, Woody RW. Estimation of protein secondary structure from circular dichroism spectra: Inclusion of denatured proteins with native proteins in the analysis. Anal Biochem 2000;287(2):243-251.

181. Bain CD, Troughton EB, Tao YT, Evall J, Whitesides GM, Nuzzo RG. Formation Of Monolayer Films By The Spontaneous Assembly Of Organic Thiols From Solution Onto Gold. J Am Chem Soc 1989;111(1):321-335.

182. Gooding JJ, Mearns F, Yang WR, Liu JQ. Self-assembled monolayers into the 21(st) century: Recent advances and applications. Electroanalysis 2003;15(2):81-96.

183. Cassim JY, Yang JT. A Computerized Calibration Of Circular Dichrometer. Biochemistry 1969;8(5):1947-&.

184. Qiu J, Lee H, Zhou C. Analysis of guanidine in high salt and protein matrices by cation-exchange chromatography and UV detection. J Chromatogr A 2005;1073(1-2):263-267.

185. Faucheux N, Schweiss R, Lutzow K, Werner C, Groth T. Self-assembled monolayers with different terminating groups as model substrates for cell adhesion studies. Biomaterials 2004;25(14):2721-2730.

186. Wagner R, Richter L, Wu Y, Weissmuller J, Kleewein A, Hengge E. Silicon-modified carbohydrate surfactants VII: Impact of different silicon substructures on the wetting behaviour of carbohydrate surfactants on low-energy surfaces - Distance decay of donor-acceptor forces. Appl Organomet Chem 1998;12(4):265-276.

187. Budzynski AZ. Difference In Conformation Of Fibrinogen Degradation Products As Revealed By Hydrogen Exchange And Spectropolarimetry. Biochim Biophys Acta 1971;229(3):663-&.

188. Kloczewiak M, Wegrzynowicz Z, Matthias FR, Heene DL. Studies On Chemically Modified Fibrinogen .2. Physicochemical Properties Of Maleylated Fibrinogen. Thromb Res 1976;9(4):359-368.

189. Lee DC, Haris PI, Chapman D, Mitchell RC. Determination Of Protein Secondary Structure Using Factor-Analysis Of Infrared-Spectra. Biochemistry 1990;29(39):9185-9193.

190. He XM, Carter DC. Atomic-Structure And Chemistry Of Human Serum-Albumin. Nature 1992;358(6383):209-215.

191. 1EI3, chicken fibrinogen. Protein Data Bank.

192. 1AO6, human serum albumin. Protein Data Bank. .

193. Damodaran S. In situ measurement of conformational changes in proteins at liquid interfaces by circular dichroism spectroscopy. Anal Bioanal Chem 2003;376(2):182-188.

194. 3GHG, human fibrinogen. Protein Data Bank.

195. Fears KP, Creager SE, Latour RA. Determination of the surface pK of carboxylic- and amine-terminated alkanethiols using surface plasmon resonance spectroscopy. Langmuir 2008;24(3):837-843.

196. Werner C, Eichhorn KJ, Grundke K, Simon F, Grahlert W, Jacobasch HJ. Insights on structural variations of protein adsorption layers on hydrophobic fluorohydrocarbon polymers gained by spectroscopic ellipsometry (part I). Colloid Surf A 1999;156(1-3):3-17.

197. Latour RA. Thermodynamic perspectives on the molecular mechanisms providing protein adsorption resistance that include protein-surface interactions. J Biomed Mater Res A 2006;78A(4):843-854.

198. de Feijter JA, Benjamins J, Veer FA. Ellipsometry as a Tool to Study Adsorption Behavior of Synthetic and Biopolymers at Air-Water-Interface. Biopolymers 1978;17(7):1759-1772.

199. Lassen B, Malmsten M. Structure of protein layers during competitive adsorption. J Colloids Interface Sci 1996;180(2):339-349.

200. Abraham GA, de Queiroz AAA, San Roman JS. Hydrophilic hybrid IPNs of segmented polyurethanes and copolymers of vinylpyrrolidone for applications in medicine. Biomaterials 2001;22(14):1971-1985.

201. Grunkemeier JM, Tsai WB, Horbett TA. Co-adsorbed fibrinogen and von Willebrand factor augment platelet procoagulant activity and spreading. J Biomater Sci Polym Ed 2001;12(1):1-20.

202. Grunkemeier JM, Tsai WB, Horbett TA. Hemocompatibility of treated polystyrene substrates: Contact activation, platelet adhesion, and procoagulant activity of adherent platelets. J Biomed Mater Res A 1998;41(4):657-670.

203. Tamada Y, Kulik EA, Ikada Y. Simple Method for Platelet Counting. Biomaterials 1995;16(3):259-261.

204. Vroman L, Adams AL. Adsorption of Proteins out of Plasma and Solutions in Narrow Spaces. J Colloid Interface Sci 1986;111(2):391-402.

205. Norde W, Favier JP. Structure of Adsorbed and Desorbed Proteins. Colloids Surf 1992;64(1):87-93.

206. Blockmans D, Deckmyn H, Vermylen J. Platelet Activation. Blood Rev 1995;9(3):143-156.

207. Clemetson KJ, Clemetson JM. Platelet Receptors. In: Michelson AD, editor. Platelets. 2nd ed: Elsevier Science, 2007. p. 117-144.

208. Shattil SJ, Kashiwagi H, Pampori N. Integrin signaling: The platelet paradigm. Blood 1998;91(8):2645-2657.

209. Ruggeri ZM. Platelets in atherothrombosis. Nature Medicine 2002;8(11):1227-1234.

210. Nurden AT. Glanzmann thrombasthenia. Orphanet J Rare Dis 2006;1.

211. Vanhoorelbeke K, Ulrichts H, Van de Walle G, Fontayne A, Deckmyn H. Inhibition of platelet glycoprotein Ib and its antithrombotic potential. Curr Pharm Des 2007;13(26):2684-2697.

212. Cook JJ, Bednar B, Lynch JJ, Gould RJ, Egbertson MS, Halczenko W, et al. Tirofiban (Aggrastat (R)). Cardiovasc Drug Rev 1999;17(3):199-224.

213. Lele M, Sajid M, Wajih N, Stouffer GA. Eptifibatide and 7E3, but not tirofiban, inhibit alpha(v)beta(3) integrin-mediated binding of smooth muscle cells to thrombospondin and prothrombin. Circulation 2001;104(5):582-587.

214. Parise LV. Integrin alpha(llb)beta(3) signaling in platelet adhesion and aggregation. Curr Opin Cell Biol 1999;11(5):597-601.

215. Chen YP, Otoole TE, Ylanne J, Rosa JP, Ginsberg MH. A Point Mutation in the Integrin Beta(3) Cytoplasmic Domain (S752-P) Impairs Bidirectional Signaling through Alpha-Iib-Beta-P3 (Platelet Glycoprotein Iib-Iiia). Blood 1994;84(6):1857-1865.

216. Horbett TA, Lew KR. Residence Time Effects on Monoclonal-Antibody Binding to Adsorbed Fibrinogen. J Biomater Sci Polym Ed 1994;6(1):15-33.

217. Agnihotri A, Siedlecki CA. Time-dependent conformational changes in fibrinogen measured by atomic force microscopy. Langmuir 2004;20(20):8846-8852.

218. Soman P, Rice Z, Siedlecki CA. Measuring the time-dependent functional activity of adsorbed fibrinogen by atomic force microscopy. Langmuir 2008;24(16):8801-8806.

219. Nonckreman CJ, Rouxhet PG, Dupont-Gillain CC. Dual radiolabeling to study protein adsorption competition in relation with hemocompatibility. J Biomed Mater Res 2007;81A(4):791-802.